INFORMATION TO USERS

This manuscript has been reproduced from the microfilm master. UMI films the text directly from the original or copy submitted. Thus, some thesis and dissertation copies are in typewriter face, while others may be from any type of computer printer.

The quality of this reproduction is dependent upon the quality of the copy submitted. Broken or indistinct print, colored or poor quality illustrations and photographs, print bleedthrough, substandard margins, and improper alignment can adversely affect reproduction.

In the unlikely event that the author did not send UMI a complete manuscript and there are missing pages, these will be noted. Also, if unauthorized copyright material had to be removed, a note will indicate the deletion.

Oversize materials (e.g., maps, drawings, charts) are reproduced by sectioning the original, beginning at the upper left-hand corner and continuing from left to right in equal sections with small overlaps. Each original is also photographed in one exposure and is included in reduced form at the back of the book.

Photographs included in the original manuscript have been reproduced xerographically in this copy. Higher quality 6" x 9" black and white photographic prints are available for any photographs or illustrations appearing in this copy for an additional charge. Contact UMI directly to order.

U·M·I

Evolution of the northern Mariana forearc between 19–21°N:
Petrologic and tectonic evidence for accretion and the formation
of a petrologically diverse forearc crustal section

Johnson, Lynn Ellen, Ph.D.

University of Hawaii, 1991

EVOLUTION OF THE NORTHERN MARIANA FOREARC BETWEEN 19-21°N:
PETROLOGIC AND TECTONIC EVIDENCE FOR ACCRETION
AND THE FORMATION OF A PETROLOGICALLY DIVERSE FOREARC CRUSTAL SECTION

A DISSERTATION SUBMITTED TO THE GRADUATE DIVISION
OF THE UNIVERSITY OF HAWAII
IN PARTIAL FULFILLMENT OF THE REQUIREMENTS
FOR THE DEGREE OF

DOCTOR OF PHILOSOPHY

IN

GEOLOGY AND GEOPHYSICS

AUGUST 1991

By

Lynn Ellen Johnson

Dissertation Committee:

Patricia Fryer, Chairperson
Rodey Batiza
Michael O. Garcia
John M. Sinton
Michael Mottl

I dedicate this dissertation to my parents,

Patricia Johnson and Alan Johnson and my

advisor and friend Dr. Patricia Fryer

Acknowledgments

It takes many years and a lot of hard work to complete a PhD dissertation; this one was no exception. Although there are many people who helped me to accomplish this undertaking, only a few are mentioned below.

I thank the two people most responsible for convincing me to attempt graduate school in the first place Marty Kleinrock and Dave Clague. Marty made graduate school sound like a fun place and convinced me I could do it if I put my heart and soul into the endeavor. Dave gave me the confidence and a headstart on the skills to undertake a PhD.

My parents both deserve recognition for the role they played in the completion of this work. My mother's constant emotional support and confidence in my abilities and my father's unwavering belief in my ability to complete anything I started gave me the courage ic keep trying when I felt overwhelmed.

Many many thanks go to my friends and fellow graduate students throughout the years. Julie Hood, who made me feel welcome at UH from the very start, and Pat Berge, whose comraderie in all things (but especially advisors , chocolate and the Club) helped to brighten even the darkest days (like right before comps), deserve special recognition. My office mates and third floor buddies Kris, Syl, Martha, Phil, Mary, Adam, Devi, Janice, and Noel deserve thanks for being both excellent friends and enlightening colleagues. Suki helped me to feel like a petrologist in the midst of marine geophysicists, and Cate always reminded me that geology was not the only thing in the world. Very special thanks go to Fernando for abundant computer assistance and friendship. I thank all the doves, especially Margaret ,who, though always from a distance, inevitably said the right thing to keep me going when everyone and everything else failed.

own way, though with a few well placed pushes. For this and her belief in my abilities I am eternally grateful.

Abstract

The Mariana forearc is a complex, changing and evolving plate boundary zone. On the basis of geophysical and geologic studies in the 1970's, the Mariana forearc was proposed to be an erosive feature. Volcanism from the arc added new crust to the region while erosion at the trench removed forearc crust and mantle. The results from this dissertation require a more complex evolution. Geochemical studies of mafic rocks dredged from a 2000 m high scarp at 19°30'N, and drilled from a serpentine seamount indicate at least three tectonic sources. Samples with low TiO_2 (<0.8 wt. %) resemble rocks typically formed in a supra-subduction zone region including island arc tholeiites (IAT) and boninites. Samples with moderate TiO_2 (1-2%) resemble basalts formed at a mid-ocean ridge (MORB). Samples with high TiO_2 (>2.5 %) and high alkali elements resemble lavas formed at an intra-plate (hotspot) seamount. Paleontologic studies of radiolarian chert and radiometric studies of lavas from the outer forearc scarp date these samples as Cretaceous. MORB in the outer forearc, over 50 km from the trench axis, could be derived by at least four mechanisms: (1) accretion from the subducting slab, (2) oceanic plate (West Philippine Sea) trapped since the initiation of subduction, (3) intrusion of backarc basin magmas, or (4) forearc magmatism with a MORB-like geochemical composition. The presence of Cretaceous cherts with these lavas is consistent with accretion. However, the presence of IAT throughout the inner trench wall and from the same dredges as MORB is consistent with erosion.

A chain of seamounts is colliding with the forearc at 20°20'N. Seamount collision, common at western Pacific subduction zones, causes fracturing and uplift of the inner trench wall and forearc facilitating erosion. However, the colliding seamounts and underlying plate are also fractured and provide a large, elevated

volume of seamount rocks, thickened crust and faulted oceanic plate to the inner trench wall which may facilitate accretion.

The Mariana forearc is a highly faulted, actively deforming, petrologically complex region. I suggest that both accretion and erosion occur and perhaps alternate both spatially (along the length of the forearc) and temporally over the history of the forearc.

Table of Contents

List of Tables

List of Figures

List of Abbreviations

MORB.....mid-ocean ridge basalt

BABB.....backarc basin basalt

DDW .....distilled deionized water

g......gram

HFSE.....high field-strength element (e.g. Zr, Ti)

IAT.....island arc tholeiite

km.....kilometer

LILE.....large ion lithophile element (e.g. K, Rb, Sr)

Ma.....millions of years ago

m.y......millions of years

OIB.....ocean island basalt

REE.....rare-earth element (the lanthanide series)

SSZ.....supra-subduction zone

Preface

The two main questions I attempt to address with this doctoral dissertation are: "What is the geochemical and structural nature, of the crust of the Mariana forearc?" and "what geologic history could explain the present structure of the Mariana forearc?"

In order to address these questions I have attempted to characterize the petrology and tectonics of the Mariana forearc and to develop a model for the evolution of the forearc. My work has been concentrated on the outer forearc, between 19 and 21°N, but has implications for the rest of the forearc. The data used here include petrography and geochemistry of dredged and drilled rocks, seismic records, gravity and magnetics measurements and SeaMARC II sidescan and bathymetry of the forearc. This work builds upon the interpretations of previous workers in the Mariana region most heavily Dan Karig, Patricia Fryer and Sherman Bloomer. Despite over a decade of concentrated study in the Mariana forearc, fundamental questions about the initiation and subsequent evolution of the forearc region still remain.

The format of this dissertation is: Chapter 1, The introduction, is a brief, but detailed, history of work in the Mariana forearc prior to my dissertation studies and a summary of my dissertation work and findings. Chapter 2 is a detailed analytical methods section and includes procedures for rock sample preparation, analyses and data reduction. The detailed nature of some of this chapter is intended to allow the reader to repeat the conditions of analyses. Chapters 3-7 are individual manuscripts which will be published and in some cases will have more than myself as author. Because of this manuscript format chapters 3-7 each have an abstract, introduction, body of text and conclusions. Analytical methods and references are presented separately to avoid excessive duplication. Listed below are the intended authors for each of these chapters and an explanation of what work was done by each author in the

preparation of each manuscript. Chapter 8 presents a short summary and conclusion of the work presented in chapters 1-7.

Chapter 3: The First Evidence for MORB-like Lavas from the Outer Mariana Forearc: Geochemistry, Petrography and Tectonic Implications.

I will be the first author on this manuscript and Patricia Fryer, University of Hawaii (UH) will be the co-author. I performed all of the analytical work, wrote the initial manuscript and revisions. Patricia Fryer was the chief scientist on the cruise where the samples were collected and assisted with the development, organization and presentation of these ideas.

Chapter 4: Mafic Clasts in Serpentine Seamounts: Petrology and geochemistry of a diverse crustal suite from the outer Mariana forearc

I am the sole author on this publication which is intended for the Ocean Drilling Program, Scientific Results volume 125B. All of the writing and the bulk of the analytical work was done by me either at sea on the JOIDES Resolution or at the UH. I was senior author for the site reports for the Ocean Drilling Program, Initial Results volume 125A for Sites 778 and 779 which are addressed in this paper.

Chapter 5: Late Cenozoic Volcanism in the Mariana Forearc Revealed from Drilling at ODP Site 781

The senior author on this paper is Michael Marlow, United States Geological Survey (USGS); I am second author; Julian Pearce, University of Durham, UK, is third; Patricia Fryer, UH, is fourth; LedaBeth Pickthorn, USGS is fifth and Bramley Murton, Institute of Oceanographic Sciences-Deacon Laboratory, UK, is sixth. The writing tasks were completed as follows: Marlow wrote the geophysical portions of

the paper and the abstract; I assisted with rewriting, clarifying and editing these sections. I wrote the introduction and the geochemistry sections, except for the isotope geochemistry section. Marlow and I collaborated extensively on the discussion and conclusions. Pearce wrote the isotope geochemistry section and provided assistance with the other geochemistry sections of this chapter. Fryer assisted with editing of the entire chapter. Analytical chores were completed as follows: Marlow processed all geophysical data, I performed microprobe analyses, rare-earth element analyses and some x-ray fluorescence (XRF) analyses. Other XRF analyses were performed on board the JOIDES Resolution. Pickthorn performed the K-Ar dating and Murton collected the trace element data in Table 5-3 and Pearce the isotope analyses.

Chapter 6: New evidence for crustal accretion in the outer Mariana forearc: Cretaceous Radiolarian cherts and MORB-like lavas

I am the senior author on this paper, Patricia Fryer, UH, is second, Brian Taylor, UH, is third, Michelle Silk, University of California at Berkeley (UCB) is fourth, David Jones, UCB, is fifth, William V. Sliter, USGS is sixth, Tetsumaru Itaya, Okayama University of Science, is seventh, Teruaki Ishii, Ocean Research Institute, is eight. I wrote the entire text and prepared the figures, however many of the ideas, both scientific and organizational, were developed through lengthy discussions with Taylor and Fryer, both of whom provided useful critiques of earlier versions of this chapter. Silk and Jones performed the Radiolarian identifications and Sliter the foraminifera identifications. Itaya provided the K-Ar dates and Ishii assisted with obtaining Itaya's help.

Chapter 7: Ridge Collision in the Northern Mariana Subduction Zone: Forearc deformation and implications for tectonic erosion and accretion in hardrock forearcs.

This paper will be authored by myself as first author and Patricia Fryer as second author. I wrote all of the text, processed all of the sidescan data, compiled all of the bathymetry, gravity, magnetics and seismic data. Fryer assisted with sidescan interpretation and the development of the ideas regarding forearc evolution. Karen Sender, UH, assisted with sidescan processing.

All other text in this dissertation was written solely by me. However, in many instances improvements in presentation and idea have been suggested by members of my dissertation committee.

Chapter 1:

Introduction

1.1 The Mariana Forearc

The forearc, which is the primary feature addressed in this work, is defined as the region between the active arc and the trench (Fig. 1.1). The Mariana subduction system presumably began forming 45 Ma, approximately coincident with the change in motion of the Pacific plate. Although the exact mechanism for subduction initiation and thus the formation of the Mariana forearc is unknown, two models have been proposed. One model suggests that subduction began along a weakness in the oceanic crust, perhaps a transform fault (Uyeda and Ben-Avraham, 1972; Hilde et al., 1977). In this model, both the overriding plate and the downgoing plate are initially mid-ocean ridge-generated crust. Thus the original forearc was the oceanic plate trapped between the subduction zone and the location where the arc formed, and was probably composed primarily of mid-ocean ridge basalt (MORB), sediment and perhaps intraplate seamounts. A second model (Klein and Kobayashi, 1980; Ogawa and Naka, 1984) proposes that a preexisting subduction system rotated into place and became the present Mariana system. Thus the forearc would be composed of arc and forearc-generated rocks. However, no evidence for arc terranes greater than 45 Ma (the Palau-Kyushu Ridge) have been found, and studies of the West Philippine basin show it to be MOR crust (Mattey et al., 1980; Hilde and Lee, 1984) suggesting the original forearc was a trapped block of oceanic plate. These data support the first model. Although the origin of the Mariana subduction system and its forearc is an important question, many of the conclusions drawn in this work will not be greatly affected by the nature of the original forearc.

Forearcs are dynamic plate boundary regions, not static features. Forearc terranes are changed by numerous processes such as arc rifting, erosion of the inner trench wall, and accretion from the subducting plate. Clues to the processes which have changed the forearc since initiation can be found in the structural and petrologic makeup of the forearc itself. There are many possible scenarios for the evolution of the forearc, and these have prompted several models of forearc evolution.

Two end-member types of subduction margins are generally recognized. Type 1 is an accretionary margin such as the Barbados margin where large volumes of sediment are accreted to the forearc forming a thick accretionary prism. Type 2 is an erosional margin, such as the Mariana and Tonga margins, where little sediment is accreted and erosion of the inner trench wall dominates forearc morphology. Some combination of these processes can be observed in many subduction margins around the world.

1.2 The Mariana Arc System

The Mariana subduction system, located in the western Pacific (Fig. 1.1) is a well-studied intra-oceanic arc system (e.g., Karig, 1974; Hawkins et al., 1984). Subduction along the Mariana trench began about 45 Ma nearly coincident with a change in motion of the Pacific plate. The features of the Mariana subduction system, from west to east are: (1) the Palau-Kyushu Ridge, a remnant (inactive) and now submarine island arc; (2) the Parece Vela Basin, an inactive backarc spreading basin; (3) the West Mariana Ridge, also a remnant arc; (4) the Mariana Trough an active backarc spreading basin (also called the Mariana backarc basin); (5) the Mariana Arc, an active volcanic island arc; (6) the Mariana forearc, including the frontal arc

province (ie., Guam and Saipan), serpentine seamounts and steep faults; and (7) the Mariana Trench (Fig.1.1).

1.2.1 Evolution of the Mariana Arc System

Shortly after initiation of subduction, about 45 Ma (Hussong and Uyeda, 1981), arc volcanism began in response to heating of the downgoing slab forming an active island arc, the Palau-Kyushu ridge. The Palau-Kyushu Ridge was active until about 30 Ma when spreading began forming the Parece Vela basin. This rifting isolated the Palau-Kyushu ridge from the magma source and moved it to the west with respect to the trench. Spreading in the Parece Vela basin continued until about 25 Ma at a full rate of 54-64 mm/my (Kroenke et al., 1980). The West Mariana Ridge, was the active arc from 20-5 Ma; it was isolated when spreading began in the Mariana trough between 5-10 Ma at a full rate of 34-46 mm/my (Kroenke et al., 1980; Fryer and Hussong, 1981). Volcanism began on the currently active Mariana island arc about 10 Ma (Hussong and Uyeda, 1981). Throughout this evolution, the trench and forearc have remained in the same positions, relative to one another and the active arc, as they occur today. The forearc is a tectonically active environment and has undergone significant changes since subduction initiation and forearc formation. Erosion of the inner trench wall, accretion from the arc and the downgoing plate, intrusions of melts from the sub-forearc mantle and the island arc, and formation of serpentine seamounts may all have acted to modify the forearc.

The Mariana subduction system has evolved through at least two episodes of arc-rifting creating the interarc basins (Parece Vela and Mariana Trough) and remnant arcs (Palau-Kyushu and West Mariana Ridges). Two end-member models have been proposed to explain arc rifting. In model 1 the arc splits along the axis

(Karig, 1973); in model 2 the arc splits asymmetrically or primarily along the trench side of the arc (Hawkins et al., 1984). If the arc splits along its axis, it leaves the eastern portion of each active arc in the forearc region of the system. If the arc splits on the eastern edge of the active ridge the entire arc moves westward, relative to the trench, leaving the new arc to grow on rift-generated (backarc basin) or arc crust. Each of these models have implications for the structure and composition of the forearc. In model 1 part of the arc remains and is accreted to the western margin of the forearc. In model 2 the crust upon which the new arc forms will be rift-generated crust with either backarc basin basalt (BABB) composition or arc composition. If the new arc is built west of the rift boundary. portions of this rift-generated crust may be added to the western margin of the forearc. The presence of two remnant arcs and the frontal arc seamounts north of Uracas suggests that some combination of these two mechanisms must have occurred over the history of the Mariana forearc.

1.2.2 Geological Studies of the Mariana Forearc

Geophysical surveys of the Mariana forearc and inner trench wall reveal an unusually complex crustal structure: sediment thicknesses of as much as 1 km in the forearc basin, and an inner trench wall dominated by outcrops of igneous rock (Hussong et al., 1981; Mrozowski et al., 1981). Early models for the evolution of the forearc region (Karig, 1971; Karig and Sharman, 1975) proposed that accretion of oceanic plate, seamounts, and sediment has created an unusually thick and wide forearc. However, the lack of an accretionary prism, the lack of sediment in the trench axis (Hussong and Uyeda, 1981), and the crustal structure, continuous from the arc to the trench, determined from seismic refraction studies (LaTraille and Hussong, 1980) and studies of the rock types recovered from the forearc (Bloomer

and Hawkins, 1983; 1987; Bloomer, 1983) suggested that little, if any, of the subducting plate was preserved in the forearc.

Diverse rock types recovered through dredging in the outer forearc, south of latitude 18°N, include siltstone, chert, lava (basaltic and andesitic), gabbro, and ultramafic rocks; they represent all the elements of an ophiolite suite (Bloomer and Hawkins, 1983) with supra-subduction zone (SSZ) chemical characteristics. SSZ rocks include all igneous rocks generated beneath the active volcanic front and in the forearc. Prior to the work presented in this dissertation the composition of lavas recovered by dredging (Bloomer and Hawkins, 1983; 1987; Bloomer, 1983) and drilling (during DSDP Leg 60, (Meijer et al., 1981; Sharaskin, 1981; Wood et al., 1981) in the forearc were all, with one exception, of SSZ composition (island arc tholeiites [IAT], boninite). The presence of solely arc-generated rocks in the outer forearc and primarily arc rocks exposed in the inner trench wall require approximately 50-100 km of erosion of the inner trench wall (Bloomer, 1983). However some evidence supports an accretion model: (1) A few fragments of high TiO_2 alkalic basalt, thought to be locally accreted·seamount fragments, were recovered during dredging of the inner trench wall (Bloomer, 1983). (2) Sparse Cretaceous microfossils were recovered at DSDP Sites 460 and 461 (Azema and Blanchet, 1981; Hussong et al., 1981) drilled in the inner trench wall. These examples were primarily dismissed as reworked, exotic fragments. (3) Karig and Ranken (1983) suggested at least one incidence of post-Oligocene accretion based on seismic profiles of the southern forearc. No rocks with MORB compositions were recovered from the forearc during these earlier studies. On the basis of these seismic and geochemical data, the dominant mechanism of forearc evolution were proposed to be tectonic erosion of the inner trench wall and igneous accretion from the arc

(Mrozowski and Hayes, 1980; Hussong and Uyeda, 1981; Bloomer and Hawkins, 1983; Bloomer, 1983).

More recent sampling of the forearc includes the first samples recovered from a fault exposure in the forearc west of the break in slope of the inner trench wall (Chapters 3 and 6) and the first description of mafic clasts recovered from the serpentine seamounts (Chapter 4) (Fryer et al., 1989; Johnson et al., 1989). Sample suites with distinct similarities to MORB, OIB and transitional (tholeiitic-alkalic) basalt as well as IAT and boninite were recovered (Chapter 3). This dissertation presents new evidence for accretion in the outer Mariana forearc. The discovery of lavas with MORB-like composition and accreted sediments in this setting requires a reassessment of the existing models for Mariana forearc evolution. Rocks with MORB-like geochemical characteristics are discussed in Chapter 3, evidence for a complex forearc crustal structure over 80 km from the trench are discussed in Chapters 4 and 5, and evidence for accretion of Cretaceous radiolaria and foraminifera in cherts dredged from a deep scarp in the outer forearc over 50 km from the trench axis is discussed in Chapter 6.

Prior to this work in the outer Mariana forearc, the accepted model for formation of the Mariana forearc was subduction initiation in an intraplate setting creating a forearc composed primarily of MORB and subsequent erosion sufficient to remove all of the original forearc. According to this model, the forearc was replaced by volcanic rocks with SSZ characteristics (IAT and boninite) as erosion occurred. The lack of ocean plate rocks (MORB) in the inner trench wall and the lack of any non-arc derived rocks from the forearc west of the break in slope of the inner trench wall (prior to my work, Chapters 3, 4, 6) supported the two conclusions that tectonic accretion was very limited or non-existent and the exposure of SSZ rocks in the inner

trench wall suggested that some erosion must have occurred. However, the discovery of rocks with ocean plate chemical affinities in three separate locations within the forearc (Chapters 3, 4, and 6) indicates that tectonic accretion occurs over at least a 7000 km^2 area.

1.2.3 Causes and Consequences of Forearc Erosion

Erosion of the inner trench wall can be accomplished in several ways. The most obvious cause of erosion is the interaction of the inner trench wall and outer forearc with a seamount, chain of seamounts or an aseismic ridge on the downgoing plate (e.g., Smoot, 1983; Fryer and Smoot, 1985) (Chapter 7). Vertical faulting in the forearc, perhaps caused by seamount subduction, will oversteepen the inner trench wall causing mass wasting (Smoot, 1983; Fryer and Smoot, 1985; Ballance et al., 1989).

The intersection of seamounts or ridges with a subduction zone has profound morphologic effects on the inner trench wall and the outer forearc. Ridges and isolated seamounts are quite common on the Pacific plate; eventually these edifices reach the trench and must either be subducted or become part of the overriding plate (through tectonic accretion). Morphologic effects consistent with erosion include (1) structural disruption of the inner trench wall and shallowing of the trench axis (Fryer and Hussong, 1985; Collot et al., 1985); (2) subsidence and basin formation in the forearc (Collot and Fisher, 1989) and uplift of the forearc (Fryer and Smoot, 1985); and (3) accelerated tectonic erosion of the inner trench wall (Ballance et al., 1989). Erosion rates up to 50 km/my have been proposed for the Tonga forearc where it intersects the Louisville Ridge (Ballance et al., 1989).

Grabens have been shown to form in response to the bending of the plate at weaknesses associated with the original seafloor spreading fabric (e.g., Jones et al., 1978). The products of mass wasting can be carried beneath the forearc in these grabens. The faulted plate may also create a rough surface that may enhance erosion of the outer forearc.

The morphology of the Mariana forearc is typical of an erosional forearc; (1) rock outcrops in the inner trench wall; (2) little or no sediment is present in the forearc or trench axis; (3) no sedimentary accretionary wedge is developed; and (4) erosion of the overriding plate at the inner trench wall is characteristic (Mrozowski and Hayes, 1980; Hussong and Uyeda, 1981; Bloomer, 1983).

In the Mariana forearc, one of the most important consequences of erosion of the inner trench wall is exposure of crust formed from SSZ magmas. Bloomer (1983) proposes that the exposure of SSZ rocks in the inner trench wall is the result of at least 50 km of erosion.

1.2.4 Causes and Consequences of Accretion in the Forearc

Evidence for accretion where large accretionary prisms are developed is obvious. Accretion at hardrock or erosional margins, such as the Mariana subduction margin, may be much more subtle and represented by fragments of intra-plate seamounts or faulted blocks of oceanic plate and/or minor off-scraped sediment. These fragments may accrete quite easily to the inner trench wall (Bloomer, 1983; Ballance et al., 1989; Yamazaki and Okamura, 1989). Accretion into the outer forearc, arcward of the break in slope of the inner trench wall, is more difficult as it requires that the accreted fragments be thrust tens of km over the outer forearc or faulted into the forearc from depth. The erosive action of subducting seamounts as they

collide with the inner trench wall coupled with vertical tectonic movement in the forearc may create steep-sided reentrants which may later become forearc basins (Collot and Fisher, 1989). Accreted fragments may reside along the walls of these reentrants allowing for accretion of subducting plate rocks far from the trench axis (Chapter 6).

Although not truly accretion the forearc may be modified by the intrusion of metamorphic rock. A large number of seamounts (up to 2000 m high) lie in the outer Mariana forearc, 60 to 100 km from the trench axis. Previous investigations (including dredging, diving and side-scan sonar studies) show that these seamounts consist primarily of variably serpentinized ultramafic rock and serpentine muds (Bloomer and Hawkins, 1983; Fryer et al., 1985; 1990; Hussong and Fryer, 1985; Fryer and Fryer, 1987; Saboda et al., 1987; Saboda, 1991). Previous investigators proposed that serpentine bodies are formed when fluids from the subducting Pacific Plate, released by compaction and dehydration reactions, become incorporated into the overlying mantle wedge (Bloomer, 1983; Fryer and Fryer, 1987). The serpentine muds which form these edifices carry blocks of ultramafic rock and a few fragments of mafic rock (Chapter 4). The serpentine seamounts intrude a large volume of mud and rock into the forearc and affect the composition, volume and tectonic history of the forearc.

1.3 Summary

There is no evidence for in-situ rocks (for instance those drilled during DSDP Leg 60) older than about 45 Ma in the Mariana forearc, indicating that the Mariana forearc is a region formed since the initiation of subduction coincident with the change

in motion of the Pacific plate. The primary conclusions of this dissertation work are the following.

(1) The Mariana forearc and in fact entire subduction region is much more complex than previously realized.

(2) Rocks with tectonic affinities of oceanic plates (MORB, OIB) and rocks with SSZ affinities (IAT, boninite) are present throughout much of the forearc and are found together in several locations throughout the forearc.

(3) Cretaceous cherts, MORB and OIB have been documented in the outer forearc west of the break in slope of the inner trench wall indicating that accretion is possible not only in the inner trench wall but in the outer forearc despite the presence of a large amount of SSZ lavas (e.g., DSDP leg 60 results) recovered from the forearc west of the break in slope.

(4) A simple erosional model for the evolution of the forearc is insufficient to explain the geochemical suites of igneous rocks and the sediments present in the outer forearc. Conversely, a simple accretion model is also unable to explain the forearc structure and composition.

(5) Significant vertical, and perhaps lateral, faulting and uplift must occur throughout the forearc and probably is assisted by the subduction of seamounts and aseismic ridges.

(6) Episodes of tectonic erosion of the inner trench wall and outer forearc must alternate both in time and along strike in the Mariana subduction margin.
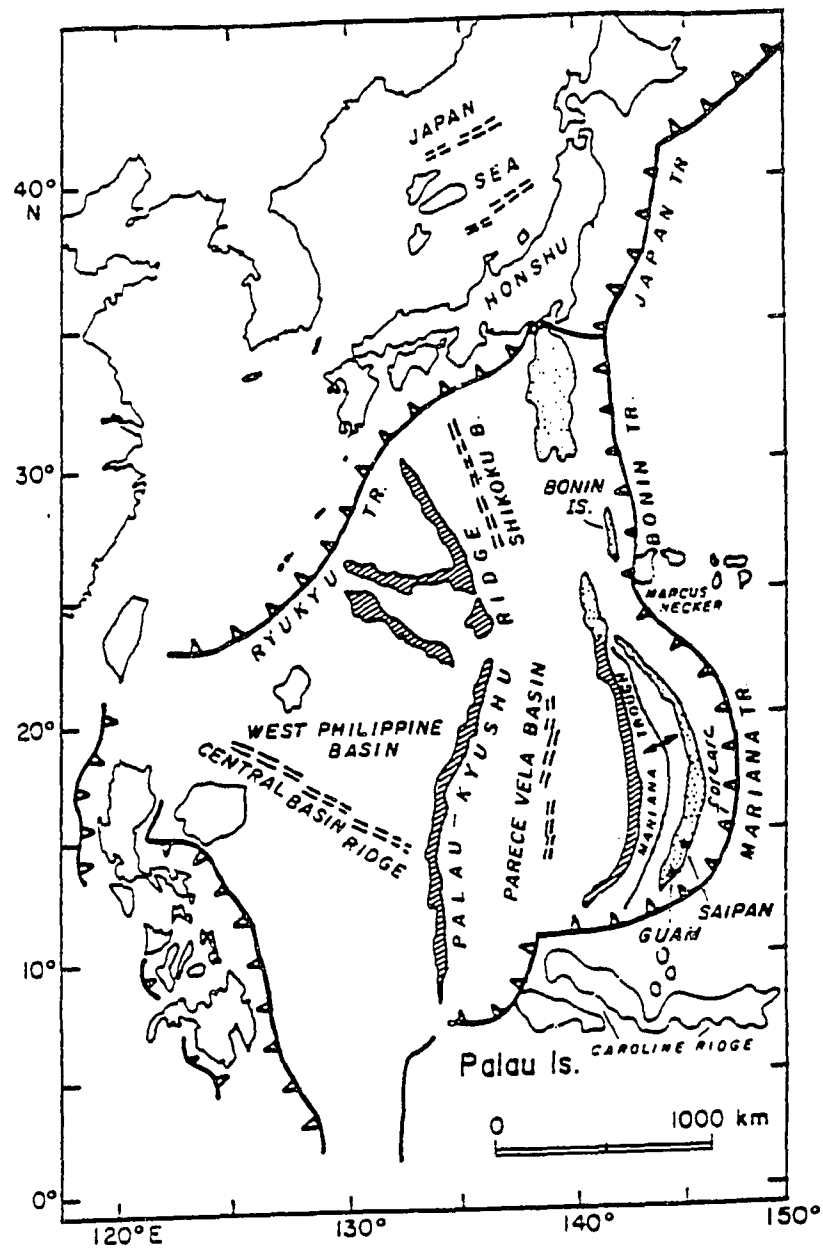
Figure 1.1: General western Pacific map showing the entire Mariana
subduction system from the W. Philippine Basin to the trench and Pacific
plate. Note the two remnant arcs, the Palau-Kyushu ridge and the West
Mariana Ridge, the active arc, the Mariana Island Arc, the remnant backarc
basin, the Parece-Vela Basin, the active backarc basin, the Mariana Trough,
the frontal arc, the islands of Guam and Saipan, the forearc dotted with
serpentine seamounts, the deep trench and the subducting Pacific plate covered
with ridges and seamounts.

Chapter 2:

Analytical Methods

2.1 Samples Available

Rock samples discussed in this dissertation were collected during three research cruises. Samples were dredged during R/V Kana Keoki cruise KK-81-06-26-03 in 1981 and R/V Atlantis II cruise AII-118-15 in 1987. Samples were recovered by drilling from the D/V JOIDES Resolution during Ocean Drilling Project (ODP) Leg 125. Samples were analyzed by X-ray fluorescence (XRF) at the University of Massachusetts, (UMASS) at the University of Hawaii (UH) and on board the JOIDES Resolution (JR). Microprobe analysis was performed at the UH and rare-earth elements (REE) were determined at Lamont-Doherty Geological Observatory (LDGO).

2.2 Geochemical Sample Preparation and Analyses

Representative samples from the entire dredge suite were chosen to be thin sectioned. Wherever possible larger and fresher rocks within each group, identified by hand-sample characteristics, were selected. Only a few mafic rocks were recovered in Holes 778A and 779A during ODP Leg 125. All of the rocks of sufficient size were selected for thin sectioning and analysis. Because of the small size of drill samples, no selection based on size or freshness was possible.

The following sections discuss sample preparation methods for dredged samples. Methods for drilled samples are discussed in Fryer, Pearce, Stokking et al., (1990)

Dredge samples were first inspected in thin section, and assigned to categories on the basis of petrologic features. The freshest samples of each category were selected for chemical analysis. Each sample was then trimmed with a diamond saw to remove altered surfaces. This was not possible in some cases, depending on the size of the sample and the extent of alteration. Cut surfaces were lapped with 200 mesh alumina grit to remove saw marks and contamination. Samples were washed in an ultrasonic bath in tap water until water remained unclouded for 5 minutes and dried overnight on a hot plate at low (<50°C) temperature.

Trimmed samples were crushed in a hydraulic crusher to produce pieces less than 0.5 cm in size. These pieces were washed in an ultrasonic bath in tap water until water remained unclouded for 5 minutes and dried overnight on a hot plate. The freshest pieces were chosen by hand for analysis, washed in an ultrasonic bath in distilled and deionized water (DDW) until water remained unclouded for 5 minutes and dried overnight on a hot plate. The definition of fresh depended on the sample. If there were sufficient chips with no visible alteration then only these were chosen. If there was insufficient material, chips showing the least amount of alteration were chosen. In some samples carbonate veining was so intense that it was not possible to eliminate all veins from the chips used for analysis; in these cases no attempt was made to eliminate them in order to reduce biasing the sample composition.

Each washed and picked sample was powdered in a tungsten-carbide or alumina mill. The mill was cleaned between samples by (1) brushing all particles free; (2) blowing out the compartment with pressurized air; and (3) cleaning with DDW and alcohol until kimwipes remained unsoiled. After cleaning the mill was pre-contaminated by powdering excess rock chips (those not chosen as freshest), cleaned again (steps 1-3) and then the picked sample was powdered.

Sample powders were stored in glass jars that had been washed with laboratory soap and hot water and rinsed with DDW and acetone and dried for several hours in a laboratory oven.

2.3 X-ray Fluorescence Analyses

2.3.1 XRF Analyses (UMASS)

Approximately 1 gram of rock powder (prepared as discussed above) was placed into a quartz crucible and heated at 1050°C for a minimum of two hours in order to oxidize all iron to Fe_2O_3 and to drive off any volatiles that may be present. Loss on ignition (LOI) was calculated as [(original weight - post ignition weight)/ original weight]. Following ignition 0.3000+/-0.0003 g of rock powder were thoroughly mixed with 1.6070+/-0.0005 g of flux. The sample was heated in a platinum crucible in a furnace for six minutes at 1000°C and mixed by swirling two-three times during the six minute heating period. Following heating the melted rock was poured onto a graphite disk, pressed into a thin glass disk, cooled on a covered insulated hot plate at approximately 200°C for two to four hours, and allowed to cool slowly to room temperature to avoid cracking. The edges of the disks were filed smooth and washed with acetone to remove any residue before analysis. Pt crucibles were cleaned in strong HCl between each use to dissolve any remaining sample residue. All other labware was cleaned with acetone before use.

Approximately 2 grams of powder were pressed into a pellet with a boric acid casing for trace element analysis.

The elements Nb, Zr, Zn, Ni, Cr, V, Ce, Ba, and La were analyzed using a Au source tube; Y, Sr, Rb, and Ga were analyzed using a Mo source tube. Precision of the

data was determined by repeat analysis of a single a basaltic standard (BHVO 'new')
with each run of unknowns (Table 3-2).

2.3.2 XRF Analyses (UH)

Analyses at UH were performed in a similar manner to those at UMASS. The
primary difference was in the volumes of rock powder used for analyses.

Approximately 1.5 gram of rock powder (prepared as discussed above) was
placed into a ceramic boat and heated at 950°C overnight to determine LOI. Following
ignition 0.4500+/-0.0002 g of rock powder were thoroughly mixed with
2.9500+/-0.0004 g flux. The sample was heated in a platinum crucible for four
minutes at 1000°C, mixed by swirling, heated for two minutes, removed from the
furnace and swirled for 30-45 seconds over an acetylene torch to assure complete
mixture. The melted rock was poured onto a graphite disk heated to 250°C and pressed
into a thin glass disk. The glass disk was transferred to a hotplate at 200°C for two to
four hours, covered with a ceramic lid and allowed to cool slowly to room temperature
to avoid cracking.

Approximately 4.5 to 5 grams of powder, pressed into a pellet with a boric
acid casing were used for trace element analysis.

2.4 Electron microprobe Analyses (UH)

Thin sections were prepared and polished to 0.03 microns and coated with a
thin film of carbon to assure electrical conductivity and to dissipate heat.

Analysis at UH was performed on a fully automated, 3-spectrometer, Cameca
microprobe using the methods of Byerly et al., (1977; Table 4). For mineral
analyses, the beam was focused to its smallest possible diameter, approximately 2-3

μm, counting time was 20 s/element per each spot analyzed; and a beam current of 10-15 nA at 15 kV was used. All calibration was accomplished on natural minerals. Elements that are abundant in a given mineral were calibrated on the same phase as that being analyzed (e.g. Al for plagioclase was calibrated on plagioclase). Final data were corrected by comparison to repeat analyses of known values of standard minerals and adjusted linearly for drift. All mineral analyses presented are the result of averaging of several spots per crystal and in some cases for several crystals of a given morphology type within a single sample. Repeat analyses of standards was less than 7% for all elements and less than 2% for MgO, SiO$_2$, CaO and FeO.

2.5 Rare-Earth Element Analyses (LDGO)

2.5.1 REE Preparation

Rock powders were prepared (see above) from clean, whole rock samples, ignited at 950°C and fused with a flux in a graphite crucible at 1060°C. Molten sample was poured into 50 ml of 1 N HCl and dissolved. This solution was loaded onto ion exchange columns and followed with a wash of weak HCl and HNO$_3$ to remove most elements except the REE. The REE were collected in 6N HNO$_3$. This solution was dried down and re-dissolved into 7.5 ml base solution and analyzed by DCP (directly coupled plasma) spectrometry.

All acids for REE work were prepared using milli-Q (DDW water further purified to less than 80 ohms) pure water. Acids were commercial (Fisher) reagent grade further distilled to assure purity. Tolerance for all normalities was 2% of acid strength and was determined by titration.

All samples were ignited prior to weighing for analyses to remove adsorbed water and structural volatiles. This step was particularly important for altered

samples that may contain up to 5-10 wt % volatiles. Approximately 0.6 g of powder was weighed into a small aluminum crucible and placed into a furnace at 950°C for 2-2.5 hours. Ignited powder was stored in a desiccator until weighed for analyses.

Following ignition, most samples were simply rolled gently between the folds of weighing paper to return to a powder state. Several samples of boninite, however, appeared to be on the verge of melting and required crushing in an agate mortar to a powdered state so that they could be accurately weighed and mixed with the flux.

Graphite crucibles were used for fusion for DCP analyses to assure that all of the fused sample rolled cleanly out of the crucible. New crucibles were ignited in a furnace at 900°C for 20 minutes and wiped out with a kimwipe and blown clean with compressed air. Previously used crucibles were wiped out with a kimwipe and blown clean.

Johnston Mathey Puratronic LiB_2O_4 flux was used. This flux was in a small ball form (as opposed to a powder form) and was easier to weigh. 1.6000 +/- 0.0001 g flux was weighed into each graphite crucible and a small well formed in the center with a tiny spoon. The final weight was taken after forming the well and removing the spoon. 0.4000+/- 0.0001 gram of ignited rock powder was weighed directly into the well in the flux in the crucible. The sample was then thoroughly mixed with the flux by means of the tiny spoon. Mixing was considered complete when the color of the sample plus fusion was homogeneous.

The fusion furnace was pre-heated to 1060°C. Six samples (flux plus rock) were placed into the furnace at a time and the furnace allowed to regain a stable temperature. Samples remain undisturbed in the furnace for 15 minutes at 1060°C. After 15 minutes one sample was removed from the furnace swirled for approximately 5 seconds to assure mixture and complete fusion and replaced for one

minute. After one minute a second sample was removed and swirled and replaced, the first swirled sample was removed and poured immediately into a 150 ml plastic bottle containing 50 ml of 1 N HCl, capped and shaken for 30 seconds. This procedure was repeated for all six samples and the bottles were all shaken for an additional 10-15 minutes until the sample has completely dissolved and no trace of glass was observed in the bottom of the bottles. In most cases the fused sample rolls cleanly out of the graphite crucible as a single bead, however, occasionally a small fleck of flux (a small white ball) was left in the crucible. This was mixed with the sample and will dissolve. All samples were fused in this manner and allowed to cool for 2-3 hours before loading onto columns.

The ion exchange columns used were 1 cm diameter, 33 cm long quartz glass tubes with a tapered bottom and a reservoir (approximately 180 ml) at the top. Columns were loaded with 1.6 grams of analytical grade, (Bio-Rad: AG50W-X8, 200-400 mesh) cation exchange resin, retained in the column by means of a small wad of silica wool. The resin was cleaned using 150 ml of 2N HNO_3 followed by 450 ml of 6N and backwashed with ultra-clean water using a plastic syringe and long teflon tube. Back-washing removed all traces of acid from the resin and allowed the resin to re-settle to a loosely packed state. Glass watch plates were placed over the top of each column and columns were set up in banks of 4 inside plexiglass housings to prevent dust and other contaminants from gathering on the columns. A total of 20 columns were available in the lab at LDGO for REE separation.

Cooled, dissolved samples were loaded through a plastic funnel lined with filter paper to remove any graphite particles remaining from the fusion. The sample was washed out of the bottle and lid and through the funnel with ultra pure water. Abundant

water was used to assure that no solution remained in the bottle, or on the lid, filter paper or funnel, usually about 100-150 ml, and was allowed to drip through.

All acids were poured onto the top of the columns and allow to drip through entirely before the next acid was added. Most of the major elements were removed with 80 ml of 2N HCl. The remainder of the major elements and most of the minor elements were removed by 170 ml of 2N HNO_3. The REE and any other remaining elements (including abundant Zr, and all the Y) were stripped from the resin with 100 ml of of 6N HNO_3 and collected in 300 ml teflon beakers covered with teflon watch covers. Watch covers have a small hole where the end of the glass column fits to contain any drops or spatters that might otherwise be lost. Following collection of concentrated REE, watch covers were rinsed with milli-Q and the beakers were placed uncovered on a large hot plate. The hot plate was housed inside of a plexiglass box open to a fume hood at one end and equipped with fans at the other end to blow away the vapors from the evaporating solutions. The hot-plate was set at high (approximately 350-400°C) and the samples allowed to remain until completely dry (approximately 12-15 hours). Samples fumed, they did not boil. The beakers were then allowed to cool for at least 30 minutes.

Sample were re-dissolved in 7.5 ml of a base solution that consisted of 1.5 N HNO_3 with 1000 ppm of K, 10 ppm of P and 2 ppm of Be. K acted as a signal enhancer in the plasma, and was added by means of a pure KCO_3 powder. P and Be acted as internal standards used to correct short term drift of the plasma. A re-pipette system was used to assure a uniform delivery of base solution for each sample. Base solution was re-pippetted directly into a small (15 ml) Sevlex beaker with an airtight screw-on cap. This base solution was then poured into the Teflon beaker containing the dried sample and swirled until all the sample was dissolved. Liquid rolled cleanly and

completely out of the sevlex container. Most samples re-dissolved easily (within 15-30 seconds), and poured cleanly from teflon beakers, although occasionally a "wet-spot" remained. However, as it appears that all the dried REE concentrate has gone into solution the concentration of the solution will not be effected by the presence of a "wet spot". Re-dissolved solution was then poured into the small sevlex beakers. Beakers were immediately capped to prevent evaporation. Solutions were drawn directly out of these beakers during analyses.

Of the 20 columns available, 2 were used for the standards, discussed below, 3 were used to repeat analyses of unknowns from run to run to test repeatability and one was used for a blank containing pure flux to correct for blank contamination. The flux solution was prepared in a manner identical to that of the standards and unknowns. I discovered a random La contamination in the Puratronic flux that could not be corrected for by the blank analyses. Thus La determinations are suspect in all cases and have been included (see Table 3-3) only where duplicate or independent analyses suggest they are accurate.

2.5.2 REE Analysis

The instrument used was a directly coupled plasma with 20 simultaneous spectrometers. "HIGH" and a "LOW" REE solutions were used to monitor and correct for secular drift during analyses. Three to five analyses were made from each sample and 20 readings were taken for each analysis. These readings were averaged and any that fell significantly outside the mean were discarded.

Prior to each REE run all tubing that came in contact with the REE solution was replaced or thoroughly cleaned with 2N HNO_3 to remove any contaminants from previous runs. New anodes made of ultra-pure carbon and a freshly polished and

sharpened W cathode were installed and centered inside new ceramic sleeves to focus

the plasma. Ar gas was run through the instrument at 80 psi to create the plasma. By

adjusting the pressure of the Ar through the ceramic sleeves and over the electrodes, a

plasma with the form of a smooth, straight limbed "Y" centered over the spectrometer

slits was created. Spectrometer slits were both set at 100 microns for REE work.

Calibration was accomplished by peaking the spectrometer readings based on a

"HIGH" solution and direct comparison to analyses of known samples. The "HIGH"

solution was a synthetic REE solution made in the lab to a concentration similar to that

of the unknown samples. The "HIGH" solution was made in the same base solution as

that used to re-dissolve the samples. The "LOW" solution was simply the base solution

and acts as a blank or background measurement. Photo-multiplier tubes and the exact

location of the plasma "Y" were adjusted to give readings (raw counts) of the REE in

the "HIGH" solution of at least 3,000 although a reading of 10,000 was preferred if

attainable. A ratio of 3:1 between the "HIGH" and the "LOW" solutions was considered a

minimum acceptable condition for analysis. The "HIGH" solution was analyzed several

time and the residual % standard deviation was checked to assure a stable plasma. Both

the "HIGH" and "LOW" were analyzed at intervals throughout the plasma run.

2.5.3 REE Data Reduction

Data reduction was accomplished in 4 steps. (1) Raw data was screened to

remove any readings, of the 20 taken, that fell significantly outside of the mean of the

reading from each analysis. (2) The data was blank- and drift-corrected using the

"HIGH" solution and the "LOW" solution. It was assumed that the concentration of these

was constant throughout the plasma run. Any deviation from a straight line fit through

the results of these analyses were adjusted to fit a straight line. Internal standard

correction was performed by comparing short term deviations (deviations during the analysis of one or two samples) in the internal standard (P or Be). (3) The blank and drift reduced data were corrected for elemental interferences. These were small except for that caused by Zr. Zr was known to cause a large interference, especially with Ce, and because of chemical similarities between Zr and the REE not all Zr can be removed during column separation. The correction factor was determined using a solution of only Zr in the base solution that was analyzed during each run. The signal created by this solution over and above that present in the blank was used to correct each element. The following formula was used for all elements, Ce is used here as an example. [Ce corrected = Ce measured -((Zr in REE solution/concentration of Zr solution) x Ce measured in Zr solution))]. (4) This data was then compared to the known PPM concentration of two known standards (an alkalic basalt K1919, collected from the same flow as BHVO, and a mid-ocean ridge basalt AII-92-29 from the mid-Atlantic Ridge). Each standard analysis was also blank, drift and interference corrected. Unknowns were converted to PPM by direct comparison. All data reduction programs were written at LDGO by various researchers in the DCP lab.

Data was converted to chondrite normalized values using the values shown in 4-2. These data were then plotted for each plasma run for each sample (typically 3-5 individual analyses) and any obviously spurious points removed (typically those values that fell more that 5% away from the % standard deviation from 1 sigma were removed). The final data were considered precise to within 2% based on the repeatability of several samples.

Chapter 3:

The First Evidence for MORB-like Lavas from the Outer Mariana Forearc:Geochemistry, Petrography and Tectonic Implications

3.1 Abstract

The Mariana forearc, the region between the active Mariana volcanic arc and the trench axis, is considered to be composed of rocks entirely of arc origin. This conclusion was based upon the lack of an accretionary wedge and recovery of arc volcanics from sites throughout the forearc (including the inner trench wall). New chemical data from dredged samples demonstrate that exposures of altered basalts similar to mid-ocean ridge basalt (MORB) and of ocean island basalt (OIB) exist in the Mariana forearc. Several forearc sites, including a 2000 m scarp bounding a large graben at 19°30' N, two small scarps in the inner trench wall, and a seamount were dredged. MORB-like and OIB lavas in addition to island arc tholeiite (IAT) and boninite were recovered. All samples exhibit low temperature seafloor alteration, and some are metamorphosed to lower greenschist facies. IAT samples have low TiO_2 (<1%) and Zr (<56 ppm). The MORB samples have TiO_2 of 1-2% and Zr of 60-93 ppm. OIB samples typically have high TiO_2 (> 3%) and Zr (> 180 ppm). Several OIB samples contain modal nepheline and all have high alkali contents. The presence of OIB and MORB-like lavas in the outer forearc may suggest either that entrapment of Philippine Sea or Kula Plate or that obduction of Pacific Plate has occurred in the evolution of the Mariana forearc. However, the intimate association of MORB-like lavas with arc lavas in the fault scarp requires that either IAT magma was injected into entrapped or obducted oceanic crust or that MORB-like magma was injected into an arc crust during forearc rifting or deformation.
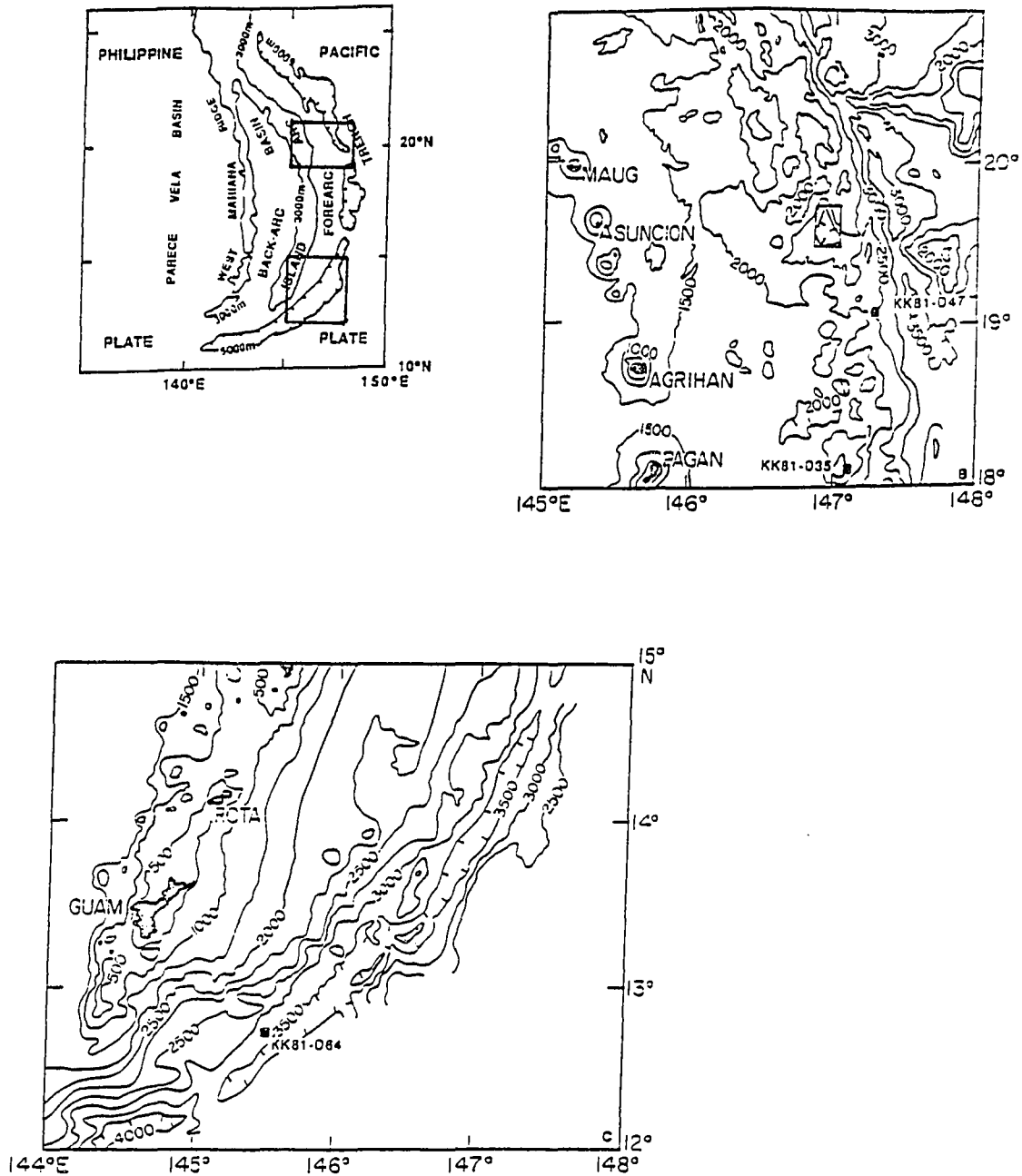
Figure 3.1: Location diagram for dredges discussed in the text. (a) General morphology of Mariana Arc system, boxes show location of figures 1b (northern) and 1c (southern). Bathymetry, contoured in 500 fathom intervals (from Smoot: 1983, 1988); (b) central Mariana forearc, 18-21°N showing large graben near 19°30'N and location of dredge hauls KK81-D47 and KK81-D35, box shows location of figure 3.2 which gives details of dredge location on eastern wall of graben; (c) southern Mariana forearc 12-15°N showing location of dredge KK81-D64.

3.2 Introduction

The tectonic history and the petrologic and geochemical nature of the central western Pacific (Fig. 3.1), from the Philippine Sea to the active Mariana trench have been the focus of numerous studies (Karig, 1971; Uyeda and Ben-Avraham, 1972; Karig, 1974; Hilde et al., 1977; Mattey et al., 1980; Hussong and Uyeda, 1981b; Meijer et al., 1981; Wood et al., 1981; Bloomer, 1983; Bloomer and Hawkins, 1983; 1987; Hawkins et al., 1984; Ogawa and Naka, 1984; Fryer et al., 1985; Fryer and Hussong, 1985; Hussong and Fryer, 1985; Fryer and Fryer, 1987; Fryer et al., 1989). A sequence of rifting events have created several marginal and backarc basins in this region (Karig, 1974; Hawkins et al., 1984). With each successive rifting event a portion of the active arc system has been detached and rafted away from the active volcanic arc to form an inactive remnant arc, bounding each newly formed basin. The record of tectonic and petrologic evolution of the arc systems and the history of rifting events is most likely preserved in the forearc region, a tectonically and magmatically active portion of the arc system, between the active volcanic arc and the trench axis. In this region the development of the lithosphere is influenced by four factors: 1) the nature of any preexisting oceanic plate material that may have been trapped during initiation of subduction; 2) the magmatic and tectonic processes associated with the evolution of the active frontal arc volcanoes; 3) the generation and emplacement of magmas peculiar to forearcs (such as the boninite suite); and 4) collision with and incorporation of small fragments of subducted oceanic plate or seamounts. Thus, the ophiolite sequences formed in forearcs are likely to be complex, both petrologically and structurally. A great deal of controversy over the nature and history of ophiolite sequences is currently centered on the question of whether these suites are supra-subduction zone (SSZ) formed in a convergent setting (the active volcanic arc, the backarc basin, or in the forearc

region), or are pieces of true oceanic crust formed at a mid-ocean ridge. Previous studies indicate that many ophiolites were formed in a SSZ environment (Pearce and Cann, 1971; Pearce, 1975; Hawkins, 1979; Pearce, 1981; Pearce, 1988). As studies of forearcs continue it is becoming increasingly evident that these regions are highly complex and can exhibit elements of all three of the possible arc tectonic regimes (the active volcanic arc, the backarc basin, and the forearc region) in which SSZ ophiolites form.

Previously published data for igneous samples from the Mariana forearc region are from dredges on the inner trench slope, several mid-forearc seamounts (Bloomer, 1983; Bloomer and Hawkins, 1983; 1987), and from four Deep Sea Drilling Project (DSDP), Leg 60 sites (458-461) (Meijer et al., 1981; Wood et al., 1981). The igneous rocks recovered in these studies were largely of IAT and boninite composition, although a small amount of OIB was also recovered (Bloomer, 1983; Bloomer and Hawkins, 1983). The composition of these samples indicated to previous workers that the Mariana forearc had formed as a consequence of island arc volcanism and tectonic erosion modified only by incorporation of a very few, small fragments of oceanic plate seamounts (Hussong and Fryer, 1981; Bloomer, 1983; Bloomer and Hawkins, 1983).

My more recent sampling of the forearc includes the first samples recovered from a fault exposure in the forearc west of the break in slope of the inner trench wall. Sample suites with distinct similarities to MORB, OIB and transitional (tholeiitic-alkalic) basalt as well as IAT and boninite chemical signatures, were recovered. Recently, the Ocean Drilling Program, Leg 125, drilled 4 sites in the Mariana forearc, 3 into a serpentinite seamount in the outer forearc and one in the mid-forearc (Fryer et al., 1989; Johnson et al., 1989). IAT was the primary
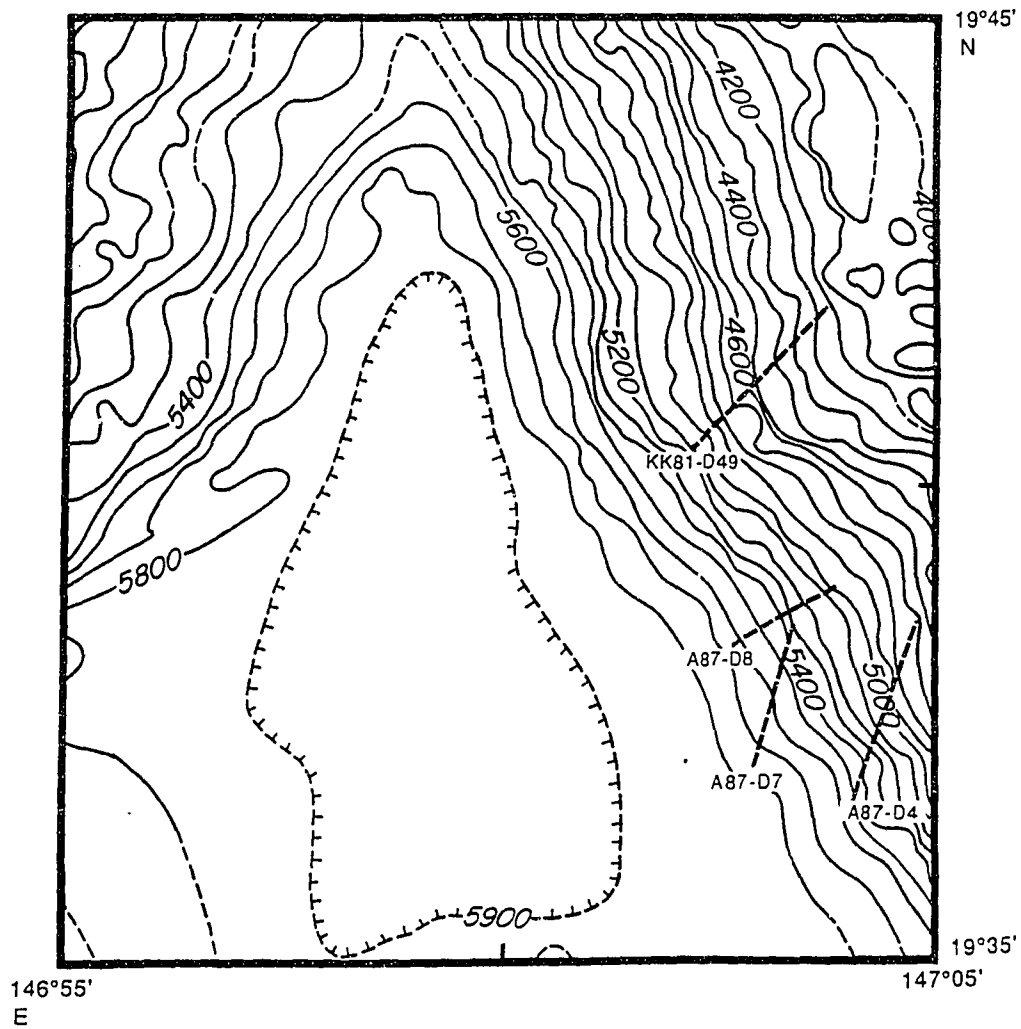
Figure 3.2: Locations of dredges A87-D4, -D7, and -D8, and KK81-D49 on steep scarp in outer Mariana forearc. Bathymetry is unpublished SeaMARC II data.

igneous rock type recovered from these holes, although a few fragments of material with MORB composition were also recovered. The discovery of lavas with MORB-like composition in this setting requires a reassessment of the existing models for Mariana forearc evolution. In this paper we present the results of analyses of these dredge samples and discuss their implications for evolution of the Mariana forearc.

3.3 Tectonic History of the Mariana Forearc

Subduction of the Pacific plate beneath the Philippine Sea plate began by the middle Eocene and formed the proto Mariana arc system (Uyeda and Ben-Avraham, 1972; Karig, 1975; Hilde et al., 1977; Ogawa and Naka, 1984). Spreading, between about 17-30 Ma, formed the Parece Vela Basin and isolated the Palau-Kyushu Ridge, now a remnant arc, from its magma source. The West Mariana Ridge, now a remnant arc, formed to the east from 29-5 Ma and was isolated when spreading began in the Mariana backarc basin (or Mariana Trough) (Mattey et al., 1980). The Mariana island arc has been active and the Mariana backarc basin has been spreading since 5-6 Ma (Fig. 3.1) (Karig, 1971; Hussong and Uyeda, 1981b).

Despite extensive studies of the Mariana forearc (Karig, 1971; Mattey et al., 1980; Meijer et al., 1981; Wood et al., 1981; Hussong and Fryer, 1981; Hussong and Uyeda, 1981b; Mrozowski et al., 1981; Karig and Ranken, 1983; Bloomer, 1983; Bloomer and Hawkins, 1983; 1987; Ogawa and Naka, 1984; Fryer et al., 1985; Hussong and Fryer, 1985; Fryer and Fryer, 1987) the fundamental problems concerning the nature of the forearc basement remain unsolved. Of the three previously suggested models for basement origin, i.e., entrapment of oceanic lithosphere (Hilde et al., 1977; Mattey et al., 1980), sediment and Pacific plate accretion (or obduction) (Hussong and Uyeda, 1981a), or arc volcanism (Hussong and Uyeda, 1981a) only arc volcanism satisfies the previously available seismic,

petrologic, and geochemical data. If the forearc is composed solely of arc related material, a significant amount (at least 50 km) of erosion of the forearc is necessary to explain the presence of arc volcanics exposed in the inner trench wall (Bloomer and Hawkins, 1983; Bloomer, 1983). However, the presence of a small quantity of OIB material in the inner trench wall and seismic and bathymetric data from the southern part of the forearc suggest at least one post-Oligocene episode of accretion (Bloomer, 1983; Karig and Ranken, 1983). Based on our new data no single explanation or mechanism for the formation of the Mariana forearc appears capable of explaining the tectonic and petrologic evolution of the entire forearc over time.

3.4 Current Study

3.4.1 Samples and Analytical Methods

Samples described in this study were collected from 7 dredges (Table 3.1). The deepest exposure in the Mariana forearc yet sampled occurs on the eastern side of a large graben, located approximately 60 km west of the trench axis at approximately 19°40'N (Figs. 3.1 and 3.2). Over 2000 m of forearc basement are exposed in a steep scarp on the northeast wall of this graben. Four dredges were taken from this scarp A87-D4, D7, D8 (Atlantis II cruise All-118-15) and KK81-D49 (Kana Keoki cruise KK810626-03). Two dredges were taken from scarps on the inner trench wall, KK81-D64 (Fig. 3.2c) at approximately 12°44' and KK81-D47 (Fig. 3.2b) at approximately 19°48N. One dredge, KK81-D35 (Fig. 3.2b) , was taken from a serpentinite seamount about 60 km from the trench axis at 18°08'N.

Basalt, diabase, andesite and minor amounts of partially lithified sediment were recovered from all dredges, in addition serpentinized ultramafic rocks were recovered from KK81-D35 and D64.

Table 3.1: Dredge Summary

dredge/ location	depth (m)	N latitude/ E longitude	estimates of volume/[1] rock types recovered
mid-forearc fault scarp			
[2]A87-D4	5360-5255	147°03.85	19°36.88* 110 kg gabbro (33%), diabase (25%) manganese and breccia (20%) volcanic(13%), sediment(9%)
A87-D7	5800-5400	147°02.71	19°37.13* 140 kg volcanic(69%), breccia (17%) chert (8%), boninite (4%) gabbro (2%)
A87-D8	5550-5125	147°03.88	19°39.33* 300 kg chert (60%), silicified clay (20%), volcanic(15%) gabbro (3%) diabase (2%)
[3]KK81-D49	5080-4420	147°01.5	19°41.9* 160 kg volcanic (80%), gabbro (15%) sediment (5%)
outer forearc seamount			
KK81-D35	2050-1760	147°07.84	18°08.29* 350 kg volcanic (50%), ultramafic (40%) gabbro (5%) sediment (5%)
scarps in inner trench wall			
KK81-D47	4450-4400	147°17	19°05** 200 kg gabbro (55%), volcanic (35%) sediment (10%)
KK81-D64	7390-7195	145°30.6	12°44.7* 900 kg ultramafic (40%), gabbro (25%), volcanics (20%), sediment (15%)

[1]based on hand sample descriptions, all percentages are approximate
[2]A87 refers to dredges taken on Atlantis II cruise, AII-118-15, in 1987
[3]KK81 refers to dredges taken on Kana Keoki cruise KK810626-03, in 1981
position during dredge *dead-reckoning **satellite

Thirty-three whole-rock samples were selected for X-Ray fluorescence

(XRF) major and trace element analysis from over 200 thin sections chosen from the

7 dredge locations (Johnson et al., 1987). Analytical methods are given in Chapter 2.

3.4.2 Geochemical and Petrographic Descriptions

All of the analyzed samples show secondary mineralization. Secondary

processes affecting the samples range from low temperature seafloor alteration to

lower greenschist facies metamorphism. The primary petrographic features of some

of the rocks are often obscured and the chemical signatures that allow unambiguous

identification of rock type and provenance are disrupted. The minor and trace

elements Ti, P, V, Cr, Y, Zr, and Nb are immobile or only slightly mobile during

greenschist facies metamorphism and seafloor weathering even over a wide range of

temperatures and high degrees of chlorite alteration (Cann, 1970; Thompson, 1973;

Pearce and Cann, 1973; Pearce, 1975; Floyd, 1975; Humphris and Thompson,

1978; Shervais, 1982; Pearce, 1988). These elements can be used to define

petrologic groups and determine the tectonic environment in which a suite of igneous

rocks is formed. Plots of Zr vs. Ti (Pearce and Cann, 1973) and Ti vs. V (Shervais,

1982) discriminate provenance of basalt samples. Our samples fall into five fields on

such plots (Figs. 3a and 3b) representing distinct chemical groups and implying

different provenance.

3.4.2.1 Geochemical Characteristics:

Sample groups are distinguished primarily by concentrations of immobile

minor and trace elements (Tables 3.2 and 3.3). A summary of the criteria

distinguishing these groups is shown in Table 3.3.

Sample groups can be distinguished by their tholeiitic or alkalic composition (Fig. 3.4) (Floyd, 1975). Groups 1, 2 and 3 all fall in the tholeiitic field (Fig. 3.4) while group 5 falls in the alkalic field and group 4 is transitional. The scatter in (Figs. 3.5a and 3.5b) demonstrates the difficulty of deriving the entire group of samples from a single parent by crystal fractionation and suggests a minimum of three parental groups. Each group is internally coherent, and genetic similarities between the groups are not apparent.

3.4.2.2 Petrographic Characteristics:

The five sample groups denoted above can also be distinguished on the basis of petrographic characteristics.

Group 1 samples are glassy, sparsely pyroxene-phyric with abundant quench crystals and are petrographically identified as boninites. Modally they are 30->60% glass, up to 30% microlite (or quench) pyroxenes, up to 20% microphenocrysts and <20->41% phenocrysts of pyroxene and <1% olivine. These samples are relatively fresh although the glass is 30-50% devitrified and 2-4% chlorite is present.

Most group 2 samples are aphyric to fine-grained (0.01-0.1 mm average) and contain altered glass (10-35%). Two samples in this group are coarse-grained diabase. All samples have 30-50% matrix (comprised of altered glass and microlites of plagioclase), 10-30% clinopyroxene, and <1-5% Fe-oxides, <5% orthopyroxene and <1% olivine. Extensive quartz and calcite veins comprise up to 20%; orthopyroxene and glass are locally replaced by chlorite.

Group 3 samples are primarily aphyric. These samples have 10-20% altered glass, and microlites of plagioclase (10-50%), clinopyroxene (15-40%), Fe-Ti oxide, (1-4%), and olivine (<1%) with <1-5% vesicles. Some samples have a few

percent clinopyroxene microphenocrysts and most have highly altered plagioclase (+/- pyroxene) glomerocrysts (up to 7%). Calcite veins comprise up to 20%.

Group 4 samples are fine- to medium-grained and have 10-14% altered glass, 35-48% plagioclase, 20-24% clinopyroxene, <4% Fe-oxides, 1.5-3% olivine, <1.5% orthopyroxene.

Group 5 samples are medium- to coarse-grained and have 30-80% matrix material (comprised of altered glass and microlites of plagioclase), 5-40% plagioclase, 0-5% nepheline and up to 18% clinopyroxene phenocrysts with 10% vesicles. Calcite and chlorite are present as veins, patches and pseudomorphs after nepheline, plagioclase, pyroxene and possibly olivine.

3.4.3 Provenance Determinations

Petrogenetic discrimination diagrams can be used to distinguish between suites of rocks from different genetic (tectonic) origins (Pearce and Cann, 1973; Shervais, 1982). These diagrams are empirical and indicate the statistical likelihood that a given suite of rocks was formed in the environment indicated. A major failing of these diagrams in the present study is the inability to distinguish backarc basin basalts (BABB) from true MORB; this is discussed in detail below.

The sample groups referred to above fall quite well within single provenance fields in the discrimination diagrams (Figs. 3.3a and 3.3b). On both the Zr-Ti diagram (Pearce and Cann, 1973) (Fig. 3.3a), and the Ti-V diagram (Shervais, 1982) (Fig. 3.3b) group 1 samples plot below (to the more depleted side) of the IAT field where boninite would be expected. Group 2 samples fall into the low-K tholeiite field and are thus classed using the more broadly recognized term IAT. Most group 3 samples fall within the ocean floor basalt field and are thus classed as MORB, while group 5 samples fall in or around the OIB field. Group 4 samples are intermediate

between groups 3 and 5 and appear to be transitional between MORB and OIB. Despite the small region of overlap between the MORB and IAT fields in the Zr-Ti diagram (Fig. 3.3a), most group 3 samples clearly fall within the MORB field in both diagrams.

Samples with MORB affinity previously have not been found in the Mariana forearc. A review of literature from the Mariana arc and forearc (Wood et al., 1981; Bloomer, 1983; Bloomer and Hawkins, 1983) and the Philippine Sea, (Mattey et al., 1980; Meijer et al., 1981), (Figs. 3.6a and 3.6b) shows that, with few exceptions, all of the published data fall into the IAT or boninite fields of both discrimination diagrams. The only exception to this is a small number of OIB samples (Bloomer, 1983; Bloomer and Hawkins, 1983) from the southern part of the forearc which were recovered within the inner trench wall.

A distinction between MORB and BABB is impossible to establish in altered samples such as these. The elements critical to the distinction such as water and the major elements, FeO^*, and Al_2O_3 at a given value of MgO, which were originally used to define Mariana BABB (Fryer et al., 1981), are disturbed by alteration and metamorphism. On the two immobile element discrimination diagrams used above, BABB samples from the Mariana, Lau and North Fiji backarc basins plot in essentially the same location as MORB from a true ocean basin (Figs. 3.6a and 3.6b), however, the Mariana samples do appear to have slightly lower Ti than the field designated for MORB. Figure 3.7 suggests that these samples may have BABB affinities, however the distinction is not unequivocal. Based solely on discrimination diagrams we are unable to distinguish BABB from MORB, but the distinction between MORB/BABB and IAT is clear.

Table 3.2a: Major and trace element abundances for Mariana forearc mafic samples

OXIDE	GROUP 1					GROUP 2								
	7-26	4-10	7-77	4-11	47-22	4-2	4-65	47-25	4-72	4-66	4-12	4-5	64-28	47-23
SiO_2	63.62	62.10	61.04	61.03	56.79	57.47	56.58	55.35	54.91	54.81	54.58	53.71	54.83	51.38
TiO_2	0.20	0.21	0.18	0.18	0.20	0.98	0.58	0.70	0.58	0.57	0.44	0.80	0.21	0.67
Al_2O_3	11.97	11.85	11.77	11.56	10.27	14.25	15.71	15.86	14.98	15.73	15.75	14.49	13.32	15.98
Fe_2O_3	0.95	1.11	1.15	1.14	1.27	1.92	1.48	1.67	1.52	1.52	1.41	1.83	1.19	1.65
FeO	4.84	5.66	5.84	5.81	6.50	9.81	7.56	8.54	7.75	7.76	7.18	9.32	6.09	8.44
MnO	0.10	0.12	0.13	0.13	0.16	0.20	0.17	0.10	0.23	0.16	0.20	0.23	0.12	0.14
MgO	8.51	9.27	10.04	10.20	15.45	3.88	6.04	5.17	7.60	7.36	7.27	6.72	11.31	8.76
CaO	5.22	5.70	6.27	6.12	6.20	3.53	5.78	7.62	5.83	5.58	7.68	5.47	9.83	7.56
Na_2O	2.60	2.19	2.03	2.06	1.88	6.67	4.02	3.66	5.03	4.75	3.78	4.80	1.78	3.09
K_2O	1.02	0.87	0.75	0.76	0.49	0.07	1.35	0.74	0.70	0.66	0.91	1.42	0.13	1.54
P_2O_5	0.04	0.04	0.03	0.03	0.03	0.09	0.06	0.07	0.05	0.05	0.04	0.07	0.01	0.08
TOTAL	99.61	99.75	99.88	99.67	99.97	99.96	100.17	100.43	100.04	99.82	100.04	99.90	99.50	100.23
Mg#	54	52	53	54	61	21	35	29	39	38	40	32	55	41
LOI	6.47	3.77	3.53	2.72	5.40	1.36	2.82	3.07	3.27	2.82	2.72	5.60	2.62	6.71
TRACE ELEMENTS														
Cr	556	631	762	784	1194	bd	18	8	59	32	29	33	541	75
Ni	196	190	199	207	466	13	39	27	57	43	43	35	186	48
Zn	49	58	59	57	69	162	98	58	71	61	144	71	41	86
V	153	174	180	177	131	317	227	261	237	260	217	280	139	279
Ga	9	6	9	9	9	14	14	21	14	13	14	14	13	13
Rb	27	23	19	21	7	bd	12	17	3	4	5	7	bd	14
Sr	66	63	62	62	101	47	119	124	99	112	106	170	142	405
Y	5	5	5	5	5	24	15	14	14	13	11	18	7	16
Zr	49	42	36	38	28	56	43	41	32	33	28	39	27	43
Nb	2	1	2	2	tr	1	tr	1	bd	tr	tr	1	bd	tr
Ce	5	7	6	7	6	9	tr	5	7	6	tr	tr	7	8
Ba	62	47	43	47	9	tr	122	17	tr	21	53	21	tr	29
La	bd	tr	tr	bd	tr	bd	bd	tr	tr	bd	bd	tr	bd	bd
Ti/Zr	23	29	28	29	41	94	68	82	99	87	78	85	40	93
Ti/V	7	7	6	6	9	19	15	16	15	13	12	17	9	14

All abundances are XRF whole rock analyses performed at the University of Massachusetts, Amherst, analyst: L. Johnson
oxides are in wt percent, trace elements are in parts per million, Fe_2O_3 assumed =0.15% total FeO

Mg#=((mol% Mg + mol% Fe)/mol%Mg))x100, LOI:loss on ignition at 950°C, bd:below detection, tr:trace amounts detected

	GROUP 3											GROUP 4	
OXIDES	7-30	7-56	7-79	7-23	7-15	7-75	7-1	7-51	7-50	7-12	8-58	49-21	7-16
SiO_2	49.72	49.68	48.52	47.94	49.31	48.52	48.10	49.19	49.12	50.17	49.18	49.43	49.33
TiO_2	1.37	1.46	1.42	1.29	1.35	1.29	1.11	1.40	1.39	1.42	1.35	1.78	1.99
Al_2O_3	15.08	14.82	14.39	13.32	15.95	15.41	17.02	15.76	15.73	15.96	19.34	15.70	16.99
Fe_2O_3	1.66	1.62	1.79	1.57	1.56	1.47	1.70	1.93	1.92	1.68	1.45	1.56	1.49
FeO	8.47	8.24	9.15	8.02	7.96	7.49	8.66	9.84	9.78	8.58	7.40	7.93	7.60
MnO	0.22	0.20	0.28	0.19	0.19	0.22	0.23	0.16	0.16	0.16	0.15	0.17	0.14
MgO	7.63	7.46	7.11	6.90	6.63	6.40	6.13	5.81	5.74	5.68	5.15	9.41	6.72
CaO	11.09	11.78	12.06	15.40	12.38	14.22	12.24	12.18	12.03	12.24	8.91	7.80	10.57
Na_2O	3.17	3.45	3.52	3.60	3.43	2.93	3.11	2.56	2.64	2.64	4.97	4.09	3.37
K_2O	0.45	0.29	0.83	0.80	0.27	1.13	0.75	0.26	0.27	0.26	0.54	1.55	1.09
P_2O_5	0.11	0.11	0.16	0.15	0.11	0.14	0.11	0.11	0.11	0.11	0.16	0.19	0.30
TOTAL	99.91	100.02	100.25	100.07	100.02	100.05	100.12	100.30	99.98	99.86	99.43	100.49	100.44
Mg#	37	37	34	36	35	36	32	28	28	30	31	44	37
LOI	2.65	3.08	6.42	6.47	3.29	5.54	5.51	2.44	2.50	2.49	4.51	5.39	3.52
TRACE ELEMENTS													
Cr	326	311	156	295	281	239	333	294	297	299	193	301	233
Ni	78	75	98	58	81	70	123	77	78	81	123	121	92
Zn	90	89	99	82	82	79	82	105	115	108	91	76	76
V	282	284	320	265	256	256	250	284	285	280	152	221	186
Ga	17	17	16	14	16	16	16	18	18	18	22	18	20
Rb	6	5	12	15	5	17	8	5	6	5	6	8	11
Sr	152	161	135	145	183	160	194	132	133	135	326	191	522
Y	27	28	29	25	25	25	21	26	26	27	19	27	21
Zr	79	85	85	72	83	77	60	81	77	79	93	120	182
Nb	5	5	5	4	4	4	3	4	4	5	10	4	19
Ce	9	18	15	14	15	13	10	12	10	13	25	18	45
Ba	19	17	32	32	tr	32	36	tr	12	13	78	30	180
La	bd	bd	5	tr	bd	tr	tr	tr	bd	tr	9	6	16
Ti/Zr	107	107	98	103	103	96	105	109	113	111	88	76	61
Ti/V	29	31	27	29	32	30	27	30	29	30	53	48	64

All abundances are XRF whole rock analyses performed at the University of Massachusetts, Amherst, analyst: L. Johnson oxides are in wt percent, trace elements are in parts per million, Fe_2O_3 assumed =0.15% total FeO

Mg#=((mol% Mg + mol% Fe)/mol%Mg))x100, LOI:loss on ignition at 950°C, bd:below detection, tr:trace amounts detected

Table 3.2c: Major and trace element abundances for Mariana forearc mafic samples

GROUP 5

OXIDE	7-38	7-39	7-31	7-17	8-102	35-20	35-21	BHVOnew[1] ($\pm$ wt %) (average/total deviation)	
SiO_2	46.52	44.83	43.14	48.65	47.56	51.06	55.76	49.86	(0.1)
TiO_2	3.58	3.41	3.20	4.07	2.13	2.64	3.21	2.74	(<0.1)
Al_2O_3	19.10	18.03	17.21	15.05	12.48	11.61	11.67	13.76	(0.2)
Fe_2O_3	1.40	1.70	1.88	1.90	1.99	1.53	1.32	12.11	(<0.1)
FeO	7.13	8.68	9.60	9.69	10.17	7.82	6.72	0.17	(none)
MnO	0.17	0.19	0.16	0.12	0.16	0.14	0.16	7.17	(0.6)
MgO	3.10	3.28	3.52	4.14	13.83	6.31	5.45	11.39	(<0.1)
CaO	11.00	12.43	13.81	8.60	6.18	11.69	8.38	2.29	2.6
Na_2O	3.26	3.31	2.42	3.77	3.06	5.93	5.09	0.52	(none)
K_2O	3.14	2.70	3.45	1.52	0.94	0.22	1.27	0.28	(3.6)
P_2O_5	0.53	0.50	0.42	1.00	0.42	0.35	0.51	100.29	
TOTAL	99.72	100.03	99.88	99.59	100.06	100.17	100.29		
Mg#	22	20	19	22	47	35	35		
LOI	10.75	11.43	14.09	2.12	3.73	5.26	3.98		

TRACE ELEMENTS ($\pm$ ppm)

	7-38	7-39	7-31	7-17	8-102	35-20	35-21		
Cr	20	21	142	56	353	242	127	298	(5)
Ni	59	60	50	64	361	·74	120	134	(3)
Zn	110	107	173	121	121	100	85	110	(2)
V	167	191	190	196	108	199	292	290	(6)
Ga	22	23	20	26	19	15	10	22	(1)
Rb	47	65	101	23	13	3	18	9	(<1)
Sr	377	365	253	700	577	89	94	385	(2)
Y	24	22	19	33	19	26	31	24	(<1)
Zr	217	206	181	251	157	203	276	185	(5)
Nb	38	36	32	24	21	19	28	19	(<1)
Ce	58	57	48	79	45	42	61	42	(4)
Ba	331	283	272	600	416	25	134	134	(8)
La	22	24	16	29	24	14	20	13	(5)
Ti/Zr	89	90	106	96	75	68	69		
Ti/V	128	107	101	125	118	80	66		

All abundances are XRF whole rock analyses performed at the University of Massachusetts, Amherst, analyst: L. Johnson oxides are in wt percent, Fe_2O_3 assumed =0.15% total FeO, Mg#=((mol% Mg + mol% Fe)/mol%Mg))x100,

LOI:loss on ignition at 950°C, trace elements are in parts per million, bd:below detection, tr:trace amounts detected

[1] average analysis and total deviation for standard sample analyzed with each run,

Table 3.3: Discriminants of Geochemical Groups

	group 1	group 2	group 3	group 4	group 5
immobile elements[1]					
Y (ppm)	5	16	25	24	25
Zr (ppm)	38	38	79	151	213
Ti (wt%)	0.19	0.61	1.35	1.89	3.18
Ti/V (ppm)	7	17	30	56	99
LREE[2]	low	lo w	medium	med-high	high
Provenance	boninite	IAT[3]	MORB[4]	transit.[5]	OIB[6]

[1]elements considered immobile during alteration, values are averages for each group
[2]light rare-earth elements [3]island arc tholeiite [4]mid-ocean ridge basalt
[5]transitional between tholeiitic and alkalic basalt [6]ocean island basalt
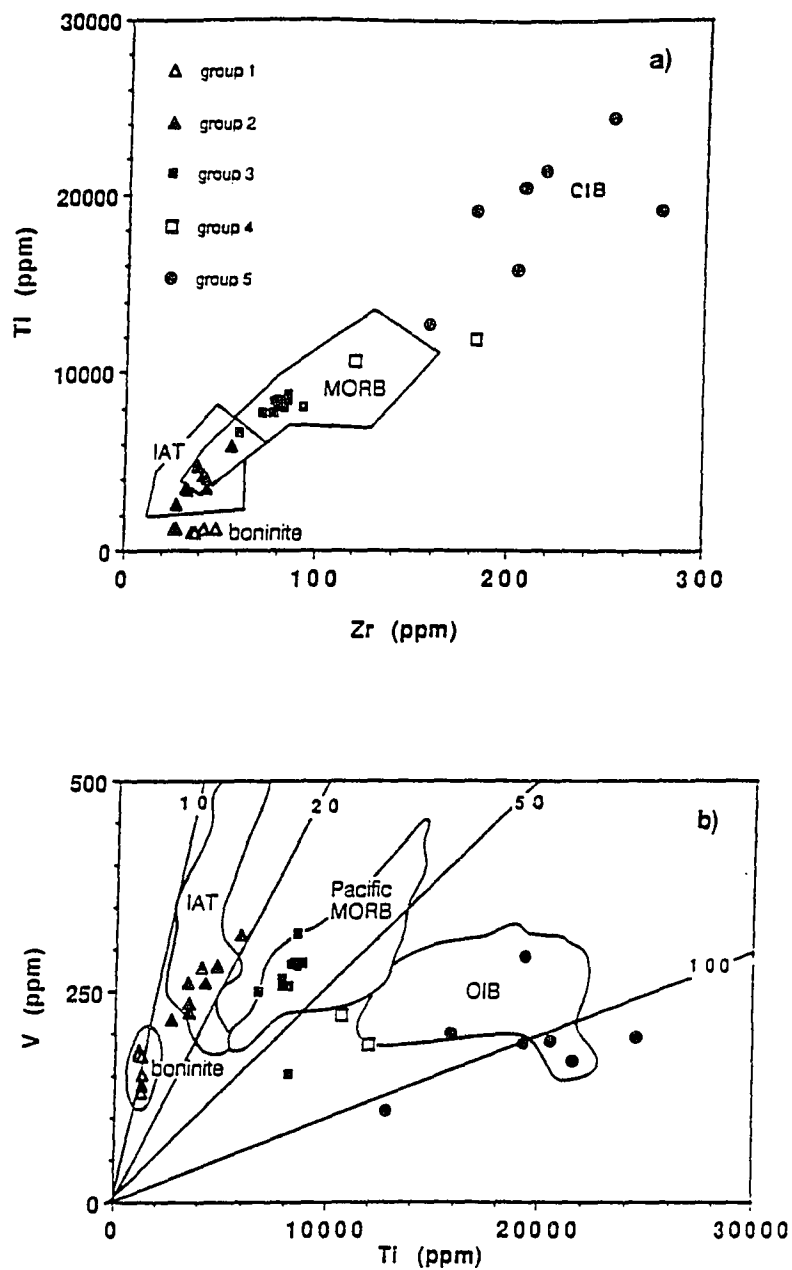
Figure 3.3: Petrogenetic discrimination diagrams to indicate tectonic provenance; (a) Zr-Ti diagram (Pearce and Cann, 1973), (b) Ti-V diagram (Shervais, 1982) symbols are the same as in (a).
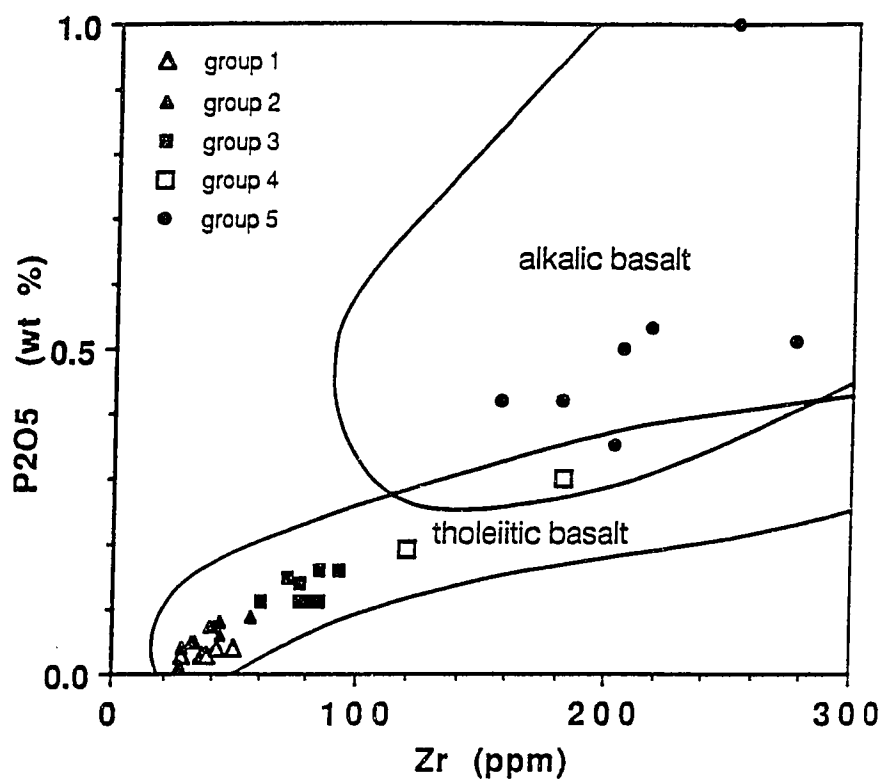
Figure 3.4: Tholeiitic versus alkalic discrimination plot of P_2O_5 vs. Zr, elements considered immobile during low T/P metamorphism (Floyd, 1975).
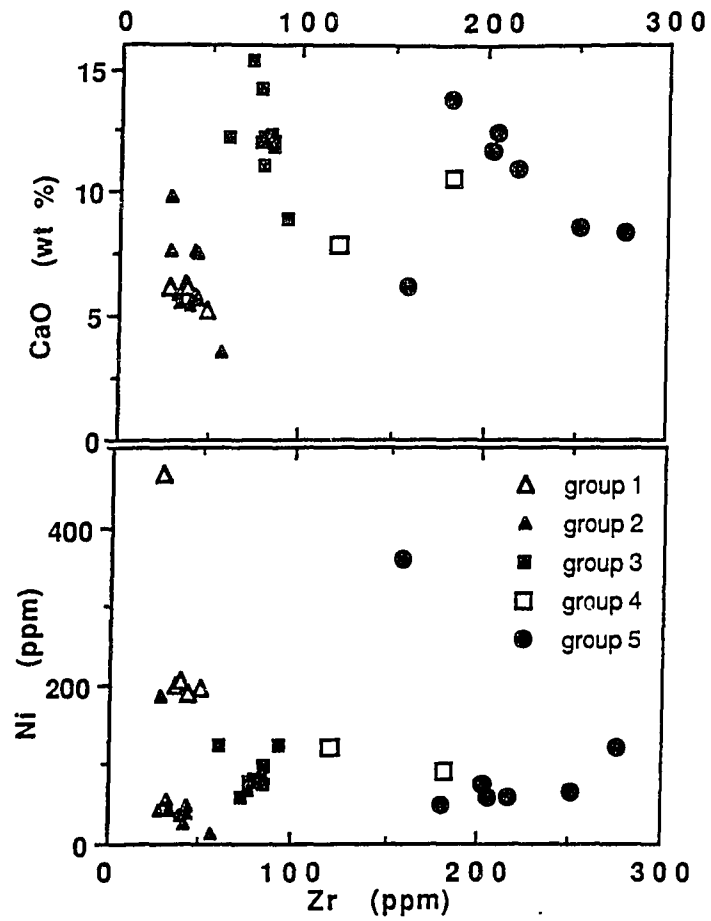
Figure 3.5: Variation diagrams Zr vs. CaO (a) and Ni (b) illustrating that these rocks are not derived by fractionation from a single parent.

500

1 0   2 0

5 0

V (ppm)

IAT

Pacific
MORB

OIB

250

100

boninite

0

0   10000   20000

Ti (ppm)

20000

OIB

a)

Ti (ppm)

MORB

10000

IAT

boninite

0

0   100   200

Zr (ppm)
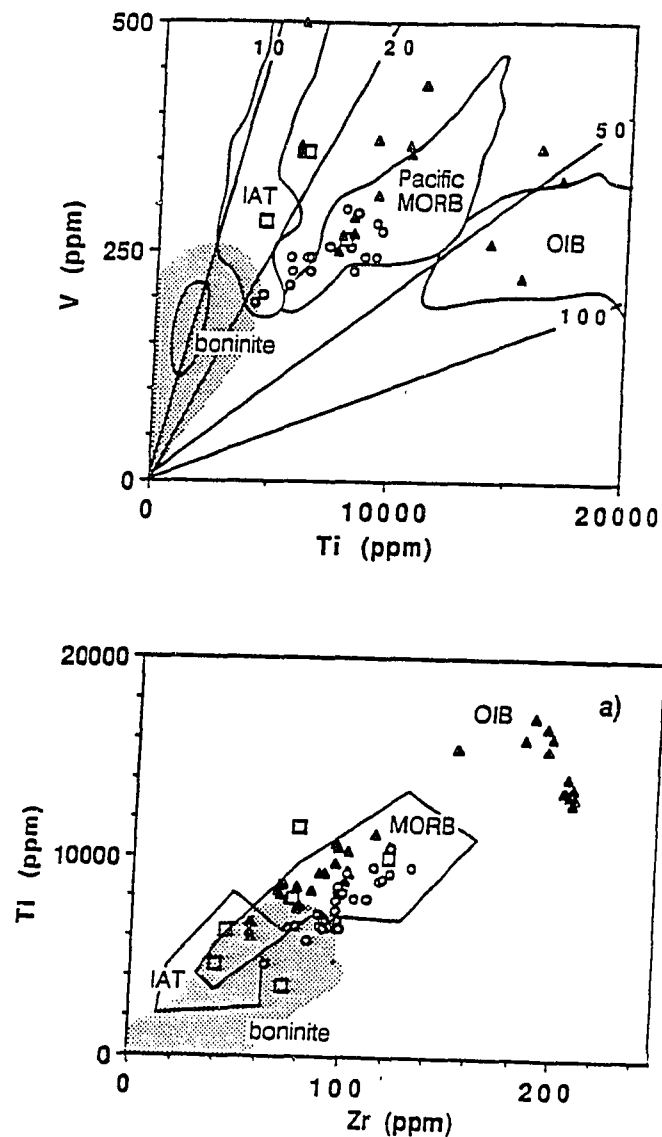
Figure 3.6: Petrogenetic discrimination diagrams after Pearce (Pearce and Cann, 1973) (a) and Shervais (b) (Shervais, 1982) (as in figure 3.3) for previously published data from the Mariana forearc (stippled) (Bloomer, 1983; Bloomer and Hawkins, 1983; Meijer et al., 1981; Wood et al., 1981) and representative backarc basin analyses: open squares are Lau Basin (Gill, 1976; Hawkins, 1985), filled triangles are N. Fiji Basin, (Price et al., 1990) open circles are Mariana backarc basin (Hawkins, 1985; Sinton and Fryer, 1987). Previous Mariana forearc data all plot within the island arc or boninite fields. No MORB-like lavas have been previously recovered. Back-arc basin samples span the entire range for the MORB fields of both diagrams indicating that these discrimination diagrams cannot be used to distinguish altered MORB from altered BABB.
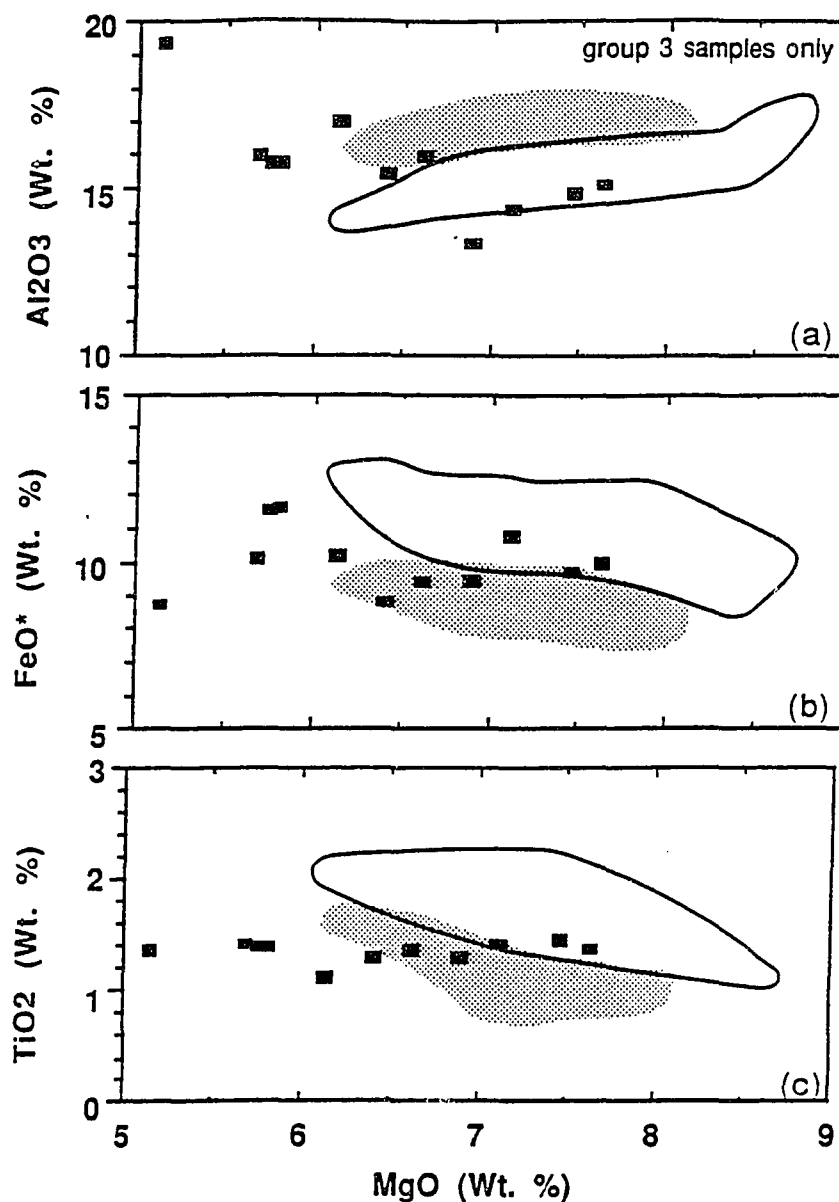
Figure 3.7: MgO (Wt. %) vs. (a) Al_2O_3 (Wt. %), (b) FeO* (Wt. %) (total Fe as FeO) and (c) TiO_2 (Wt. %). The shaded field shows the range of glass compositions from the Mariana backarc basin and the open field is average MORB from Fryer (1981). Group 3, MORB-like lavas from this study show similarities to BABB particularly in TiO_2 and FeO*, however the results are unequivocal because alteration and metamorphism of the samples can change concentrations of many major elements.

3.5 Discussion

The hypothesis that the forearc was generated solely by eruption/injection of IAT associated with frontal arc volcanism is clearly no longer acceptable. The discovery and documentation of MORB (or BABB) composition rocks in the Mariana forearc constrains models for forearc formation to two possibilities. If the group 3 rocks are true MORB then either accretion or trapping of oceanic plate has occurred in the forearc. If the group 3 rocks are BABB they could be explained by the intrusion of dikes and sills of BABB into a forearc composed primarily of IAT.

In addition to the MORB/BABB rocks, any model for the formation of the forearc must also account for the abundance of IAT and boninite composition lavas and the absence of MORB composition lavas recovered in the inner trench wall and the DSDP Leg 60 sites (Meijer et al., 1981; Wood et al., 1981; Bloomer and Hawkins, 1983; Bloomer, 1983). Volumetric calculations, based on bathymetry from the GEBCO map of the northwest Pacific (Iwabuchi, 1979), the forearc cross section at 18°N from DSDP Leg 60 (Hussong and Uyeda, 1981a), and assuming a uniform production rate for the arc over time (Gill, 1981; Sample, 1982) suggest that the volume of the forearc is 50-300% too large to have been formed solely by arc volcanism. Another factor which must be considered in any new model for forearc formation is the close association of diverse rock types which were recovered from a 3 km^2 area on the fault scarp. Two dredges less than 2 km apart (Fig. 3.2, A87-D4 and D7) contained all five of the igneous rock types present (boninite, IAT, MORB, transitional, OIB) as well as sedimentary rocks. Thus, the crust in this region is petrologically complex at a small scale.

If the MORB composition rocks found in the forearc are trapped pieces of oceanic plate, the close association of IAT and MORB composition rocks could result from extensive intrusion of IAT dikes and sills into a forearc region composed

primarily of oceanic plate. Both accretion and trapping of crust are considered unlikely because it seems probable that this would result in exposure of some MORB-like lavas in the inner trench wall. None has been recovered. Alternatively, magmatic stoping of pieces of oceanic plate by an intruding IAT magma could account for both the presence of MORB and the close proximity of diverse rock types.

If the rocks are of BABB composition and if, as previously suggested (Wood et al., 1981; Bloomer, 1983; Bloomer and Hawkins, 1983) the forearc is primarily IAT, it is likely that during forearc rifting, magma with BABB characteristics is intruded into a predominantly IAT forearc. Emplacement of BABB magmas during a forearc rifting or deformation event could explain the diversity of rock types present in the fault scarp.

3.6. Conclusion

Samples with distinct petrochemical signatures of oceanic plate related rocks, MORB (or BABB) and OIB, exist in the Mariana forearc, proving that the forearc does not consist solely of arc related rocks. The data from this study show the first evidence for emplacement of lavas with MORB- (or BABB-) like compositions in the Mariana forearc, and demonstrates the close proximity of MORB (or BABB) and OIB to arc derived material (IAT, boninite). However, the method of emplacement remains problematic. We suggest that this material was emplaced either through the process of IAT intrusion into trapped or accreted oceanic plate or more likely, the injection of MORB-like magma into predominantly IAT crust during forearc rifting or deformation.

Chapter 4:

Mafic Clasts in Serpentine Seamounts: Petrology and Geochemistry of a Diverse Crustal Suite from the Outer Mariana Forearc

4.1 Abstract

Clasts of metamorphosed mafic igneous rock of diverse composition were recovered in two drill sites on a serpentine mud volcano in the outer Mariana forearc during Leg 125. These clasts are xenolithic fragments that have been entrained in the rising serpentine mud, and make up less that 9% of the total rock recovered at Sites 778 and 779. Most samples are metabasalt or metadiabase, although one clast of possible boninite and one cumulate gabbro were recovered.

On the basis of trace element signatures, samples are interpreted to represent both arc-derived and mid-ocean ridge derived compositions. Rocks with extremely low TiO_2 (<0.3 %) and Zr (<30 ppm) are similar to boninite series rocks. Samples with low TiO_2 (<0.9 %) and Zr (<50 ppm) and extreme potassium enrichment (K_2O/Na_2O >3.9) may represent island arc rocks similar to shoshonites. However, the K_2O/Na_2O ratios are much higher than those reported for shoshonites from modern or ancient arcs and may be the result of metamorphism. Samples with moderate TiO_2 (1.4 to 1.5 %) and Zr (72 to 85 ppm) are similar to rocks from mid-ocean ridges. A few samples have TiO_2 and Zr intermediate between island arc and MORB-like rocks. Two samples have high iron ($Fe_2O_3^* =$ >12.8 to 18.5%) ($Fe_2O_3^* =$ total iron calculated as Fe_2O_3) and TiO_2 (>2.3 %) and resemble FeTi basalt recovered from mid-ocean ridges. Metamorphism in most samples ranges from low-temperature zeolite, typical of ocean floor weathering, to prehnite-pumpellyite facies and perhaps lower greenschist. Blue amphibole and lawsonite minerals are present in several samples. One diabase clast (Sample 9) exhibits Ca enrichment,

similar to rodingite metamorphism, typical of mafic blocks in serpentinized masses. The presence of both low grade (clays and zeolites) and higher grade (lawsonite) metamorphism may indicate retrograde processes in these clasts.

These clasts are fragments of the forearc crust and possibly of the subducting plate that have been entrained in the rising serpentine and may represent the deepest mafic rocks ever recovered from the Mariana forearc. The variable compositions and degree of metamorphism of these clasts requires at least two tectonic origins. The recovery of clasts with mid-ocean ridge and arc chemical affinities in a single drill hole requires these clasts to have been "mixed" on a small scale either (1) in the forearc crustal sequence, or (2) after inclusion in the rising serpentine mud. The source of the MORB-like samples and an explanation for the presence of both MORB-like and arc-like rocks in close proximity is critical to any model for the evolution of the Mariana forearc. The source of the MORB-like samples likely will be one (or more) of the following: (1) accretion of Pacific plate lithosphere, (2) remnants of original forearc crust (trapped plate), (3) volcanism in the supra-subduction zone (arc or forearc) environment, or (4) derivation from the subducting slab by faulting along the décollement.

4.2 Introduction

4.2.1 Objectives of ODP Leg 125

Approximately one-half of the time devoted to Leg 125 was spent drilling at four sites on a serpentine seamount in the outer Mariana forearc (Conical Seamount, 19°30'N, 146°40E') (Fig. 4.1). One of the two primary objectives of the leg was to drill through the flanks of the seamount into underlying basement to investigate the origin and evolution of forearc terranes. Igneous forearc crust recovered in the

vicinity of the serpentine seamounts can provide a comparison with the 340 m of igneous crust recovered during DSDP Leg 60 (Hussong et al., 1981).

Two sites are located on the southern flank (Sites 778 and 779) and one at the summit (Site 780) of the seamount (Fig. 4.1). The fourth site (Site 781) is located just northwest of the topographic expression of the serpentine seamount and is discussed in Chapter 5. This paper discusses the mafic clasts recovered in Holes 778A and 779A and their importance in understanding intra-oceanic forearc development.

As expected from previous studies (Bloomer and Hawkins, 1983; Fryer et al., 1985; Fryer and Fryer, 1987; Saboda et al., 1987; Fryer et al., 1990b; Saboda, 1991), sheared serpentine muds and homogeneous serpentinized harzburgite are the primary rock types that were recovered from the seamount sites (778, 779, 780) (Fryer, Pearce, Stokking et al., 1990; Fryer et al., 1990a) (Fig. 4.1). Hole 780A at the summit of Conical Seamount (Fig. 4.1) was drilled to a depth of 163.5 m below sea floor (mbsf) and encountered serpentine muds with infrequent blocks of serpentinized ultramafic rock; no mafic rocks were recovered. Drilling on the flanks of the seamount at Holes 778A and 779A (Fig. 4.1) reached 107.6 and 317.2 mbsf respectively. Although drilling ceased at Sites 778 and 779, before reaching in-situ basement beneath the seamount, sparse fragments of mafic igneous rock are intimately intermixed with the serpentine mud and serpentinized ultramafic rock (Fryer, Pearce, Stokking et al., 1990). The mafic rocks are present primarily as small (4.8 cm), fine-grained, rounded clasts of metabasalt; however, one large interval (392 cm) of coarser-grained, possibly intrusive, rock was cored at Hole 779A. The sparse volume of these mafic clasts suggests that they are present as "xenoliths" in the serpentine seamounts. The drilling results indicate that the
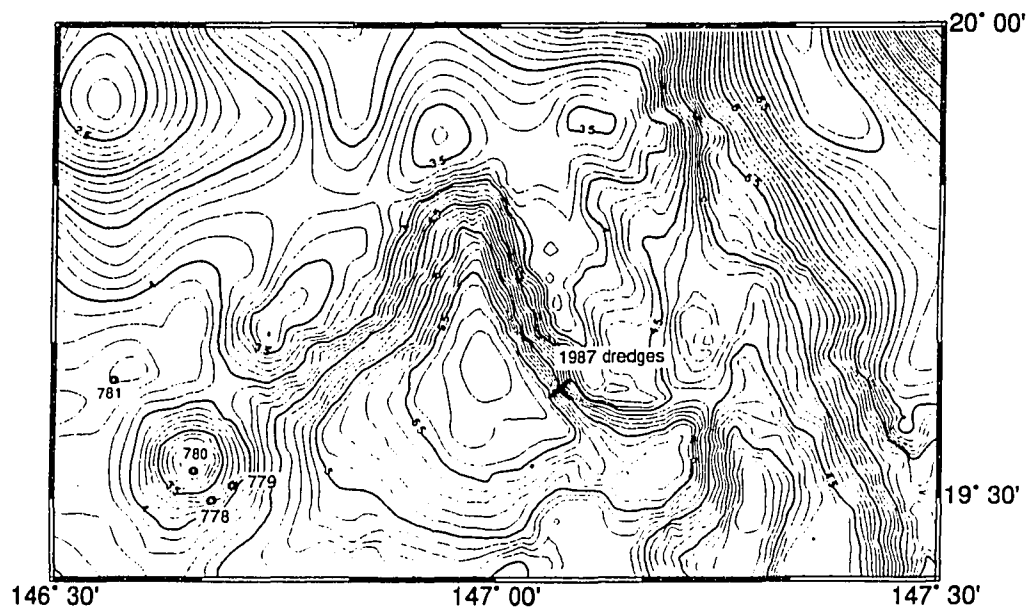
Figure 4.1: Bathymetric map showing the Serpentine Seamount drilled during Leg 125 and a steep scarp in the outer Mariana forearc. Filled circles are locations for samples discussed, open circles are other drill sites, line represents dredge tracks of Chapter 3.

seamount is a large mud volcano venting deep seated fluids (Mottl et al., Leg 125

Scientific Results Volume) and erupting serpentine muds and entrained

clasts from depth through a central conduit (Fryer et al., Leg 125 Scientific Results

Volume). Metamorphic minerals in most of these clasts are typical of the prehnite-

pumpellyite to greenschist facies. However, in some of these clasts minerals typical

of the blueshist facies are present (Maekawa et al., Leg 125 Scientific Results

Volume), suggesting they may have been plucked from deep within the forearc. The

Torishima Forearc Seamount, a serpentine seamount drilled in the Izu-Bonin forearc

at 31°N (Sites 783 and 784), yielded only a few small clasts of mafic rock.

Although mafic fragments from Conical Seamount represent less than 9% of

the total rock recovered (in drill holes), the great chemical diversity and the wide

range in metamorphic grade suggests that they may represent fragments of forearc

crust as well as fragments of the subducting plate. The presence of these rocks have

significant implications for the formation and evolution of the Mariana forearc and

may help broaden our understanding of the tectonic processes that control the

composition, structure, and development of intra-oceanic forearc regions.

4.2.2 Tectonic Setting and Description of Serpentine Seamounts

A large number of seamounts (up to 2000 m high) lie in the outer Mariana

forearc, 60 to 100 km from the trench axis. Previous investigations (including

dredging, diving and side-scan sonar studies) show that Conical Seamount (Fig. 4.1)

consists primarily of variably serpentinized ultramafic rock and serpentine muds

(Hussong and Fryer, 1985; Fryer et al., 1987; 1990b). Previous investigators

proposed that serpentine bodies are formed when fluids from the subducting Pacific

Plate, released by compaction and dehydration reactions, become incorporated into the

overlying mantle wedge (Bloomer, 1983; Fryer and Fryer, 1987). Formation of

serpentine mud volcanoes probably results from serpentinization of forearc mantle by interaction with this fluid, causing a decrease in density and allowing ascent of serpentinized mantle along fractures in the forearc. Serpentine mud carrying large, often rounded, blocks of ultramafic rock erupts from a central conduit and forms a large edifice, probably within a period of 1.5 to 2 m.y. (Fryer et al., 1990b). Blocks observed during ALVIN dives range in size from 0.5 to 2 m in diameter and blocks up to 4 m were drilled. Smaller fragments of mafic rock, such as those found in Holes 778A and 779A may be brought to the sea floor together with the serpentine, although none have yet been identified in dredge hauls from Conical Seamount.

4.2.3 Previous Studies of Mafic Rocks in the Mariana Forearc

Previous drilling in the Mariana forearc during DSDP Leg 60 recovered a total of 340 m of igneous basement at two forearc sites (Sites 448 and 449). All of the igneous rock recovered (Mattey et al., 1980; Meijer et al., 1981; Wood et al., 1981; Sharaskin, 1981) can be grouped into the single chemical-tectonic affinity of the island arc tholeiite series (Hickey and Frey, 1982) that includes boninites and island arc tholeiitic basalts (IAT). Dredges from the inner trench wall recovered mafic igneous rocks almost solely of IAT affinity (Bloomer and Hawkins, 1983;1987; Bloomer, 1983). A small amount of alkalic basalt recovered in three dredges from the inner trench wall is an exception and probably represents local accretion of seamount fragments (Bloomer and Hawkins, 1983). A more recent study of rocks dredged from a steep scarp in the outer forearc (~ 60 km from the trench axis and 40 km northeast of the Leg 125 drill sites) (Johnson et al., 1987) (Chapter 3) did however, discover a very diverse suite of rocks including metabasalts with geochemical signatures indicative of rocks formed in four different tectonic environments: (1) oceanic spreading centers that create mid-ocean ridge basalt

(MORB), (2) intra-plate hotspots that create oceanic island basalt (OIB); (3) supra-subduction zone (SSZ) margins that create IAT, and (4) forearc igneous rocks such as boninites or forearc rift-related lavas. Cretaceous cherts recovered with these rocks are consistent with accretion of Pacific plate crust (Chapter 6).

Despite petrologic and compositional overlap, there is a difference in the style of occurrence of the mafic samples between Sites 778 and 779. Mafic rocks account for approximately 9% of total recovery from Hole 778A and are present in 6 of 13 cores taken. These samples, as well as the sparse clasts from Holes 783A and 784A, are present as isolated, rounded fragments of brecciated metabasalt, 2 to 8 cm in diameter, that ordinarily lie in direct contact with serpentine clay. Compositionally and petrographically distinct clasts are found adjacent to one another and do not appear to be part of continuous blocks. In contrast, Hole 779A mafic rocks, approximately 7% of the total recovery, are present in only three intervals within 37 cores recovered. Hole 779A mafic clasts are larger, constituting a 62- and a 390-cm section of core for each of a single rock type (Samples 11 and 9 respectively). One exception is a single, isolated, rounded clast of cumulate gabbro at the bottom of the hole (Core 36, Sample 1). The different manner of occurrence of clasts between the two holes (small, scattered fragments for Hole 778A compared with large blocks for Hole 779A), may be related to the source area of the serpentine flows that carried these clasts or, perhaps, to variable internal structure of the seamount itself.

4.3 Petrography and Geochemistry: Mafic Igneous Clasts

4.3.1 Analytical Procedures

Thin sections of 36 samples were prepared, and 18 whole-rock analyses were made from 11 of the meta-mafic samples that were of sufficient size for analyses

(Table 4.1). Major and trace element analyses by X-ray fluorescence (XRF) were performed both on board the JOIDES Resolution and at the University of Hawaii (Table 4.2). See chapter 2 for details.

4.3.2 Petrography

The mafic igneous clasts, though sparse in number and volume, are diverse in rock type; this diversity precludes any attempts to place these samples into geochemical groups (Table 4.1).

Of the 34 thin sections of mafic rock examined (Table 4.1), 24 are metabasalts, and 10 are metadiabase. One is a boninite (Sample 125-778A-8R-1, 18-20 cm), and one is a breccia (Sample 125-778A-7R-1, 1-2 cm) of mixed boninite and basalt clasts. Because of the high degree of metamorphism, the diverse assemblage of clasts and the lack of a clear petrographic grouping, only a brief summary of the petrography is given here (Table 4.1). Detailed descriptions for most samples are given in Fryer, Pearce, Stokking, et al. (1990). Metabasalts at Holes 778A and 779A are typically aphyric and fine-grained (Table 4.1). Some preserve a sparsely intersertal to intergranular texture of plagioclase needles and equant clinopyroxene microphenocrysts in a glassy to very fine-grained holocrystalline matrix. Metamorphic textures are discussed below.

The metadiabase (Sample 9, Table 4.1) occurs in Hole 779A, Cores 31 and 32 (Samples 125-779A-31R to 32R) and comprises a continuous 390 cm segment (recovered length) of variably crystallized metabasalt to diabase. The degree of crystallization increases from glassy to aphyric and fine-grained at the top to subophitic and medium- to coarse-grained towards the center of the block suggesting that it is a single cooling unit. The original rock had a modal composition of 20 to

Table 4.1a: Brief petrographic descriptions of mafic clasts from ODP Leg 125.

Hole:	Core:Interval(cm)	#	Analyses	Rock Type	TiO2 %	Texture		
778A-4R1	1-2			bas		aph		subophitic, shear
	5R1 7-10	2	M, T, R	bas	0.29	aph		subophitic
	6R1 20-23			bas		spph	mg	blastic, shear
	7R1 1-2			breccia				intergranular
	7R1 2-3			and		spph	mg	shear
	8R1 18-20			bon(?)		aph	fg	glassy
	9R1 15-18	3	M, T	bas	0.92			
	9RCC 28-31			bas		aph	vfg	brecciated
	9RCC 9-12	4	M, T, R	bas	0.94		fg	intersertal, veined
	10RCC 1-3			bas		aph	mg	
	10RCC 22-24			bas		spph	fg	brecciated
	11R1 0-3	10	M, T, R	bas	2.32			
	11R1 4-7			bas	1.10	spph	mg	
	11R1 5-7	5	M, T, R	bas	1.12			
	11RCC 79			bas		spph	mg	veined
	13R1 4-6	6	M, T	bas				
	13R1 9-12			bas			glassy	
	13R1 12-14	7	M, T	bas	1.09	aph		
	13RCC 4-6	8	M, T, R	bas	1.33	aph		veined
779A-	9R1 66-68			bas			fg-mg	
	9R1 97-99			bas		aph	fg	veined
	9R1 106-108	11a	M, T, R	bas	2.50		vfg	
	9R1 117-119	11b	M, T	bas	2.38	aph	fg	veined
	31R1 102-103			dia		ph	fg	quench, veined
	31R1 112-115			dia		aph	fg	intersertal
	31R1 119-121	9a	M, T	dia	1.41	ph	mg	intersertal
	31R2 0-4	9b	M, T, R	dia	1.38	ph	mg	intergranular
	31R2 100-102			dia		ph	mg	
	31R2 103-105	9c	M, T, R	dia	1.40	ph	mg	intergranular
	31R2 119-122			dia		oh	fg-mg	
	31R3 32-34	9d	M, T	dia	1.26	ph	mg	intersertal
	31RCC 25-27	9e	M, T, R	dia	1.51	ph	cg	
	31RCC 39-41	9f	M, T	dia	1.48	ph	vfg	
	36R3 0-3	1	M, T	cum	0.19			
783A	15R2 84-86			dia		aph	mg	veined
784A-	39R1 5-6			bas		aph	glassy	veined

See Initial Reports Volume (Fryer, Pearce and Stokking, et al., 1990) for more detailed descriptions.
Elements analyzed: M= major, T=trace, R=rare-earth.
#= sample number discussed in text.
Rock type: bas=meta-basalt, and=meta-andesite, dia=meta-diabase, cum=cumulate, bon=boninite.
Texture abbreviations: shear=sheared, aph=aphyric, ph=phyric, spph= sparsely phyric.
Grain size: vfg=very-fine, fg=fine-grained, mg=medium, cg=coarse.

Table 4.1b: Brief petrographic descriptions of mafic clasts from ODP Leg 125

Hole:	Core:Interval(cm)	plag	cpx	spinel	glass	other	chl	clay	carb	p-p	other
		Original Mineralogy					Metamorphic Minerals				
778A-	4R1 1-2	x	x	x	x		x	x			
	5R1 7-10	x(m)	x(m)	x	x		x				
	6R1 20-23	x(m)	x(m)	x	x	ap	x	x		x	l w
	7R1 1-2	x(m)	x(m)	x	x			x	x		q
	7R1 2-3	x(m)	x(m)	x	x		x	x		x	ep
	8R1 18-20		x		x	ol		x	x		
	9R1 15-18										
	9RCC 28-31	x(m)	x(m)	x	x		x	x		x	z, ep, ox, q, lw
	9RCC 9-12	x	x	x	x		x	x		x	talc
	10RCC 1-3	x(m)	x(m)	x			x	x	x		ox
	10RCC 22-24	x	x				x		x	x	talc, q, lw
	11R1 0-3										
	11R1 4-7	x	x?	x	x	ol	x	x	x		q
	11R1 5-7									x	l w
	11RCC 79	x	x			ol	x				ox
	13R1 4-6	x	x	x	x			x			
	13R1 9-12	x	x	x	x		x	x	x	x	
	13R1 12-14	x(m)	x(m)	x	x		x			x	z
	13RCC 4-6	x(m)	x(m)	x	x			x		x	gt, q, ba
779A-	9R1 66-68	x	x								z
	9R1 97-99		x(m)				x	x			z
	9R1 106-108	x(m)	x(m)	x							z
	9R1 117-119	x?	x				x				q
	31R1 102-103	x(m)	x	x	x		x	x			serp
	31R1 112-115	x	x				x	x			
	31R1 119-121	x	x	x			x	x			
	31R2 0-4	x	x				x	x			
	31R2 100-102	x	x	x			x	x			gt
	31R2 103-105	x	x	x			x	x			gt
	31R2 119-122	x	x	x			x	x			gt
	31R3 32-34	x	x	x			x	x			
	31RCC 25-27	x	x				x	x			gt
	31RCC 39-41	x	x				x	x			gt
	36R3 0-3		x			ol					
783A	15R2 84-86	x(m)	x(m)		x		x				q, ep
784A-	39R1 5-6	x(m)	x(m)	x	x		x		x		ox

See Initial Reports Volume (Fryer, Pearce and Stokking, et al., 1990) for more detailed descriptions.
Mineral abbreviations: plag=plagioclase, cpx=clinopyorxene, (m)=present in groundmass only,
ap=apatite, ol=olivine, chl=chlorite, carb=carbonate, p-p=prehnite-pumpellyite association
z=zeolite, gt=hydrogrossular garnet, q=quartz, ep=epidote, ox=oxide, serp=serpentine,
lw=lawsonite and ba= blue amphibole.
lw and ba identified by Maekawa et al., (Fryer, Pearce, Stokking, et al., in prep).

40% clinopyroxene and 10 to 45% plagioclase and a weakly intersertal texture. This unit is overlain by serpentinized ultramafic rocks and serpentine mud and overlies a fragmented mixture of serpentinized dunite and metabasalt/diabase similar in composition to Sample 9.

A single sample with classic boninitic textures (Sample 125-778A-8R-1, 18-20 cm) is fine-grained with 10% microphenocrysts of orthopyroxene. The brecciated sample (Sample 125-778A-7R-1, 1-2 cm) consists of 0.5 to 1.5 cm clasts of boninite and metabasalt similar to those already described in a matrix of detrital metamorphosed mafic rock.

4.3.3 Secondary Textures and Metamorphism

Most samples, especially the isolated clasts from Site 778, have developed secondary sheared or brecciated textures. Extensive chlorite, carbonate, and prehnite-pumpellyite veining commonly overprint primary igneous textures. All samples exhibit low-temperature, possibly sub-seafloor metamorphism that is characterized by the replacement of glassy and fine-grained matrix by amorphous clay and chlorite. However in some clasts this low temperature metamorphism appears to be retrograde following higher pressure metamorphism such as that described by Maekawa et al., (Leg 125 Scientific Results Volume). Zeolites and epidote are present in some samples (Table 4.1), much of the plagioclase has been albitized, and chlorite and fibrous hornblende commonly replace pyroxene. Relict crystals of clinopyroxene are present in most samples, but relict plagioclase is rare. Lawsonite and sparse blue amphibole are present in some clasts (Maekawa et al., Leg 125 Scientific Results Volume). Sample 9 (Table 4.1) has undergone pervasive metamorphism to the prehnite-pumpellyite facies.

Sample 9 exhibits the extreme Ca-enrichment (up to 25%) and the complete

loss of alkalis (K, Na, and Rb) characteristic of rodingite metamorphism (Coleman,

1967); metamorphism is pervasive with no relict plagioclase remaining and only

sparse, skeletal remnants of clinopyroxene. Rodingite metamorphism is a common

phenomenon in ophiolite exposures, for instance New Zealand (Coleman, 1966) and

California and Oregon (Coleman, 1967). Blocks of mafic rock intruded into or

tectonically emplaced into ultramafic rocks are metamorphosed simultaneously with

serpentinization of the ultramafic rock. The metamorphism of Sample 9 is

homogeneous throughout the block, as demonstrated by the REE and incompatible

element patterns (Figs. 4.2 and 4.3). A particularly interesting observation is that

the REEs of Sample 9 form smooth chondrite-normalized patterns consistent with

immobile trace element interpretations of pre-metamorphic compositions. I conclude

that REE are either immobile during rodingite metamorphism or have been mobilized

as a coherent group. The extent and homogeneity of rodingitization suggests intrusion

or tectonic incorporation of the mafic block into the ultramafic rocks prior to or

during serpentinization and emplacement into the Mariana forearc. However, the

higher than normal concentrations of serpentinizing fluids present within Conical

Seamount may accelerate the reaction time for rodingitization allowing for

emplacement of this block into the serpentine muds after initial serpentinization and

seamount formation.

4.3.4 Major and Trace Element Abundances

The generally high degree of metamorphism of the rocks requires that the

geochemical discussion be centered on elements believed to be immobile during most

metamorphic processes. Many of these samples have unusual major element

abundances, and in some cases these abundances can be explained by the metamorphic

process. For example, the high Ca and lack of alkalis in Sample 9 is characteristic of

rodingite metamorphism. Other unusual values, such as the high MgO for Samples 7

and 8 remains unexplained by either primary igneous processes (e.g., fractionation,

crystal accumulation) or observable metamorphic processes (e.g., veining, addition

of metamorphic minerals). Major elements (Al_2O_3) (Pearce, 1975), minor

elements (Ti, P) (Pearce and Cann, 1973), trace elements (V, Cr, Y, Zr, Nb)

(Shervais, 1982), and the REEs (Ce-Lu) (Humphris and Thompson, 1978;

Morrison, 1978) have been shown to be to be relatively immobile during normal

seafloor weathering. Samples are numbered with respect to increasing

TiO_2 concentration (Table 4.2), and the abundance of immobile incompatible

elements (Ti, Zr, Y and the REE) (Fig. 4.3) generally increases with sample number.

Analyses from several intervals are presented for two of 11 clasts analyzed

(Samples 9 and 11; Table 4.2). On the basis of REE and immobile element patterns

(Figs. 4.2 and 4.3), and two trace element discrimination diagrams (Figs. 4.4a and

4.4b); these clasts can be identified as (1) SSZ rocks (Samples 1 through 4), (2)

depleted MORB-like rocks (Samples 5 through 7), (3) MORB-like rocks (Samples 8

and 9) and (4) high Fe and Ti rocks (Samples 10 and 11).

The incompatible trace element characteristics of basaltic rocks can be demonstrated

and different samples compared using multi-element plots normalized to N-type

MORBs (normal MORB) (Pearce, 1983; Sun and McDonough, 1989). In Figure 4.3

high field strength elements (HFSE: P, Y, Ti, Zr, and the REEs), considered immobile

during normal seafloor metamorphism, have been plotted with the degree of

incompatibility during melting (of a lherzolite source) increasing to the right.

Magmas derived from a mantle source similar to a MORB source will show a flat

pattern, with deviations from this pattern suggesting (1) a different mantle

Table 4.2a: XRF major and trace element data for mafic clasts
from Leg 125, Holes 778A and 779A.
Samples are numbered in order of increasing TiO_2

Sample	1	2	3	4	5	6	7	8
Hole	779A	778A	778A	778A	778A	778A	778A	778A
Core	36-3	5-1	9-1	9-CC	11-1	13-1	13-1	13-CC
Interval	0-6	7-10	15-18	9-12	5-8	5-8	12-14	4-6
Oxides (%)								
SiO_2	46.24	57.70	49.58	48.02	47.94	44.53	43.17	44.28
TiO_2	0.19	0.30	0.92	0.94	1.15	1.17	1.18	1.44
Al_2O_3	14.07	14.81	17.88	16.05	15.49	13.06	12.93	10.07
Fe_2O_3	4.40	8.45	8.22	8.73	13.37	12.52	11.44	10.86
MnO	0.17	0.17	0.17	0.18	0.18	0.27	0.25	0.24
MgO	19.70	7.80	7.03	7.92	2.63	7.04	18.27	23.69
CaO	15.70	3.11	11.88	12.71	9.62	18.19	10.89	6.72
Na_2O	nd	6.16	0.97	0.92	6.14	1.82	0.28	1.14
K_2O	0.10	0.16	3.79	3.14	0.83	0.31	0.83	0.02
P_2O_5	nd	0.03	0.06	0.14	0.05	0.08	0.09	0.11
Total	100.55	97.81	100.48	98.58	96.51	98.67	99.22	98.36
LOI	6.94	2.91	6.10	3.78	3.95	4.45	7.30	7.94
trace elements (ppm)								
Nb	nd	1.5	1.8	1.8	1.4	1.2	5.0	2.4
Zr	1.6	31.0	43.4	50.1	60.3	64.3	57.0	77.6
Y	4.0	9.1	17.5	21.3	22.4	28.4	28.0	28.1
Sr	48.5	50.9	66.0	94.8	61.6	95.4	82.3	43.6
Rb	2.6	2.9	66.7	57.1	16.3	6.1	16.7	nd
Zn	20.5	55.5	63.8	70.7	100.3	92.2	94.7	73.5
Cu	19.1	298.8	35.0	35.4	205.7 ·	75.4	51.2	49.1
Ni	135.5	53.9	38.1	44.0	46.7	41.6	41.1	28.4
Cr	660.7	85.0	119.7	116.5	68.3	150.5	170.0	42.6
V	146.0	215.3	219.0	239.2	357.2	316.8	242.4	280.9
Ce	na	5.9	na	nd	nd	16.2	10.3	8.3
Ba	29.9	2.3	43.3	53.6	46.3	57.8	33.0	14.2
U	2.0	na	2.1	na	na	na	na	na
Sc	42.8	na	26.8	na	na	na	na	na
Co	39.0	na	47.8	na	na	na	na	na
Zr/Y	0.41	3.41	2.47	2.35	2.69	2.26	2.04	2.76
Ti	1109	1768	5485	5640	6863	7013	7073	8631
	b	a	b	a	a	a	a	a

analyzed (a) on board the JOIDES Resolution, analyst D. Sims; (b) at the University of Hawaii,
analyst: L. Johnson. nd = none detected; na = not analyzed; bd = below detection;
LOI = loss on ignition.

Table 4.2b
XRF major and trace element data for mafic clasts
from Leg 125, Holes 778A and 779A.
Samples are numbered in order of increasing TiO2

Sample	9a	9b	9c	9d	9e	9f	10	11a	11b
Hole	779A	779A	779A	779A	779A	779A	778A	779A	779A
Core	31-1	31-2	31-2	31-3	31-CC	31-CC	11-1	9-1	9-1
Interval	119-121	0-4	103-105	32-34	25-27	39-41	0-3	106-108	117-119
Oxides (%)									
SiO_2	41.34	42.27	39.92	40.89	41.68	40.06	45.98	45.98	46.51
TiO_2	1.48	1.38	1.46	1.40	1.51	1.54	2.36	2.65	2.38
Al_2O_3	12.64	14.33	15.20	13.51	14.35	14.38	6.51	15.79	13.62
Fe_2O_3	11.56	10.55	12.46	11.47	11.98	13.25	18.53	12.76	13.73
MnO	0.22	0.19	0.19	0.19	0.22	0.19	0.26	0.16	0.19
MgO	11.97	7.29	7.81	7.00	7.99	7.89	11.93	8.08	7.90
CaO	19.10	24.16	22.61	23.88	22.67	21.96	9.43	7.77	12.41
Na_2O	nd	nd	nd	nd	nd	nd	4.14	4.31	3.18
K_2O	nd	nd	nd	nd	nd	nd	0.03	0.55	0.28
P_2O_5	0.09	0.11	0.08	0.09	0.11	0.09	0.23	0.23	0.27
Total	98.38	100.27	99.70	98.42	100.50	99.36	98.78	98.26	100.44
LOI	4.47	4.33	4.02	9.76	4.62	3.96	1.74	5.44	5.79
trace elements (ppm)									
Nb	0.5	2.1	1.1	1.2	2.0	0.2	2.5	2.6	5.0
Zr	81.0	72.3	84.6	82.2	78.0	85.3	149.7	186.9	178.9
Y	33.8	28.9	35.2	33.7	31.1	35.4	62.0	47.7	56.8
Sr	62.0	58.1	92.3	49.0	58.1	57.5	40.9	168.7	163.4
Rb	nd	nd	nd	nd	nd	nd	nd	9.9	5.0
Zn	92.8	74.6	93.6	104.0	96.0	99.2	93.1	131.6	124.4
Cu	55.6	56.0	48.6	38.0	60.4	55.1	56.9	50.7	45.5
Ni	69.3	79.2	56.9	71.6	82.9	75.0	563.1	52.1	50.2
Cr	207.2	268.2	129.6	195.9	235.6	218.8	109.1	163.3	126.7
V	333.6	284.5	345.2	339.2	320.8	337.2	494.3	424.1	397.3
Ce	6.8	na	9.8	bd	na	14.7	11.2	22.5	na
Ba	32.5	45.2	59.1	31.6	45.4	50.4	24.8	26.7	25.9
U	na	2.8	na	na	3.1	na	na	na	1.6
Sc	na	35.3	na	na	42.1	na	na	na	40.2
Co	na	59.4	na	na	63.5	na	na	na	54.1
Zr/Y	2.40	2.51	2.40	2.44	2.51	2.41	2.41	3.92	3.15
Ti	8841	8272	8721	8392	9051	9231	14146	15854	14236
	a	b	a	a	b	a	a	a	b

analyzed (a) on board the JOIDES Resolution, analyst D. Sims; (b) at the University of Hawaii,
analyst: L. Johnson. nd = none detected; na = not analyzed; bd = below detection;
LOI = loss on ignition. Samples 9a - 9e and 11a - 11b are each from a single clast.

Table 4.3: Rare-earth-element data and selected chondrite normalized ratios.

Sample	2	4	5	8	9b	9c	9e	10	11a	% Std. dev.[a]	Norm. factor[b]
Hole:	778	778	778	778	779	779	779	778	779		
Core:	5R1	9RCC	11R1	13RCC	31R2	31R2	31RCC	11R1	9R1		
Interval	7-10	9-12	5-7	4-6	0-4	103-105	25-27	0-3	106-108		
(ppm)											
La	1.05	na	na	na	2.62	2.99	2.38	na	6.34	na	0.315
Ce	2.92	5.64	6.72	10.08	8.62	9.57	9.63	17.28	21.30	1.9	0.813
Nd	2.47	5.18	5.90	9.32	7.98	8.85	8.97	16.92	18.18	1.7	0.597
Sm	0.77	1.89	2.25	3.11	2.86	3.25	3.33	6.22	6.03	1.9	0.192
Eu	0.25	0.80	0.86	1.17	1.11	1.17	1.13	2.08	2.09	0.5	0.072
Gd	1.09	2.74	3.03	4.27	3.97	4.58	4.67	8.41	7.67	0.4	0.259
Dy	1.33	3.27	3.76	4.61	4.91	5.59	5.82	10.55	8.88	1.6	0.325
Er	0.97	2.10	2.48	2.94	3.20	3.67	3.82	7.15	5.25	1.2	0.214
Yb	1.09	2.05	2.56	2.76	3.18	3.69	3.71	7.22	4.78	1.6	0.208
Lu	0.17	0.31	0.41	0.42	0.50	0.58	0.57	1.07	0.66	1.9	0.032
Selected chondrite normalized ratios											
(Ce/Yb)N	0.69	0.70	0.67	0.93	0.69	0.66	0.66	1.14	0.61		
(Ce/Sm)N	0.90	0.70	0.71	0.76	0.71	0.69	0.68	0.83	0.66		
(Sm/Lu)N	0.76	1.01	0.93	1.24	0.97	0.95	0.98	1.53	0.98		
(Gd/Lu)N	0.80	1.09	0.93	1.25	1.00	0.99	1.01	1.44	0.98		
(Dy/Lu)N	0.77	1.04	0.92	1.08	0.98	0.96	1.01	1.33	0.98		

Data determined by directly coupled plasma (DCP), at Lamont-Doherty Geological Observatory, analyst: L. Johnson.

[a] Percentage of standard deviation [(1 std. dev. /average)*100] for four analyses of a Mid-Atlantic ridge basalt.

[b] Chondrite factor used for normalization for Figure 2; na=La values not determined.

source, (2) a mantle source modified by the addition or loss of selected elements, or (3) metamorphism of the lavas after eruption. Magmas derived from a convecting mantle wedge overlying a subducting slab should be similar to those of MORB, though more depleted in the incompatible and HFSEs by the melting event that extracted the MORB. Other factors such as crystal accumulation or extensive crystal fractionation may also affect the MORB normalized ratios (Fig. 4.3).

Samples 1 and 2 have very low abundances of incompatible (and immobile) elements (Figs. 4.3 and 4.4) such as TiO_2 (<0.3 %), P_2O_5 (<0.1 %), Zr (<31 ppm), and Y (<9 ppm). Sample 1 is a metamorphosed cumulate and has high Ni and Cr contents. Sample 2 has an irregular REE pattern at 3-5 x chondrite, with a distinct negative Eu anomaly. It is light REE (LREE; La-Nd) depleted $(Ce/Yb)_N$ =0.69 and has an unusual heavy REE (HREE; Dy-Lu) enrichment trend (Fig. 4.2). Sample 2 also has an extreme Ce depletion and a small but distinct Ti depletion relative to other incompatible elements (normalized to N-MORB) (Fig. 4.3).

Samples 3 and 4 have low abundances of TiO_2 (0.9 %), Zr (43-50 ppm) and Y (18-21 ppm) relative to the N-MORB normalizing values (Figs.4.3 and 4.4). An unusual feature of these two samples is the high abundance of K_2O (>3.1 %) and Rb (57 to 67 ppm). Sample 4 is slightly LREE depleted {$(Ce/Sm)_N$ = 0.70}, has a small positive Eu anomaly and flat HREE at about 10X chondrite (Fig. 4.2). There is a slight but distinct kink in the REE pattern between Gd and Dy causing the HREE to be slightly depleted with respect to the middle REE (Sm-Gd). The extreme K_2O enrichment suggests these rocks may be related to shoshonites that are found in some of the active Mariana island arc volcanoes (Jackson et al., 1987; Bloomer et al., 1989). However, the K_2O/Na_2O ratio (>3.9) is unusually high; typical shoshonites have K_2O/Na_2O=0.4-1.2 (Bloomer et al., 1989). The extremely high K_2O/Na_2O , and elevated Rb and P may be attributed to metamorphic effects.

Samples 5, 6, and 7 (Table 4.2) have abundances of TiO_2 (1.2 %), Zr (60 ppm) and Y (28 ppm) all slightly higher than Samples 1 through 4 (Figs. 4.3 and 4.4). These three samples plot on the border of the IAT and MORB fields of Figures 4.4a and 4.4b. Sample 5 exhibits a smoother REE pattern and is more LREE depleted {$(Ce/Sm)_N$ = 0.67)} than Samples 2 and 4 (Fig. 4.2). The N-MORB normalized pattern for Sample 5 is similar to Sample 4 at ~ 0.8X N-MORB, but has a lower value of P.

Samples 8 and 9 have similar abundances of many minor and trace elements such as TiO_2 (1.4 to 1.5 %), Zr (72 to 85 ppm) and Y (29 to 35 ppm) (Table 4.2) at about 1X N-MORB (Fig. 4.3). However Ba, Ni and Cr are much lower in Sample 8 than Sample 9. Sample 8 has unusually high MgO (23.7 %), that is not caused by an accumulation of mafic phenocrysts (Table 4.1). Sample 9, represented by six analyses (9a through f), has an extremely high abundance of CaO (19.1 to 24.2%); K_2O, Na_2O and Rb are below detection for all samples, a feature characteristic of rodingite metamorphism as discussed above. The unusually low abundance of SiO_2 (40 to 42%) is probably a dilution effect associated with the increased Ca. REE patterns for Samples 8 and 9 are similar at about 10-15X chondrite. Sample 8 has greater LREE depletion {$(Ce/Sm)_N$ = 0.93} than Sample 9 {$(Ce/Sm)_N$ = 0.66-0.69}, and a distinct HREE depletion {$(Gd/Lu)_N$ =1.25}. Sample 9 exhibits a slight negative Eu anomaly in the two deeper samples (9b and e; Fig. 4.2) indicating plagioclase fractionation. Samples 8 and 9 plot in the MORB field of Figures 4.4a and 4.4b and are coincident with the field containing the MORB-like rocks of Chapter 3.

Samples 10 and 11 have high contents of $Fe_2O_3^*$ (13.6 to 18.5 %) ($Fe_2O_3^*$ = total iron calculated as Fe_2O_3), Na_2O (3.2 to 4.3%), TiO_2 (>2.4), and Zr (>150
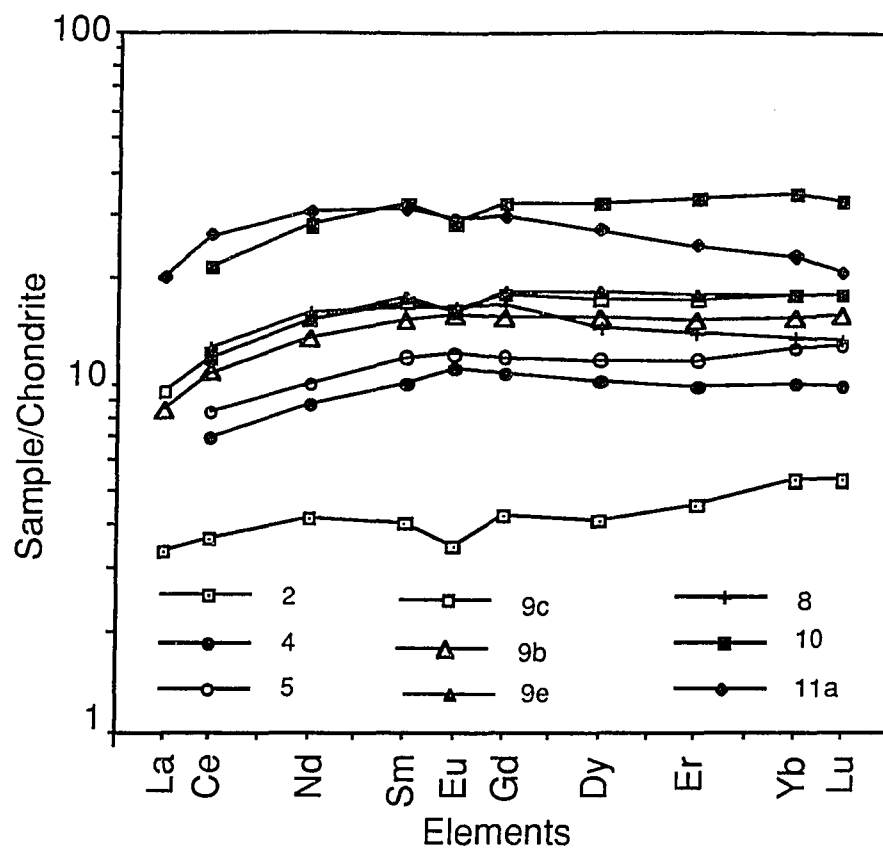
Figure 4.2: Chondrite normalized rare earth element patterns. All samples are plotted at the same scale and are identified by sample number. Note the increasing abundances of REE with sample number. Normalization values are given in Table 4.3.
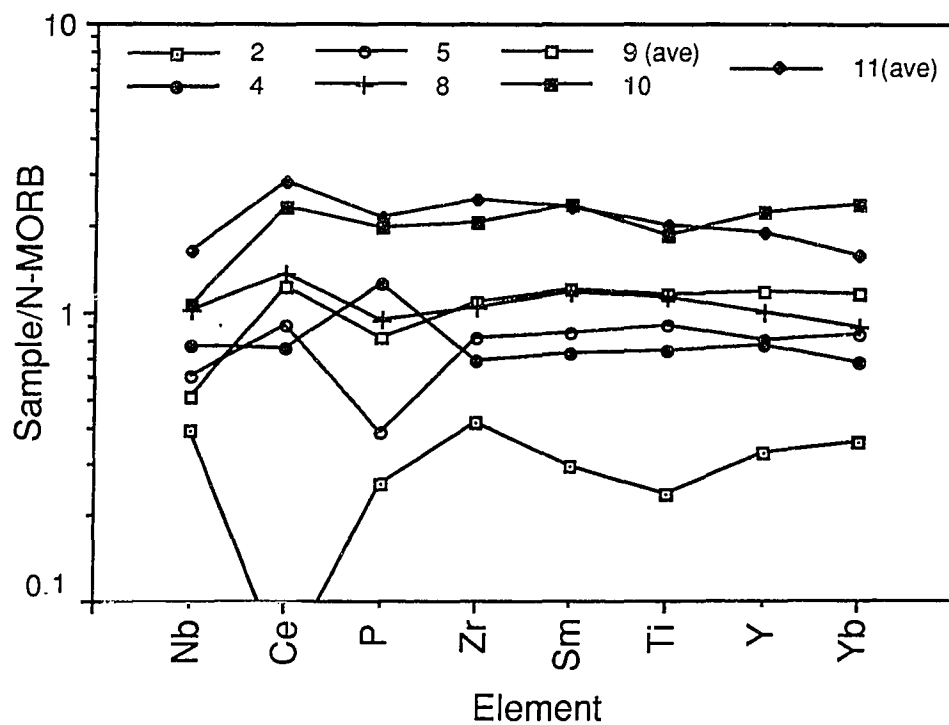
Figure 4.3: N-MORB normalized incompatible element diagrams. Values plotted are averages for each group and are normalized to the values of Sun and McDonough (1989). Note the increasing HFSE enrichment with sample number.
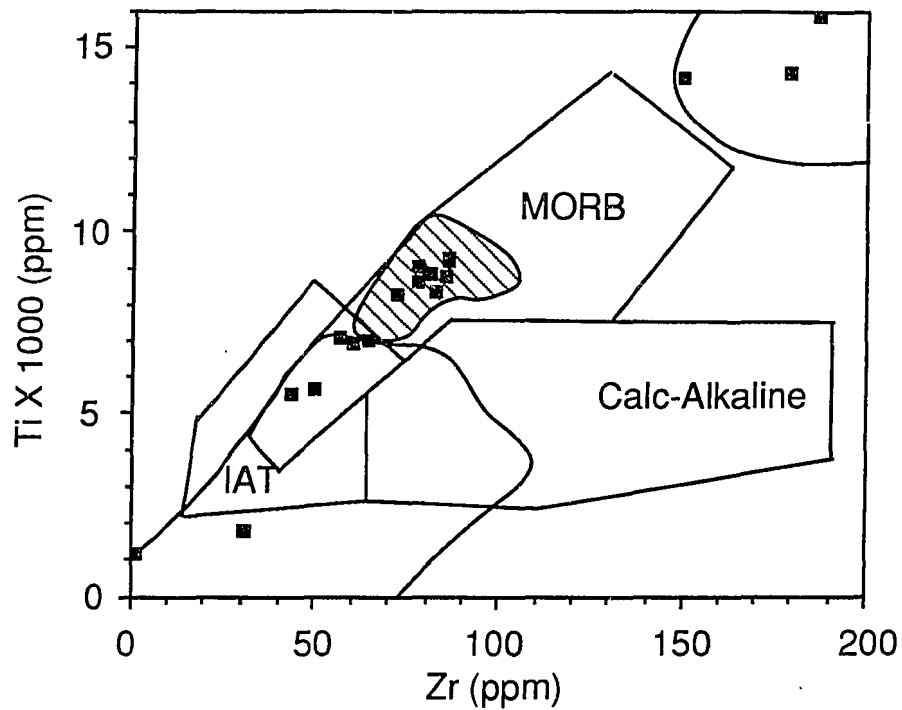
Figure 4.4: Immobile trace element co-variation diagrams to fingerprint tectonic environment of magma genesis.

Figure 4.4a: Ti-Zr diagram from Pearce and Cann (1973); Plotted symbols represent samples discussed in this paper. Fields are for previously published Mariana forearc data from (Wood et al., 1981; Meijer et al., 1981; Bloomer, 1983; Bloomer and Hawkins, 1987) (Chapter 3). Lined field is for MORB group of Chapter 3.
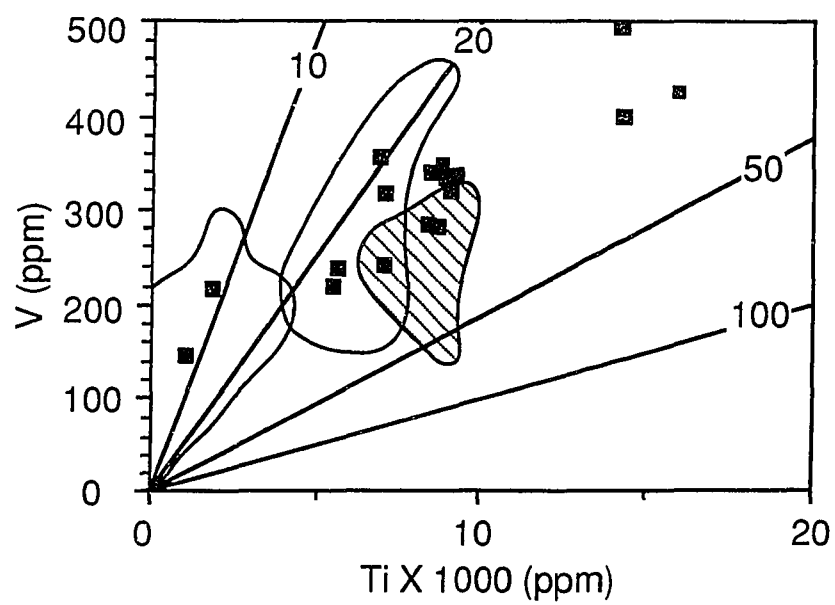
Figure 4.4b: Ti-V diagram from Shervais (1982). All symbols are the same as in Figure 4.4a
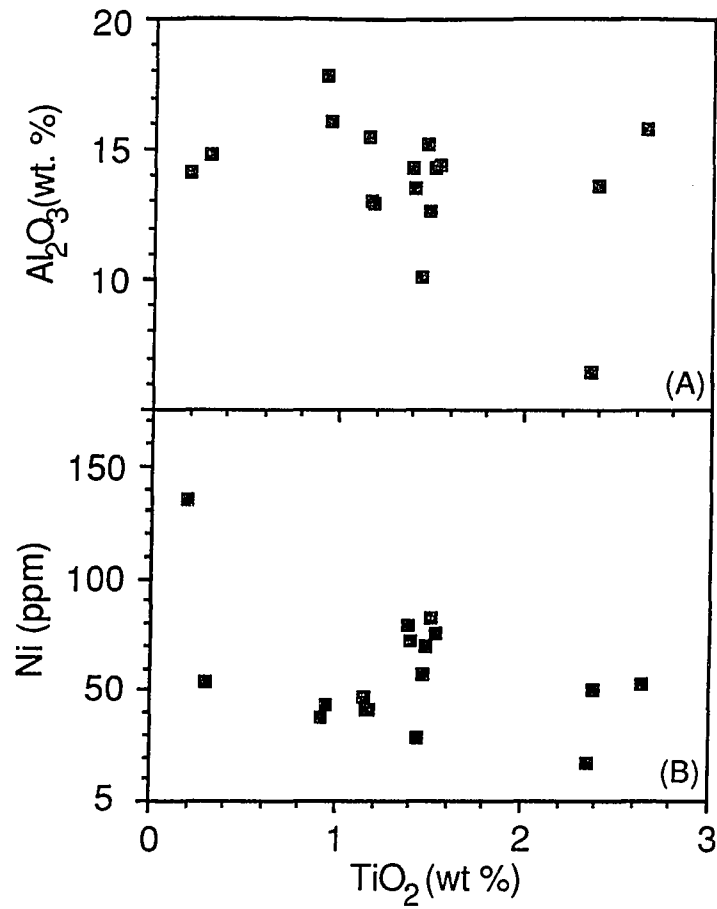
Figure 4.5: Variation plots to demonstrate the lack of fractional
crystallization control by (a) olivine (Ni vs. TiO_2) and (b) plagioclase
(Al_2O_3 vs. TiO_2).
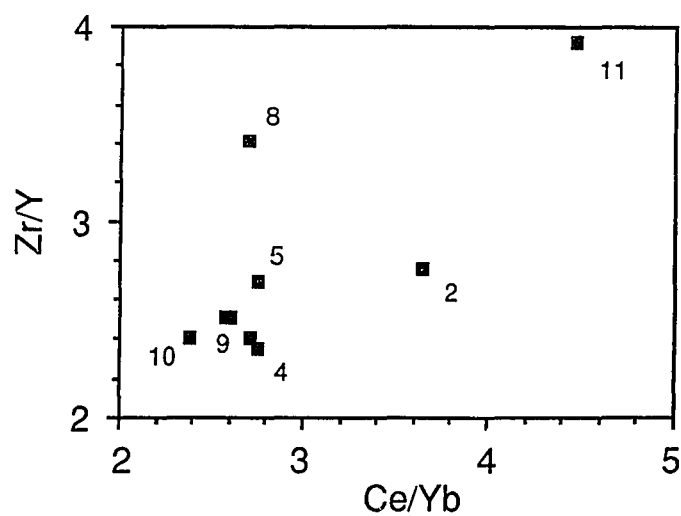
Figure 4.6: Zr/Y vs. Ce/Yb plot to test for similar source compositions. Note that Samples 4, 5, 9, and 10 cluster and may indicate derivation from a similar source, however the remaining samples are completely scattered suggesting multiple sources.

ppm), characteristics similar to FeTi basalts recovered from mid-ocean ridges

(Byerly et al., 1976; Natland, 1980). Sample 10 (Sample 125-778A-1R-1, 0-3

cm) contains the highest iron content and also has a high abundance of Ni (563 ppm)

and the REEs (20-35X chondrite). The REE pattern is slightly LREE depleted

{$(Ce/Sm)_N$ = 0.66} and has a small negative Eu anomaly (Fig. 4.2). Sample 11

(Sample 125-779A-9R-1, a: 106-108 and b: 117-119 cm) has lower contents of

Fe_2O_3, and Ni (50 to 52 ppm), and REE abundances similar to Sample 10 at 20-30X

chondrite. However Sample 11 exhibits a "humped" REE pattern with a middle REE

enrichment {$(Ce/Sm)_N$ = 1.14; $(Ce/Yb)_N$ = 1.06}. Both samples have high (2-3X

N-MORB) incompatible element abundances.

4.3.5 Geochemical Interpretations

A qualitative inspection of the immobile elements of Samples 1 through 4

suggests that these samples are probably not related to the more TiO_2 rich samples

(5 to 11) by fractionation of any common mineral phase assemblage (plagioclase,

pyroxene, olivine) (Fig. 4.5) or by different degrees of partial melting (Fig. 4.6).

A test for fractionation can be attempted, even with metamorphosed rocks, using

plots of immobile but compatible elements such as Ni (for olivine fractionation) and

Al_2O_3 (for plagioclase fractionation) vs. an incompatible and immobile element (TiO_2)

(Figs. 5a and b). During fractionation, TiO_2 should increase only gradually until the onset

of crystallization of a titanium-bearing oxide phase. Thus, if the samples are related by

fractionation, plots of Al_2O_3 and Ni vs. TiO_2 should show the same trend. However, TiO_2

shows no obvious correlation with either Ni or Al_2O_3 (Fig. 5b). Thus, if fractionation is

involved it seems likely it is only among samples with similar TiO_2, such as Samples 5,

6, and 7.

Ratios of incompatible elements (Figs. 3 and 4, Tables 2 and 3) suggest that these clasts were derived from multiple sources. However variable degrees of partial melting may also cause variable incompatible element ratios such as those exhibited by Zr/Y and Ce/Yb (Fig. 4.6).

Samples 1 through 4 have very low REE (Fig. 4.2) and incompatible elements (Fig. 4.3) and plot in the arc fields of two widely used discrimination diagrams (Figs. 4.4a and 4.4b). The kinked REE (MREE>HREE) pattern for Sample 4 is similar to that for other rocks from the Mariana arc system (Dixon and Stern, 1983). The low abundances of incompatible elements (Fig. 4.3) is consistent with a depleted source, and formation in a SSZ environment.

The slightly REE depleted patterns (Fig. 4.3) and the abundances of the immobile elements (Ti, Z, Y, P, Mn, Cr) (Fig. 4.4, Table 4.2) of Samples 8 and 9 are compatible with a mid-ocean ridge or arc-rifting (backarc) origin for these rocks. Samples 5, 6, and 7 have lower abundances of the discriminant elements than Samples 8 and 9, that may indicate greater extents of partial melt of the same, or a similar, source or may indicate lower degrees of crystal fractionation. The kink in the REE pattern of Sample 8 may indicate a transitional mantle source or a mixing of arc-derived and spreading-center derived magmas and would suggest an arc-rifting origin.

FeTi basalts are thought to form by extreme fractionation of MORB magma. However, the high Ni content of Sample 10 indicates it is not a fractionated rock, and thus that the high contents of iron and titanium may be a primary characteristic. The ratios of Ni and Al_2O_3 to TiO_2 do not support the derivation of Samples 10 and 11 from the other samples by fractionation (Fig. 4.5). A suite of Fe-gabbros was recovered from DSDP Site 458 (Wood et al., 1981). Site 458 Fe-gabbros have arc-

like geochemical signatures (TiO_2 <1.2 %) and are not similar to mafic clasts from

Conical Seamount (Fig. 4.3).

Some aspects of Figure 4.3, the Ce depletion of Sample 2, and the P

enrichment and depletion of Samples 4 and 5, may be explained by metamorphism.

However, Ce and P are typically considered immobile elements and these depletions

and enrichments may represent source characteristics. Nb depletion together with Ti

and Ta depletion is a characteristic of arc-derived rocks. The Nb depletion apparent in

all samples except 2 (enriched) and 4 (flat) is unusual and might also be attributed

to metamorphism although the values are so low that analytical error may be

significant. The lack of accompanying Ti depletion (relative to the other incompatible

elements) suggests the Nb depletion is not a primary characteristic of these samples.

Differences in incompatible element abundances can be ascribed to distinct sources

and geochemical histories. This is consistent with the lack of any apparent

relationship between the samples by crystal fractionation (Fig. 4.5) or partial

melting.

I therefore suggest Samples 1 through 4 are of SSZ origin and Samples 8-11

are of mid-ocean ridge or backarc basin ridge origin. The tectonic origin(s) of

Samples 5-7 are ambiguous.

4.4 Models for Development of the Mariana Forearc

Prior to the discovery of MORB-like rocks in the outer Mariana forearc

(Chapter 3), models for the formation and evolution of the forearc held that, since

inception, the Mariana forearc had been modified primarily by tectonic erosion of the

inner trench wall, and SSZ volcanism of IAT and boninite (Bloomer and Hawkins,

1983; Bloomer, 1983; Hawkins et al., 1984). The recovery of MORB-like, OIB, and

SSZ rocks intimately mixed on a scale of 2 to 3 km (Chapter 3 and 6) requires a much more complex model for the formation of the Mariana forearc.

An intrusion of IAT composition was drilled at Site 781 over 100 km from the volcanic front, about half way between the active arc and the trench, (Chapter 5). Intrusions of arc magma a great distance from the volcanic front, coupled with tectonic emplacement of Pacific oceanic lithosphere, can explain the close juxtaposition of IAT and MORB-like rocks in the outer Mariana forearc. However, volcanism with a MORB-like chemical character also occurs during arc rifting in backarc basins, (e.g., Fryer et al., 1981), and arcs (Hochstaedter et al., 1990; Fryer et al., 1990c). During rifting events, this magma type may become injected into or tectonically incorporated into the forearc region. Either intrusion or tectonic incorporation of these rocks may explain the close association of arc and MORB-like rocks, but these scenarios are unable to explain the presence of alkalic (OIB) rocks. The product of forearc rifting is most likely to be of island arc composition (Taylor et al., 1990); in-situ MORB-like rocks have never been documented from intra-oceanic forearcs. However, the possibility exists that some of these clasts with MORB-like compositions, especially Sample 9, may be the result of a sub-forearc melting event. This is supported by the presumed intrusive nature of the diabase into the serpentine. Near-trench magmatic intrusions in ocean-continent forearcs have been documented from the Paul Revere Ridge near the triple junction of the American-Pacific-Juan de Fuca plates (MacLeod and Pratt, 1973), from the Franciscan Complex of California (Echeverria, 1980), and from southern Chile (Forsythe et al., 1986). The Franciscan Complex and Paul Revere Ridge intrusions both contain tholeiitic rocks that plot in the MORB-IAT overlap field of the Ti-Zr discrimination diagram (Pearce and Cann, 1973). Echeverria (1980) suggests that the Ortigalita gabbro of the Franciscan Complex was intruded within 10 km of the

trench axis and resulted from decompression melting of the subducting plate caused

by plate flexure seaward of the trench during subduction. The silicic intrusions of

southern Chile are approximately 15-20 km from the trench axis (Forsythe et al.,

1986), it is unclear how far from the trench the Paul Revere Ridge samples were

intruded (MacLeod and Pratt, 1973).

In contrast, Conical Seamount is about 100 km from the trench. Thus, if the

lava of Sample 9 was intruded into the serpentinized rocks of the seamount it was .

likely a sub-forearc, not Pacific plate, melting event. A sub-forearc melting event

might be driven by pressure release caused by slab bending as the slab approaches the

arc and is perhaps aided by the influx of fluids from the downgoing plate. It is unclear

whether such a melting event might produce lavas of a MORB composition. If mantle

above the subducting slab and beneath the forearc is convecting (Kushiro, 1990) and

a source of fluids is present, sufficient hot, less depleted (than typical IAT source)

mantle might be able to melt, and produce a MORB-like magma. If such melting events

occur, the diabase intrusion (Sample 9) may be an example; however, the cold nature

of the serpentinite body and the presence of a cold slab beneath the forearc limit the

the heat available for such melting.

On the basis of the suite of mafic clasts recovered in Holes 778A and 779A and

on the results of dredging (e.g., Bloomer, 1983; Chapter 3), it seems likely that

there are four possible mechanisms for emplacement of oceanic (MORB-like) rocks

into the Mariana forearc.

1. Accretion of fragments of the downgoing oceanic plate into the outer forearc

has been documented (Chapter 6) (Fig. 4.7a). Such accretion appears to be episodic

and may alternate with tectonic erosion of the inner trench wall and toe of the

overriding plate. However, accreted fragments would have to be thrust over the outer
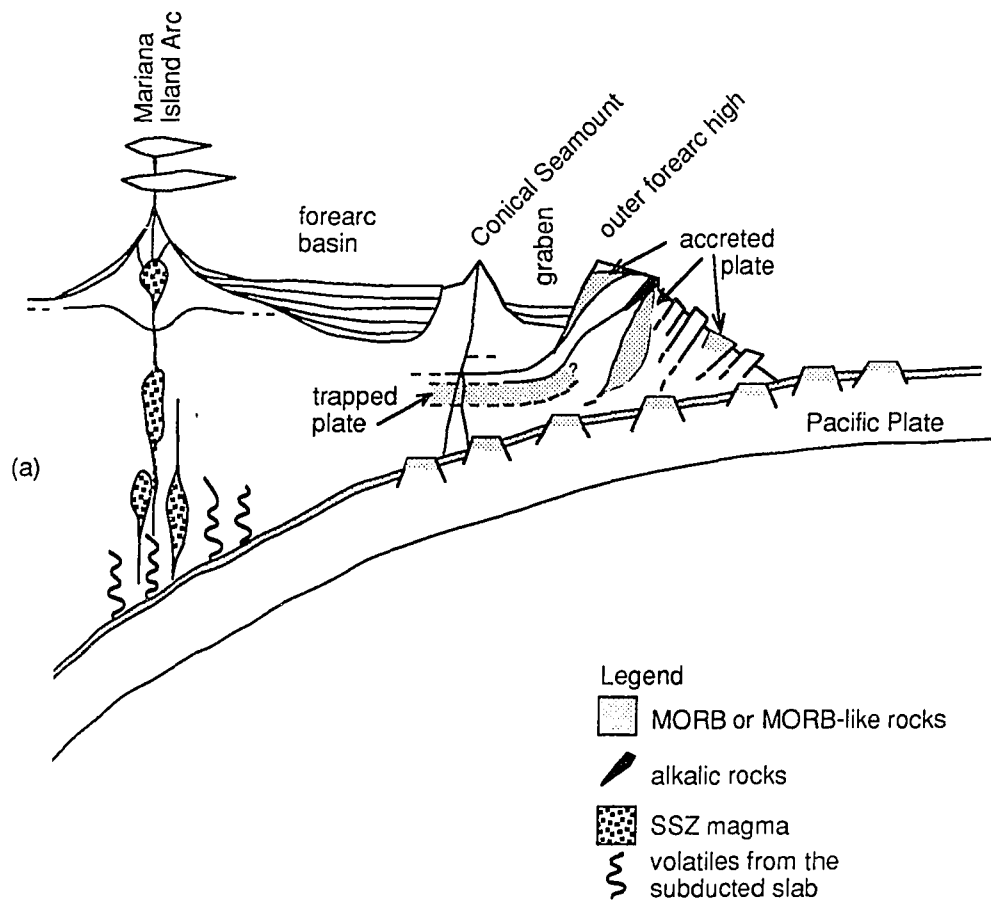
Figure 4.7: Schematic diagram of the four methods to emplace clasts with MORB-like compositions in the forearc. (a) Clasts may be derived from fragments accreted to the outer forearc. The outer forearc high is shown here as a complex block with fragments of rock of MORB, alkalic and SSZ origins. This has been documented (Chapter 6). Trapped fragments of the original oceanic plate assumed to have formed the initial forearc might also provide a source of MORB-like clasts.
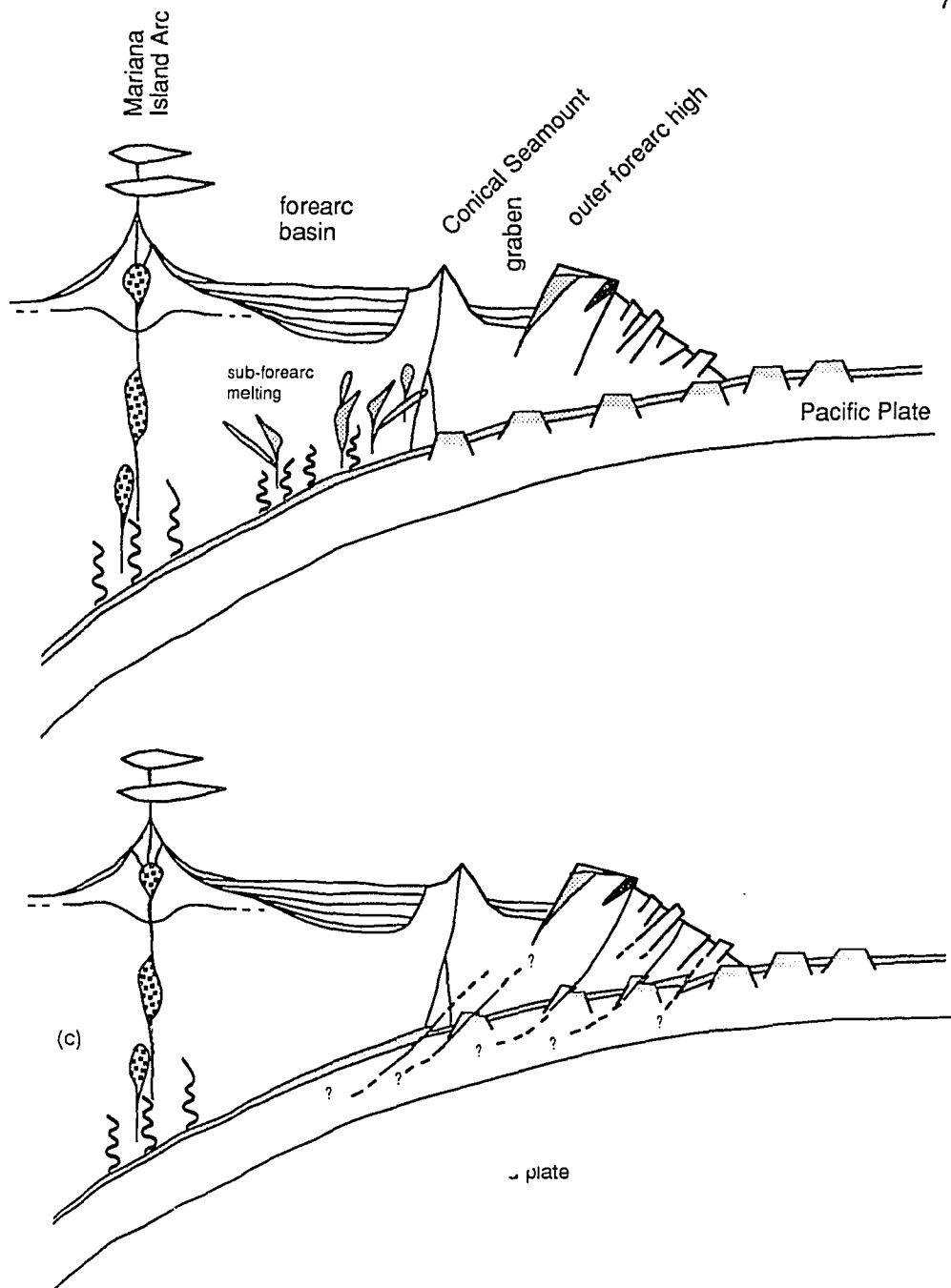
Figure 4.7b. If a sub-forearc melting event were to occur, it is possible that it would have a MORB-like composition. This is shown here as either fluid driven melting in the forearc, however decompression melting caused by a fractured subducting slab may also occur. Figure 4.7C. The outer forearc is extensively faulted; such faulting may be deep enough to intersect the décollement. Faulting along or through the décollement may move fragments of the subducted plate into the path of the rising serpentine mud.

forearc high and faulted into the pathway of the rising serpentine mud to be entrained in Conical Seamount.

2. The crustal complex in the forearc may contain fragments of oceanic plate that have remained trapped since the inception of this subduction zone and have been incorporated into a largely IAT crustal structure as xenolithic blocks (Fig. 4.7a). Seismic evidence for such blocks, at 18°N, exists as a low velocity layer in refraction surveys (Ambos, 1984) and as a strong reflector in reflection surveys (Mrozowski et al., 1981). Such blocks might supply clasts to the rising serpentine diapir. On the basis of ages of foraminifera and radiolaria (Cretaceous, >90 MA), and the maximum age estimated for the crust of the West Philippine Basin (<56 Ma, (Hilde and Lee, 1984), accreted rocks (Chapter 6) do not appear to be trapped lithosphere. No ages are available for the metamorphic clasts described in this work.

3. Following arc rifting, pieces of MORB-like, rift-related crust may become part of the forearc. This would occur if the new arc is built farther away (west) from the trench than the previous arc or backarc crust. This crust may be exposed in the outer forearc by erosion at the inner trench wall. A sill of island arc composition has been described over 100 km from the arc (Chapter 5). Thus, it is possible that intrusions of MORB-like lava, produced during arc rifting, may also be emplaced in the forearc. Sub-forearc melting, caused by the influx of fluids into the overlying mantle (Fig. 4.7b) and or decompression melting associated with bending of the subducting plate, may generate magma of MORB-like chemical composition. However we have no direct evidence for such sub-forearc melting.

4. Fragments from the subducting slab may be underplated to the forearc by extensive faulting along and through the décollement (Fig. 4.7c). These rocks are then brought into the forearc with the rising serpentine, perhaps aided by vertical tectonic processes. The presence of blue amphibole and lawsonite in some of the mafic

clasts (Table 4.1, and Maekawa et al., Leg 125 Scientific Results Volume) supports a deep origin.

In order for any of the four mechanisms described above to produce the geochemically diverse forearc sampled at Conical Seamount and at scarp exposures, rocks with MORB-like and OIB compositions must first be emplaced in the forearc. Once such rocks are present, tectonic mixing on a 2-3 km scale, perhaps accomplished through faulting parallel and normal to the trench, uplift, and intrusions of IAT and MORB (?) composition, is required to juxtapose MORB-like, OIB and IAT rocks. Erosion of the inner trench wall would allow rocks originally present or formed nearer the volcanic front to reside in the outer forearc where they may have become exposed by extensive faulting or brought to the surface by serpentine diapirism. Tectonic erosion has been proposed as a significant factor in the evolution of the Mariana (Hussong and Uyeda, 1981; Bloomer and Hawkins, 1983), the Tonga (Ballance et al., 1989), and the Japan subduction margins (von Huene et al., 1980). Bloomer (1983) estimates at least 50 km of erosion of the inner trench wall of the Mariana forearc since the initiation of subduction (45 Ma). However, erosion rates as high as 50 km m.y.$^{-1}$ have been estimated for the inner trench wall of the Tonga forearc (Ballance et al., 1989). Accretion in the Mariana forearc has also been proposed on the basis of seismic data (Karig and Ranken, 1983), and documented by paleontological data (Chapter 6). Extensive faulting would be required to allow accreted fragments to remain in the forearc once an erosional episode had begun.

The varied composition of the mafic clasts in the Mariana forearc provides direct evidence for the igneous composition of the forearc crust and indirect evidence of the tectonic processes that formed and continue to modify the forearc.

Samples 1 through 4 may have been derived from a mantle source that had

been previously melted, perhaps at a mid-ocean ridge. This is a characteristic of

many SSZ magmas and suggests these clasts represent pieces of subduction-related

forearc crust. The high K_2O/Na_2O ratio of Samples 3 and 4 may also be indicative of a

SSZ environment. The less-depleted (relative to N-MORB) Samples 5 through 9

appear to have been derived from a less depleted (in HFSE) mantle than Samples 1

through 4. Samples 5 through 9 are similar to N-MORBs and may (1) have been

derived from the subducting plate, (2) represent pieces of normal oceanic plate crust

trapped in the forearc, (3) be the result of rifting within the SSZ environment, or

(4) be the result of a sub-forearc melting event. Samples 10 and 11 are similar to

FeTi basalts that have been recovered from the mid-ocean ridges and are similar to

samples from the Galapagos spreading center (Byerly et al., 1976) and the East

Pacific Rise (Natland, 1980), suggesting that they may be pieces of the downgoing

plate or remnants of the original oceanic plate trapped in the forearc at the start of

subduction.

4.5 Conclusions

The studies of these clasts support three main conclusions.

1. The great diversity of the mafic clasts proves that the forearc basement has

a varied geochemical composition. Suites of diverse rocks (MORB-like, alkalic, IAT),

dredged from a steep scarp in the outer forearc approximately 30 km northeast of the

drill sites (Chapter 3) and from another scarp more than 170 km to the south (at

17°50'N) (Johnson and Fryer, 1990) are similar to the clasts recovered in these

drill holes, extending the area of the Mariana forearc where rocks having oceanic

affinity have been recovered to at least 7000 km^2. This is in direct conflict with

earlier models (e.g., Hussong and Uyeda, 1981; Bloomer, 1983; Bloomer and

Hawkins, 1983) that the forearc formed chiefly by intrusions of arc magmas and tectonic erosion at the inner trench wall. The suite of igneous rocks recovered from Holes 778A and 779A geochemically resembles samples dredged from fault scarps, some of which have been shown to contain tectonically accreted rocks. The recovery of widespread MORB-like rocks in the forearc requires a new model for forearc evolution.

2. The clasts are entrained in the rising serpentine muds, and therefore may have been plucked from forearc basement. The presence of lawsonite and blue amphibole (Maekawa et al., Leg 125 Scientific Results Volume) proves that samples may have been derived from depths greater than those drilled during Leg 125 (317 mbsf) or during Leg 60 (692 mbsf) (Hussong et al., 1981) and greater than those dredged (5600 m total depth) (Bloomer, 1983) (Chapter 3). Serpentine mud volcanoes, such as Conical Seamount, provide an opportunity to look deeper into the forearc than previously possible and thus sample forearc crust unavailable through other methods. If some of these clasts are derived from the downgoing slab, this provides an opportunity to study in detail the effects of subduction upon the oceanic crust.

3. The rodingite metamorphism of Sample 9 (Sample 125-779A-31R) indicates intrusion or tectonic emplacement of the mafic block into the ultramafic rock prior to or during serpentinization of the host rock. This clast may have been (1) derived from the downgoing plate and later tectonically included in the rising serpentine diapirs, or (2) intruded into the ultramafic rock or serpentine mud during a forearc magmatic event, or (3) present in the mantle that was metamorphosed to form Conical Seamount.

These conclusions support a new model for the formation of the Mariana forearc. In this model, the forearc is composed of rocks created and emplaced in a SSZ

setting and of fragments of the subducting plate. The fragments of the downgoing plate may be incorporated into the lower crust and outer forearc by faulting along the décollement or by faulting (thrusting) over the break in slope of the inner trench wall (Fig. 4.7a). Although this has not been documented, the possibility that rifting within the forearc might create volcanism with MORB-like characteristics cannot be ruled out. Unfortunately it is not currently possible to distinguish metamorphosed rocks of MORB-like character that have been formed in or near an arc (backarc basin, arc/forearc rifting) from those formed at a true mid-ocean ridge. Continuing intrusions of arc-derived magma into this oceanic/island arc mixture, such as the Pleistocene sill drilled at Site 781 (Chapter 5), may provide sufficient volcanism of IAT character throughout at least the inner forearc to create a mixed crustal sequence. I prefer a scenario where the MORB-like fragments recovered from Holes 778A and 779A are emplaced either by accretion into the outer forearc or are trapped remnants of oceanic plate; subsequent lateral faulting and vertical uplift then acted to mix these fragments with preexisting pieces of arc crust. However, the sill-like nature of Sample 9 argues for a sub-forearc emplacement of hot magma directly into or onto the serpentine mud.

The crust of the Mariana forearc is petrologically and tectonically complex. Regardless of the source of the MORB-like lavas, a multistage history and continuing magmatic and tectonic events are required to account for the current petrologic composition of the Mariana forearc.

Chapter 5:

Late Cenozoic Volcanic Rocks in the Mariana Forearc Revealed from Drilling at Ocean Drilling Program Site 781

5.1 Abstract

Geophysical surveys of the Mariana forearc, in an area equidistant from the Mariana Trench and the active Mariana Island Arc, revealed a 40-m-deep graben about 13 km northwest of Conical Seamount, a serpentine mud volcano. The graben and its bounding horst blocks are part of a fault zone that strikes northwest-southeast beneath Conical Seamount. One horst block was drilled during Leg 125 of the Ocean Drilling Program (Site 781).

Three lithologic units were recovered at Site 781: an upper sedimentary unit, a middle basalt unit, and a lower sedimentary unit. The upper unit, between 0 and 72 mbsf, consists of upper Pliocene to Holocene diatomaceous and radiolarian-bearing silty clay that grades down into vitric, silty clay and vitric, clayey silt. The middle unit is a Pleistocene vesicular, porphyritic basalt, whose top corresponds to a high-amplitude reflection on the reflection profiles. The lower unit is a middle-to-upper (and possibly some lower) Pliocene vitric silty clay and vitric clayey silt similar to the lower part of the upper unit. The thickness of the basalt unit can only be estimated to be between 13 and 25 m because of poor core recovery (28% to 55%). The absence of internal flow structures and the presence of an upper glassy chilled zone and a lower, fine-grained margin suggest that the basalt unit is either a single lava flow or a near-surface sill. The basalt consists of plagioclase phenocrysts with subordinate augite and olivine phenocrysts, and plagioclase-augite-olivine glomerocrysts in a groundmass of plagioclase, augite, olivine, and glass. The basalt is

an island-arc tholeiite (IAT) enriched in large-ion-lithophile elements relative to high-field-strength elements, similar to the submarine lavas of the southern arc seamounts. In contrast, the volcanic rocks from the active volcanoes on Pagan and Agrigan Islands, 100 km to the west of the drill site, are calc-alkaline.

The basalt layer, the youngest *in-situ* igneous layer reported from the Izu-Bonin and Mariana forearcs, is enigmatic because of its location more than 100 km from the active volcanic arc. The sediment layers above and below the basalt unit are late Pliocene (about 2.5 Ma) and normally magnetized. The basalt has schlieren-like structures, reverse magnetization, and a K-Ar age of 1.68 ± 0.37 Ma. Thus, the basalt layer is probably a sill fed by magma intruded along a fault zone bounding the horst and graben in the forearc. The geochemistry of the basalt is consistent with a magma source similar to that of the active island arc, and from a mantle source above the subducting Pacific plate.

5.2 Introduction

5.2.1 Volcano-Tectonic Setting

Subduction of the Pacific plate beneath the Philippine Sea plate began by the middle Eocene and formed the proto Mariana arc system (Uyeda and Ben-Avraham, 1972; Hilde et al., 1977; Ogawa and Naka, 1984; Karig, 1975). Sea-floor spreading, between about 30 and 17 Ma, formed the Parece Vela Basin and isolated the Palau-Kyushu Ridge, now a remnant arc, from its magma source. The West Mariana Ridge, also a remnant arc, formed to the east from 20 to 9 Ma and was isolated when spreading began in the Mariana backarc basin (or Mariana Trough; Hussong and Fryer, 1981). The modern Mariana Island Arc has been active since 5 to 6 Ma coincident with the opening of the Mariana backarc basin (Fig. 5.1; Karig, 1971;
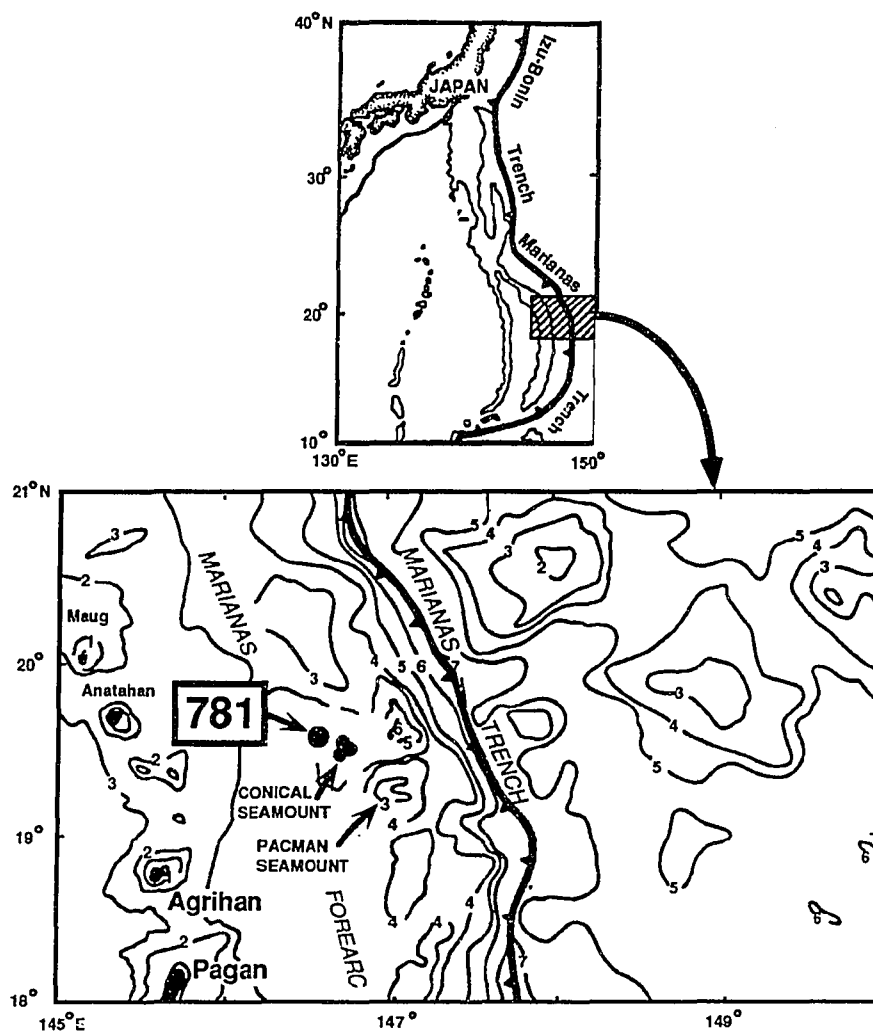
Figure 5.1. Location of ODP Site 781: (a) the regional setting of the Izu-Bonin
and Mariana island arc regions; (b) the detailed setting of Site 781 showing
the location of Agrigan and Pagan Islands and Conical and Pacman Seamounts.
Bathymetric contours in kilometers.
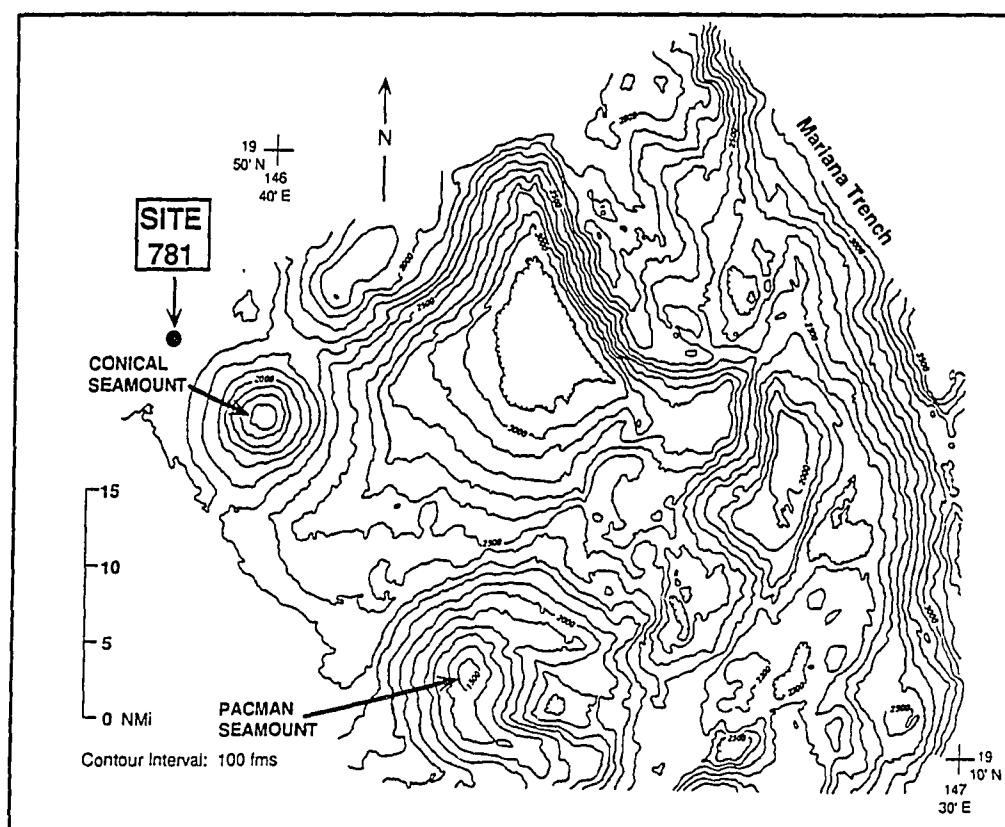
Figure 5.2. Detailed bathymetric map of the outer Mariana forearc near ODP Site 781 and Conical Seamount. Bathymetric contours in fathoms (data are from re-digitized SeaMARC, SeaBeam, and 3.5 kHz records).
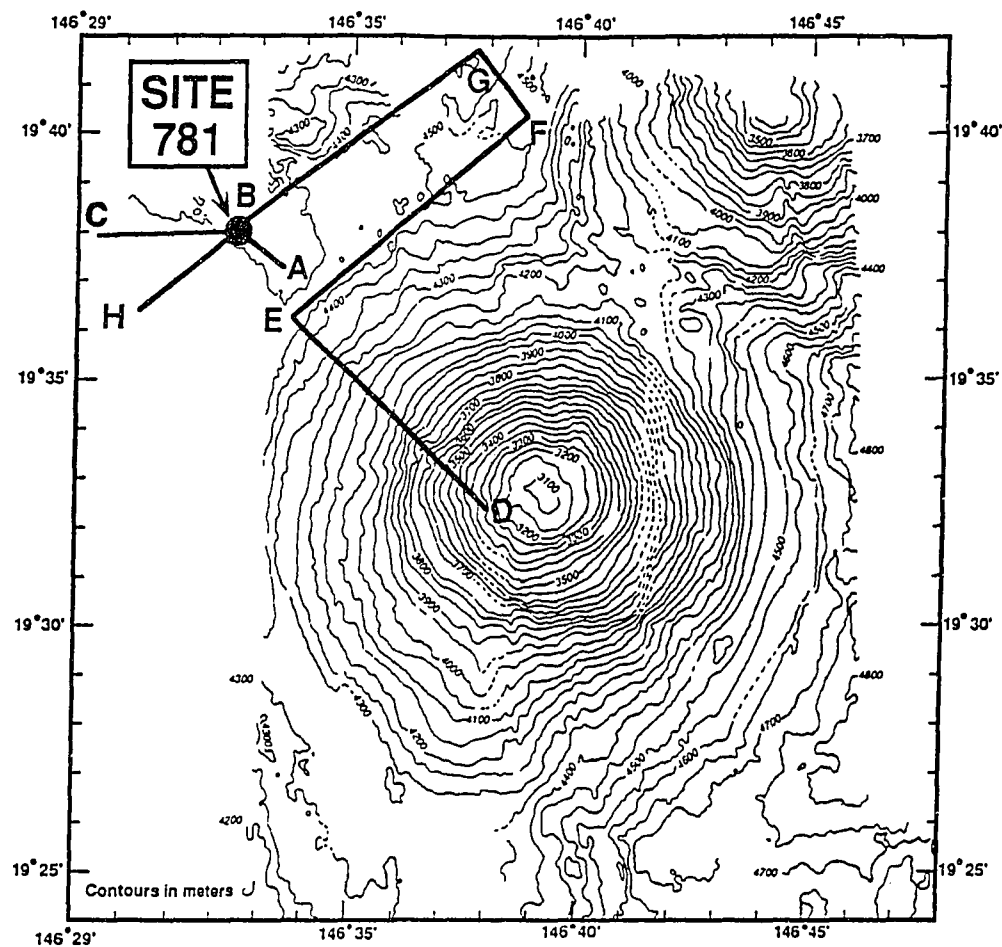
Figure 5.3. Trackline map of seismic reflection profiles across ODP Site 781 and Conical Seamount. Detailed bathymetry based on unpublished SeaBeam data collected by the University of Kiel. Contours in meters.

Hussong and Uyeda, 1981a). Despite extensive studies of the Mariana forearc (e.g., Karig, 1971; Hussong and Uyeda, 1981a; Hussong and Fryer, 1981; 1985; Mattey et al., 1980; Meijer et al., 1981; Mrozowski et al., 1981; Wood et al., 1981; Bloomer, 1983; Karig and Ranken, 1983; Bloomer and Hawkins, 1983, 1987; Ogawa and Naka, 1984; Fryer et al.,1985, 1987; Hussong and Fryer, 1985; Fryer and Fryer, 1987; and Chapter 3), the fundamental problems concerning the origin of the forearc basement remain unsolved. Of the three suggested models for basement origin, i.e., entrapment of oceanic lithosphere (Hilde and Uyeda, 1983; Mattey et al., 1980), sediment and Pacific plate accretion (or obduction) (Hussong and Uyeda, 1981b), or arc volcanism (Hussong and Uyeda, 1981b), only arc (supra-subduction zone) volcanism satisfies the previously available seismic, petrologic, and geochemical data. The recent discovery of Cretaceous mid-ocean ridge basalt (MORB), ocean island basalt (OIB), and Radiolarian chert about 50 km west of the trench slope break at the latitude of Site 781, requires reevaluation of this conclusion (Chapters 3 and 6). If the forearc is composed solely of subduction-related material, a significant amount (at least 50 km) of erosion of the forearc is necessary to explain the presence of arc volcanics exposed in the inner trench wall (Bloomer, 1983; Bloomer and Hawkins, 1983). However, the presence of a small quantity of OIB in the inner trench wall and MORB in the outer forearc, coupled with seismic and bathymetric data from the southern part of the forearc, suggest some post-Oligocene accretion (Bloomer, 1983; Karig and Ranken, 1983; Chapter 3), or the OIB and MORB in the forearc could be engulfed by later arc magmas.

The region around Site 781 from 18° to 21°N is tectonically active and characterized by vertical faulting between blocks in the forearc (Mrozowski et al., 1981; Marlow et al., 1990). For instance, a large, uplifted plateau is on strike with

the northeast-trending fault that bounds the graben adjacent to Site 781 (Figs. 5.1 and 5.4). The plateau overlies the westward extension of the Dutton Ridge, a chain of Pacific seamounts that are gradually being subducted.

5.2.2 Site 781

Seismic reflection surveys run between Sites 780 (19°32.5'N, 146°39.2'E) and 781 (19°37.9'N, 146°32.5'E) in the Mariana forearc during Leg 125 revealed an anomalously bright reflection within a horst on the edge of a small graben located about 13 km northwest of Conical Seamount (Figs. 5.1 through 5.5; Marlow et al., 1990). Two seismic reflection profiles across the horst confirmed a high-amplitude reflection located about 85 msbsf (milliseconds below sea floor, Figs. 5.3 through 5.5). The reflection, originally thought to be from a forearc basement horizon, was first penetrated by the drill at 72 meters below the sea floor (mbsf) at Site 781 and found to be a basalt unit between 12.7 and 25 m thick (poor core recovery at its base did not allow us to measure thickness accurately; Fryer, Pearce, Stokking, et al., 1990).

Here, I describe the volcano-tectonic setting of Site 781, as well as the seismic stratigraphy, petrology, and geochemistry of the basalt layer. Paleontologic, paleomagnetic, and K-Ar ages of the units drilled at Site 781 are discussed. Finally, I speculate about the origin of the basalt and its implications for models of modern convergence zones.

5.3 Seismic Stratigraphy

During Leg 125, a single-channel seismic reflection survey was run along the flanks of Conical Seamount and across the adjacent forearc to find a suitable drill site

to sample the forearc basement beneath the seamount. The survey utilized two small 80-in.^{3} water guns fired every 12 s and data were recorded using a 100-m streamer (Marlow et al., 1990).

Two single-channel, seismic reflection profiles were shot across Site 781 (Figs. 5.3 through 5.5; Marlow et al., 1990). The high-amplitude reflection, discovered during the first survey, is located about 85 msbsf at Site 781 within a horst structure adjacent to a small graben (Fig. 5.4). The 72-m-thick sedimentary sequence overlying the basalt has an average velocity of 1505 m/s (Marlow et al., 1990). The layered reflections below the basalt on Lines 4 and 5A (Figs. 5.4 and 5.5) are presumably from sedimentary sequences underlying the volcanic section (Fryer, Pearce, Stokking, et al., 1990).

On Line 4 (Fig. 5.4), a second high-amplitude reflection was recorded beneath a layered sequence filling a small graben adjacent to the horst block at Site 781. The second reflection is vertically offset from the basalt layer reflection within the horst by about 100 to 150 ms. One interpretation of the reflection geometry is shown in Figure 4, where the offset between reflections can be interpreted as faulting that post-dates the lava.

Line 5A shows the high-amplitude reflections as an irregular and "rubbly-looking" layer beneath well-layered, horizontal reflections from the overlying sedimentary sequence (Fig. 5.5). The irregular reflections are from the basalt layer drilled at Site 781 and can be traced laterally to a slightly deeper sub-bottom depth beneath the adjacent graben. In this profile, the basalt layer can be interpreted as extending laterally from the horst into the graben. The basalt layer may have continued horizontally as a sill within the horst, but dropped to a deeper level within the graben (Fig. 5.4), creating the apparent offset between the two high-amplitude

LINE 4
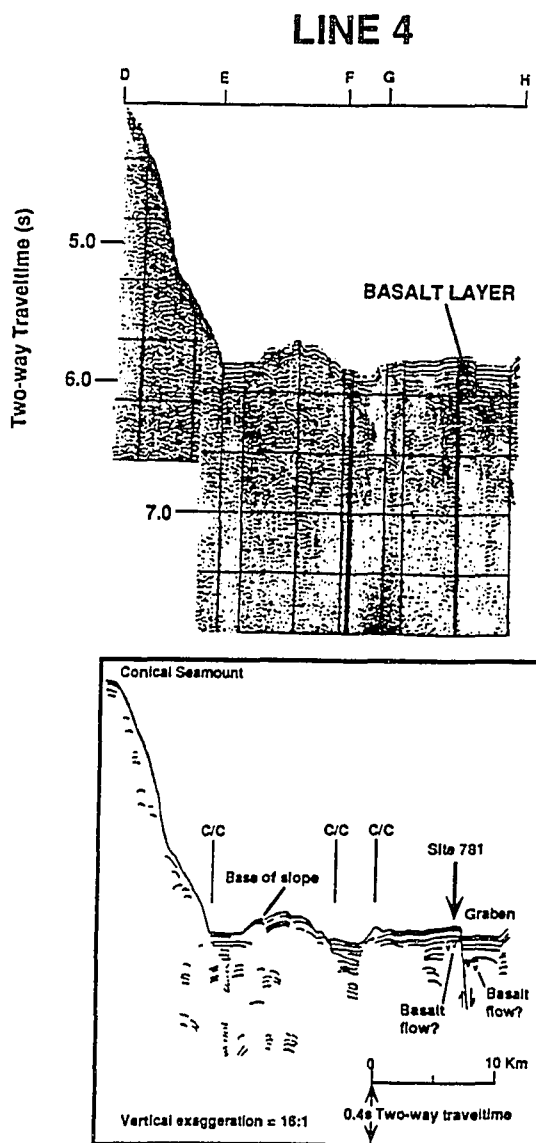
Figure 5.4. Seismic reflection profile and interpretative drawing. The high-amplitude reflector at about 85 ms two-way travel time corresponds to the top of the basalt layer penetrated at Site 781 at 72 mbsf. A similar reflector in the adjacent graben is also interpreted as a volcanic layer. The two reflectors may be part of one volcanic unit that is either displaced by young faulting, as indicated here, or is continuous and joined out of the plane of this section. The trackline location is shown in Figure 5.3.
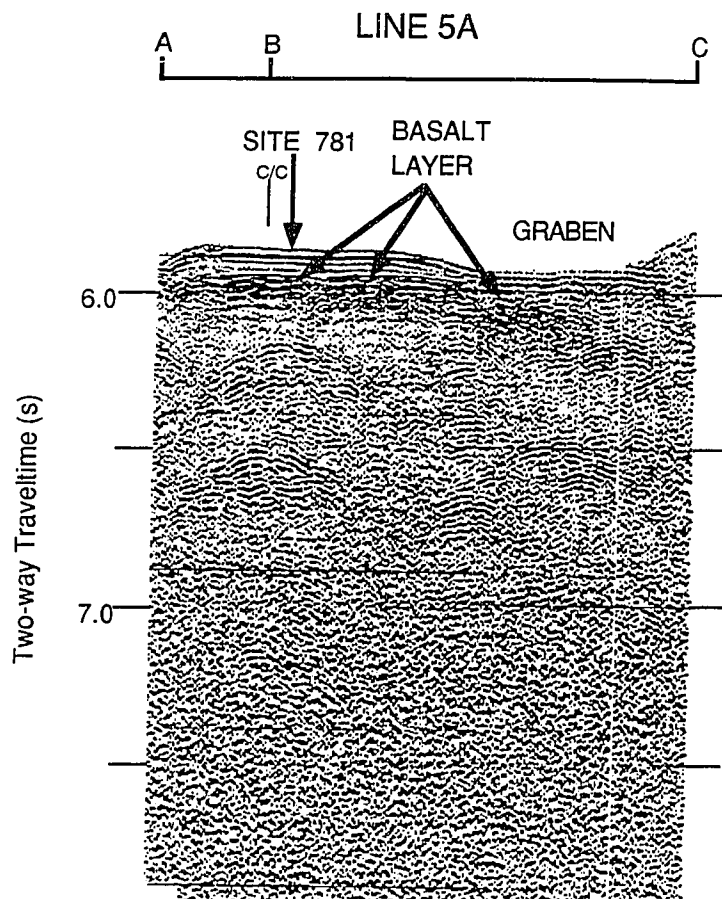
Figure 5.5. Processed digital seismic reflection data collected from survey line 125-05A, collected after leaving Site 781. Automatic gain control applied and the processing filter parameters were 25-140 Hz with a filter length of 37 Hz. Note the high-amplitude reflector corresponding to the basalt layer drilled at Site 781, that can be traced laterally beneath the adjacent graben. The trackline location is shown in Figure 5.3.

reflections on this line. This second, favored interpretation suggests that the sill post-dates the faulting along the edge of the graben. However, I cannot resolve whether the basalt layers are offset by faulting or if they occupy different levels in the section because of the sparse seismic reflection data around Site 781.

5.4 Age of Basalt

The drill encountered three stratigraphic units at Site 781: an upper sedimentary unit extending from the sea floor to a depth of 72 mbsf, followed by a vesicular, porphyritic basalt layer to about 92 mbsf, that in turn is underlain by a second sedimentary unit that extends at least to the bottom of the hole at 250 mbsf. The upper sedimentary unit consists of late Pliocene (CN12b calcareous nannofossil zone of Okada and Bukry, 1980) to Holocene diatom-radiolarian silty-clay that grades downward into vitric silty-clay and vitric clayey silt (Fryer, Pearce, Stokking, et al., 1990). The lower sedimentary unit comprises early(?) Pliocene to late Pliocene (Nannofossil Subzone CN12b) vitric silty clay and vitric clayey silt (Fryer, Pearce, Stokking, et al., 1990).

Analyses for two K-Ar ages were performed at thus U.S. Geological Survey (Menlo Park). Ages were calculated from six K_2O analyses and two argon (Ar) analyses run on an unaltered plagioclase separate from selected basalt core samples. The K_2O analyses were 0.084, 0.079, 0.075, 0.075, 0.081, and 0.082 wt% and averaged 0.079 ± 0.004 wt%. The first Ar analysis had 5.0% of radiogenic ^{40}Ar and yielded an age of 1.58 ±0.40 Ma. The second Ar analysis had 2.1% of radiogenic ^{40}Ar and yielded an age of 1.93 ±0.62 Ma. The errors are estimates of the standard deviations of analytical precision and are large mainly because of the low proportion of radiogenic to atmospheric argon 40, a common problem in very young igneous

rocks. The average of the two analyses, weighted by the inverse of the variances of the individual runs, gives an age of 1.68 ±0.37 Ma.

All the recovered basalt cores are reversely polarized. The K-Ar dating indicates that the rocks cooled through the Curie temperature during the Matuyama Reversed-Polarity Chron (0.8 to 2.5 Ma; Fryer, Pearce, Stokking, et al., 1990). The late Pliocene (Nannofossil Subzone CN12b, about 2.5 Ma) sedimentary layers above and below the basalt layer are normally magnetized and, on the basis of their paleontologic ages, were deposited during the older Gauss Normal Polarity Chron because of their paleontologic ages (Fryer, Pearce, Stokking, et al., 1990). The age data support the initial interpretation that the basalt unit is a sill. The uniform magnetization, petrology, and geochemistry of the basalt drillcores and their schlieren-like structures suggest that the cores are from one continuous sill.

5.5 Petrography and Geochemistry of Site 781 Basalt

5.5.1 Analytical Procedures

Geochemical data for the basalt samples from Site 781 are given in Tables 5.1 through 5.4.

Microprobe analyses of mineral phases were performed at the University of Hawaii on three thin sections chosen to represent, respectively, the uppermost (781A-9R1, 0-4 cm), the central (781A-10R1, 16-20 cm) and the lowermost (781A-10R3, 17-21 cm) portions of the igneous unit. Data are given in Table 5.1.

The basalt was analyzed for major and selected trace elements (Table 5.2) by X-ray fluorescence (XRF) on board the JOIDES Resolution and at the University of Hawaii and for rare-earth elements (REE) by directly coupled plasma spectrometry at the Lamont-Doherty Geological Observatory (Table 5.3). Analytical methods for

JOIDES Resolution samples are given in Fryer, Pearce, Stokking, et al. (1990); analytical methods for University of Hawaii and Lamont-Doherty Geological Observatory analyses are given in Chapter 2. The basalt was also analyzed for incompatible trace elements by inductively coupled plasma/mass spectrometry (ICP-MS) at Durham University (for analytical methods see Murton et al., in prep) and for Sr, Nd and Pb isotopic ratios (Table 5.3) by mass spectrometry at Royal Holloway and Bedford New College, London (analytical details are given in Pearce et al., in prep).

5.5.2 Petrography

The basalt sill is predominantly hypocrystalline having intersertal and intergranular to subophitic textures. Vesicles range from 0.1 to 4 mm in diameter and make up 5% to 10% of the rock. An 8- mm-thick, vesicle-free chill zone is present at the top of the sill, and sparse, very fine-grained, crystal-free zones (i.e, 781A-10R1, 17-21 cm) are present throughout the sill. The basalt is fresh except for a small amount of amorphous clay, present after glassy matrix, at the base of the recovered unit. Glomerocrysts up to 5 mm in diameter are common and are frequently composed solely of plagioclase, although about one-third include clinopyroxene and sparse olivine; opaque phases are less abundant. Individual plagioclase crystals in glomerocrysts are typically multiply-twinned, euhedral to subhedral laths, that range from 0.3 to 1.5 mm long. A few solitary plagioclase phenocrysts are present and are nearly always euhedral. plagioclase crystals frequently exhibit normal, reverse, and oscillatory zoning, with evidence for relict cores and irregular (partly resorbed?) crystal boundaries. Clinopyroxene and olivine crystals occur in glomerocrysts that have been completely surrounded or, more often, surrounded on
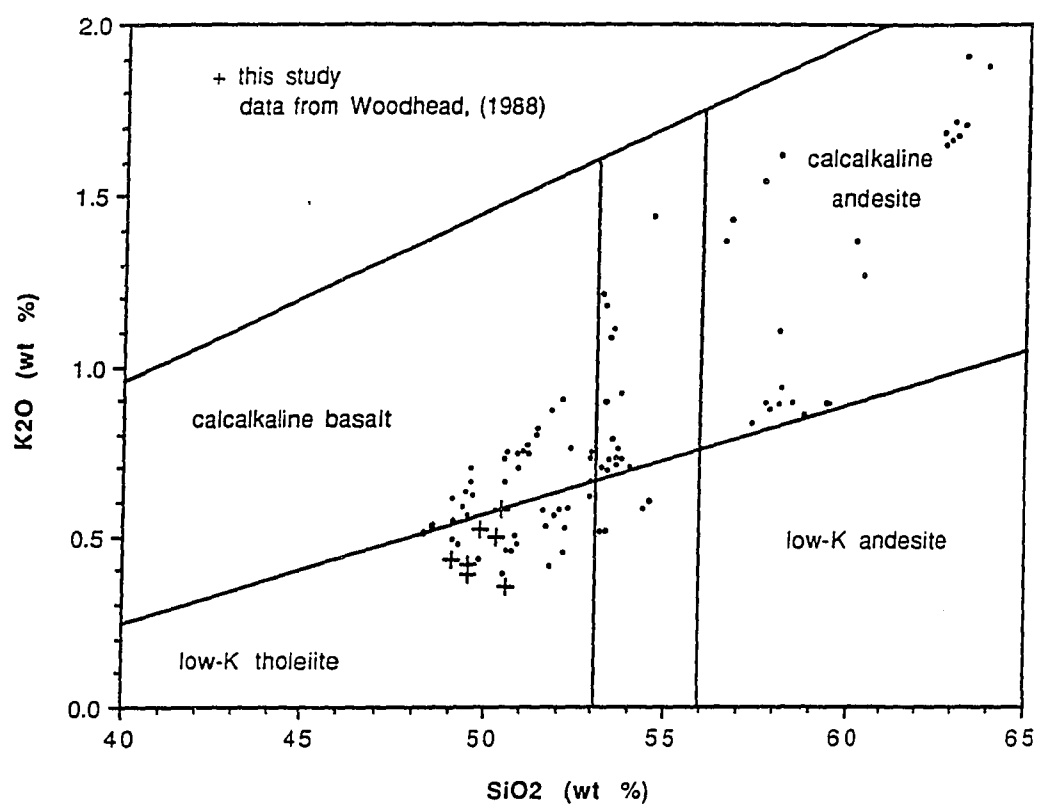
Figure 5.6. Classification of the basalt sill at ODP Site 781 based on K_2O-Si_2O co-variation. Fields are from Peccerillo and Taylor (1976). Dots are analyses of active Mariana arc volcanics (Woodhead, 1988).
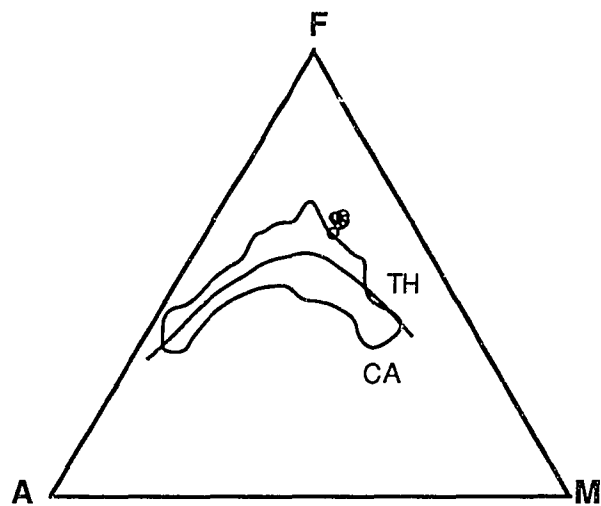
Figure 5.7. Classification of the basalt sill on the basis of iron enrichment. The dividing line is from Irvine and Baragar (1971). Field encompasses analyses of active Mariana arc volcanics (Woodhead, 1988).

three sides by crystals of plagioclase. Individual clinopyroxene crystals are 0.1 to 0.4 mm, rounded to subhedral, and often have irregular crystal boundaries. The absence of a quench texture suggests they were not in equilibrium with the surrounding melt when the sill cooled. Single clinopyroxene crystals often contain fractures filled with glass. Olivine is ubiquitous as small, rounded, anhedral crystals that are usually fractured and altered. Magnetite is common as angular to irregular crystals (<0.05 mm), increases in abundance downcore, and is infrequently included in single plagioclase or pyroxene grains. This crystal assemblage is set in a fine-grained groundmass of plagioclase, clinopyroxene and olivine microlites, that are in turn set in a dark brown glass. The modal percentage of plagioclase increases toward the center of the unit from 21% to 31% and then decreases toward the base to 24%. Clinopyroxene ranges from 1.2% to 5% and does not vary systematically throughout the core. Opaque phases comprise 3.0% to 4.5% and olivine is <1.5%. Glass + matrix (clinopyroxene + plagioclase) accounts for 55% to 65% of the rock; locally, glass comprises 20% to 45%, plagioclase 20% to 25%, and clinopyroxene 20% to 25%.

5.5.3 Mineral Chemistry

Three types of crystals, (microphenocrysts, phenocrysts, and individual crystals within glomerocrysts) consisting of plagioclase, pyroxene, olivine, and Fe-oxide were analyzed to determine compositional variability: (1) between single crystals within a glomerocryst, (2) between crystal types, and (3) vertically within the sill (Table 5.4; Figs. 5.6 through 5.8). All data points are plotted on Fig. 5.8, but only selected analyses are presented in Table 5.4. A complete set of analyses may be obtained from the ODP data base.

Table 5.1: ODP Leg 125. Site 781 mineral analyses and calculated cation proportions

PLAGIOCLASE

sample:125-781-9R1, 0-4 cm

grain/ type	mph	mph	3-1 rim	3-3 core	3-3 rim	4-1 core	4-1 rim	5 core	5 rim
SiO_2	51.76	48.04	45.28	46.92	49.12	48.93	52.11	51.47	47.65
Al_2O_3	31.09	33.68	35.09	34.56	32.29	32.93	30.63	30.91	33.21
FeO^*	1.03	0.76	0.77	0.74	0.75	0.74	0.96	0.81	0.78
MgO	1.07	0.10	nd	0.07	0.13	0.09	1.10	0.11	0.07
CaO	13.77	16.65	18.12	17.56	15.63	16.18	13.40	13.75	16.28
Na_2O	3.89	1.97	0.36	1.34	2.50	2.36	2.96	3.54	1.84
K_2O	0.08	0.06	nd	nd	0.04	0.05	0.09	0.11	0.06
Total	102.69	101.26	99.62	101.20	100.46	101.28	101.25	100.70	99.89

Ideal mineral proportions

An	65.87	82.07	96.47	87.81	77.37	78.89	71.04	67.78	82.72
Ab	33.67	17.57	3.47	12.13	22.39	20.82	28.40	31.58	16.92
Or	0.46	0.35	0.06	0.06	0.24	0.29	0.57	0.65	0.36

Cations in formula

Si	2.31	2.18	2.09	2.14	2.24	2.22	2.34	2.33	2.19
Al	1.63	1.80	1.91	1.85	1.74	1.76	1.62	1.65	1.80
Fe	0.04	0.03	0.03	0.03	0.03	0.03	0.04	0.03	0.03
Mg	0.07	0.00	0.00	0.00	0.00	0.00	0.07	0.00	0.00
Ca	0.66	0.81	0.90	0.86	0.76	0.79	0.64	0.67	0.80
Na	0.34	0.17	0.03	0.12	0.22	0.21	0.26	0.31	0.16
K	0.00	0.00	0.00	0.00	0.00	0.00	0.00	0.00	0.00

Table 5.1 (continued)

PLAGIOCLASE
sample: 125-781-10R1, 16-20 cm

grain/ type	mph	mph	1-1 core	1-1 rim	1-3 core	1-3 rim	4-1 core	4-1 rim
SiO_2	50.78	57.20	45.85	51.10	45.52	49.52	45.98	48.78
Al_2O_3	31.22	26.84	34.89	30.71	35.47	32.99	34.31	32.39
FeO^*	0.86	0.73	0.73	0.88	0.73	0.84	0.77	0.78
MgO	0.09	0.03	0.06	0.09	0.06	1.07	0.11	0.08
CaO	14.21	9.04	18.54	14.04	18.59	16.25	17.90	15.53
Na_2O	3.42	5.34	1.63	3.59	1.05	2.38	1.48	1.92
K_2O	0.10	0.21	0.03	0.10	nd	0.05	nd	0.06
Total	100.68	99.39	101.73	100.51	101.42	103.10	100.55	99.54
Ideal mineral proportions								
An	69.26	47.70	86.13	67.97	90.67	78.82	86.88	81.41
Ab	30.16	50.98	13.70	31.45	9.27	20.89	13.00	18.21
Or	0.58	1.32	0.17	0.58	0.06	0.29	0.12	0.37
Cations in formula								
Si	2.31	2.58	2.09	2.32	2.08	2.21	2.11	2.24
Al	1.67	1.43	1.87	1.65	1.91	1.73	1.86	1.75
Fe	0.03	0.03	0.03	0.03	0.03	0.03	0.03	0.03
Mg	0.00	0.00	0.00	0.00	0.00	0.07	0.00	0.00
Ca	0.69	0.44	0.91	0.68	0.91	0.78	0.88	0.76
Na	0.30	0.47	0.14	0.32	0.09	0.21	0.13	0.17
K	0.00	0.00	0.00	0.00	0.00	0.00	0.00	0.00

Table 5.1 (continued)

PLAGIOCLASE
sample 125-781-10R3, 17-21 cm

grain/			1	1	3	3	4	4
type	mph	mph	core	rim	core	rim	core	rim
SiO_2	52.81	58.70	48.85	53.09	46.14	51.60	46.61	48.55
Al_2O_3	29.09	26.15	32.80	29.78	35.05	30.03	34.05	32.83
FeO^*	0.61	0.49	0.69	0.65	0.62	1.28	0.70	0.81
MgO	0.08	1.01	0.12	0.07	0.08	0.32	0.06	1.07
CaO	12.39	8.05	16.34	12.73	18.53	13.33	17.45	15.91
Na_2O	3.54	6.34	2.13	4.17	0.46	2.94	1.48	2.31
K_2O	0.11	0.20	0.03	0.08	0.03	0.07	0.03	0.06
Total	98.63	100.94	100.96	100.57	100.91	99.57	100.38	101.54

Ideal mineral proportions

An	65.46	40.74	80.77	62.49	95.52	71.16	86.54	78.91
Ab	33.85	58.06	19.05	37.04	4.29	28.40	13.28	20.73
Or	0.69	1.21	0.18	0.47	0.18	0.44	0.18	0.35

Cations in formula

Si	2.42	2.60	2.22	2.40	2.11	2.36	2.14	2.20
Al	1.57	1.37	1.76	1.58	1.89	1.62	1.84	1.75
Fe	0.00	0.00	0.03	0.00	0.00	0.05	0.03	0.03
Mg	0.00	0.07	0.00	0.00	0.00	0.00	0.00	0.07
Ca	0.61	0.38	0.80	0.62	0.91	0.65	0.86	0.77
Na	0.31	0.54	0.19	0.36	0.04	0.26	0.13	0.20
K	0.00	0.00	0.00	0.00	0.00	0.00	0.00	0.00

Table 5.1 (continued)

CLINOPYROXENE

sample:125-781-9R1, 0-4 cm   125-781-10R1, 16-20 cm

grain/ type	mph	pheno	1 core	1 core	1 rim	4 core	mph	pheno	2 core
SiO_2	50.40	52.06	51.45	52.64	51.96	49.11	51.50	50.65	51.43
Al_2O_3	4.27	2.88	2.21	2.29	2.75	4.32	1.79	3.34	1.60
TiO_2	0.71	0.44	0.31	0.30	0.30	0.90	0.47	0.57	0.38
FeO^*	12.22	11.73	8.55	9.19	9.24	13.76	13.71	10.06	16.67
MnO	0.23	0.42	0.26	0.15	0.20	0.52	0.50	0.22	0.72
MgO	13.91	15.17	15.59	17.12	15.49	12.68	13.97	14.24	14.84
CaO	18.56	17.59	19.94	19.38	19.98	18.67	17.57	20.31	14.01
Na_2O	0.59	0.21	nd	0.25	0.26	0.26	0.16	0.24	0.12
Cr_2O_3	0.03	nd	0.17	0.58	0.60	0.17	0.24	nd	0.03
Total	100.92	100.50	98.48	101.90	100.78	100.39	99.91	99.63	99.80

Ideal mineral proportions

Wo	39.12	36.76	41.28	38.48	40.99	39.68	36.83	42.33	29.40
En	40.78	44.11	44.90	47.28	44.21	37.49	40.73	41.30	43.31
Fs	20.10	19.13	13.81	14.24	14.80	22.83	22.44	16.36	27.29

Cations in formula

Si	1.88	1.93	1.94	1.92	1.92	1.86	1.95	1.90	1.95
Al	0.19	0.13	0.10	0.10	0.12	0.19	0.08	0.15	0.07
Ti	0.00	0.00	0.00	0.00	0.00	0.03	0.00	0.00	0.00
Fe	0.38	0.36	0.27	0.28	0.29	0.44	0.43	0.32	0.53
Mn	0.00	0.00	0.00	0.00	0.00	0.00	0.00	0.00	0.00
Mg	0.77	0.84	0.87	0.93	0.85	0.72	0.79	0.80	0.84
Ca	0.74	0.70	0.80	0.76	0.79	0.76	0.71	0.82	0.57
Na	0.04	0.00	0.00	0.00	0.00	0.00	0.00	0.00	0.00
Cr	0.00	0.00	0.00	0.00	0.00	0.00	0.00	0.00	0.00

Table 5.1 (continued)

CLINOPYROXENE
125-781-10R3, 17-21 cm

grain/ type	mph	mph	4 rim	4 core	7 rim	7 core
SiO_2	50.44	50.50	51.59	51.11	51.51	52.20
Al_2O_3	1.09	2.43	3.07	2.11	2.92	2.19
TiO_2	0.31	0.36	0.26	0.38	0.36	0.33
FeO*	22.35	10.16	6.57	11.68	8.96	8.93
MnO	0.88	0.39	0.24	0.41	0.31	0.27
MgO	10.47	15.36	15.64	15.83	15.39	15.79
CaO	14.47	18.95	21.63	17.00	19.62	19.79
Na_2O	0.15	nd	nd	0.47	0.24	0.24
Cr_2O_3	nd	nd	nd	nd	0.32	nd
Total	100.16	98.15	99.00	98.99	99.63	99.74

Ideal mineral proportions

Wo	31.14	39.29	44.59	35.32	40.85	40.61
En	31.33	44.28	44.85	45.75	44.59	45.09
Fs	37.53	16.44	10.56	18.93	14.55	14.30

Cations per formula unit

Si	1.97	1.92	1.92	1.93	1.92	1.94
Al	0.05	0.11	0.13	0.09	0.13	0.10
Ti	0.00	0.00	0.00	0.00	0.00	0.00
Fe	0.73	0.32	0.20	0.37	0.28	0.28
Mn	0.03	0.00	0.00	0.00	0.00	0.00
Mg	0.61	0.87	0.87	0.89	0.85	0.87
Ca	0.60	0.77	0.86	0.69	0.78	0.79
Na	0.00	0.00	0.00	0.03	0.00	0.00
Cr	0.00	0.00	0.00	0.00	0.00	0.00

Table 5.1 (continued)

OLIVINE

sample:125-781-9R1, 0-4 cm			10R1, 16-20 cm	10R3, 17-21 cm	
grain/	2 -1	2 -1	2 -2	3		3
type	core	core	rim	core	mph	core
SiO$_2$	39.00	37.83	39.07	37.27	35.68	39.19
MgO	36.15	36.03	37.21	31.80	22.28	36.42
FeO*	26.67	26.35	26.82	33.14	44.03	26.35
CaO	0.29	0.28	0.26	0.27	0.29	0.31
MnO	0.41	0.40	0.41	0.66	0.85	0.46
NiO	nd	nd	nd	nd	nd	0.04
Total	102.52	100.89	103.77	103.14	103.13	102.77
Ideal mineral proportions						
Fo	70.73	70.91	71.21	63.11	47.43	71.13
Cations in formula						
Si	1.01	1.00	1.00	0.99	1.00	1.01
Mg	1.39	1.41	1.42	1.26	0.93	1.40
Fe	0.58	0.58	0.57	0.74	1.03	0.57
Ca	0.00	0.00	0.00	0.00	0.00	0.00
Mn	0.00	0.00	0.00	0.00	0.00	0.00
Ni	0.00	0.00	0.00	0.00	0.00	0.00

Table 5.1 (continued)

TITANO-MAGNETITE
sample:125-781-

	9R1 0-4 cm	10R1 16-20 cm	10R3 17-21 cm
FeO*	76.81	81.20	78.08
TiO_2	10.40	10.73	15.10
MnO	0.54	0.40	0.60
MgO	1.17	3.37	1.84
SiO_2	1.14	0.11	0.08
Al_2O_3	4.31	4.06	2.46
Cr_2O3	0.48	nd	0.12
CaO	0.20	0.03	0.04
Total	95.05	99.90	98.32

nd- none detected; mph- microphenocryst; FeO*- all iron as FeO
grain number (ie., 2) indicates single grain from which core and rim values were obtained
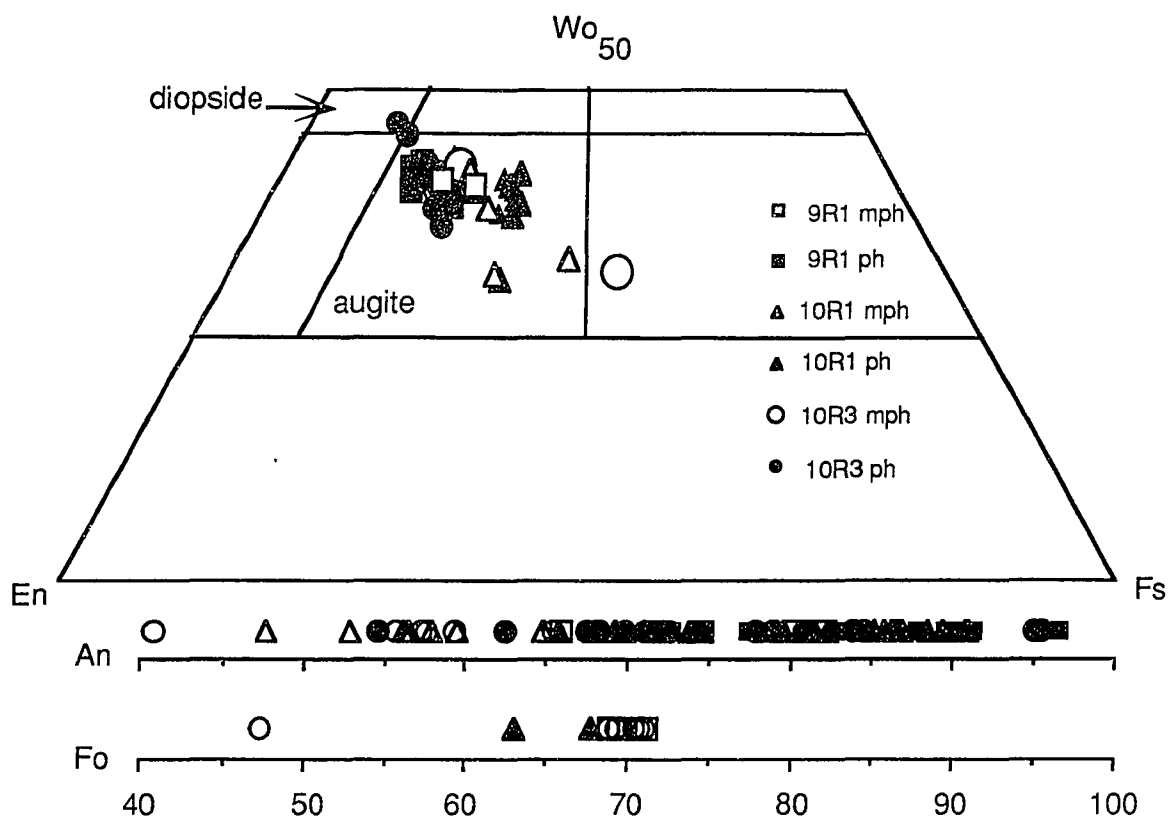All analyses from the University of Hawaii, Cameca microprobe, analyst: L. E. Johnson

Figure 5.8. Pyroxene quadrilateral. Each point represents between 2 and 6 analyses of individual crystals. No zoning between cores and rims or crystal types is observed. Fields are from Poldervaart and Hess (1951).

Total variability in plagioclase compositions ranges from An 41 to An 97. Minimum values of An decrease downhole in microphenocrysts from 66 in 781A-9R1, 0-4 cm to 41 in 781A-10R3, 17-21 cm and in phenocrysts from 68 in 781A-9R1, 0-4 cm to 55 in 781A-10R3, 17-21 cm. Maximum values of An are similar downhole for phenocrysts (91-97), but decrease (82 in 781A-9R1, 0-4 cm to 66 in 781A-10R3, 17-21 cm) for microphenocrysts. Microphenocrysts are generally lower in An (41-82) than are phenocrysts (55.97). Zoning is common and is most often normal; however, one crystal in sample 781A-9R1-0-4 was reversely zoned with An 70 (core) and An 90 (rim).

Clinopyroxenes are homogeneous and plot primarily in the augite region of the pyroxene quadrilateral (Fig. 5.8; Poldervaart and Hess, 1951). Total range of clinopyroxene compositions is: Wo 29-46 En 32-47 Fs 10-37. Clinopyroxene are homogeneous and unzoned. There are no systematic differences between microphenocrysts, phenocrysts and individual crystals within glomerocrysts (Table 5.4). Although, the total range of compositional variability is similar, microphenocrysts exhibit a greater variability within a single thin section than do phenocrysts and glomerocrysts. The greatest variability of En and Fs is found in the center of the section (781A-10R1, 16-20 cm); however, the greatest variability in Wo content is found near the bottom.

Olivine grains commonly occur as individual crystals, are unzoned and do not vary in composition downhole. Phenocrysts range from Fo 69 to Fo 71; a single microphenocryst has Fo 47.

All oxide phases analyzed were titano-magnetite; TiO_2 content increases downhole. The crystals from the upper part of the core are less titaniferous (8.5%

TiO_2) than those at the base (13% TiO_2) and an inverse relationship was observed with Cr_2O_3 (0.6% vs. 0.1%).

5.5.4 Major-Element Geochemistry

Abundances of major elements in the Site 781 lavas are similar to but not exactly like those typically found in Mariana Island Arc tholeiite basalts (Stern et al., 1989; Lin et al., 1989) and are typical of IAT basalts. Samples from Site 781 are classified as basalt and plot within the low-K tholeiite field on a SiO_2-K_2O classification diagram (Fig. 5.6; after Peccerillo and Taylor, 1976). Samples show a moderate degree of iron enrichment and plot in the tholeiite field on an AFM diagram (Fig. 5.7; after Irvine and Baragar, 1971). Basaltic abundances of SiO_2 (49.09 - 50.73 wt. %), high Al_2O_3 (17.28 - 18.17 wt. %) and high $Fe_2O_3^*$ (11.93 - 12.73 wt. %; $Fe_2O_3^*$ = total iron calculated as Fe_2O_3) coupled with low MgO (4.21 - 4.56 wt %) is a common characteristic of the IAT series. The basalt chemistry more closely resembles the lower-potassium tholeiitic lavas of Guguan, Asuncion, and the submarine volcanoes of the southern Mariana arc than the higher-potassium calc-alkaline lavas of Agrigan and Pagan (Dixon and Batiza, 1979; Stern et al., 1989; Woodhead, 1988; Lin et al., 1989; Figs. 5.6 and 5.7), or the shoshonitic and high K calc-alkaline lavas in the seamount province of the northern Mariana Island Arc (Bloomer et al., 1989).

Compositional variations within the recovered core samples are small: positive co-variations in CaO and Al_2O_3 that are inversely correlated with co-variations in MgO and $Fe_2O_3^*$ (total iron) can be explained simply by variation in the proportion of phenocrysts of plagioclase feldspar or mafic phases; a small part of the variation in potassium can be related to alteration. Overall, however, the data are

Table 5.2. LEG 125, Site 781, basalt layer XRF whole rock major and trace element abundances

Sample ID

CORE	8RCC[a]	9R1[a]	9R2[a]	9R3[b]	10R1[a]	10R2[a]	10R3[a]	10R1[b]
RANGE	11-13	69-71	49-51	88-92	84-86	68-72	65-67	131-135
Oxides in wt %								
SiO_2	49.89	49.56	49.09	50.29	50.46	49.53	50.35	50.73
TiO_2	0.86	0.88	0.85	0.91	0.89	0.85	0.90	0.91
Al_2O_3	17.87	17.69	17.31	17.79	17.10	17.57	17.28	18.17
$Fe_2O_3 \cdot §$	12.09	12.43	12.03	12.45	12.36	12.02	12.73	11.93
MnO	0.25	0.23	0.25	0.20	0.24	0.22	0.24	0.18
MgO	4.21	4.40	4.45	4.64	4.25	4.45	4.45	4.56
CaO	11.18	11.32	11.09	11.13	10.95	11.08	10.89	11.24
Na_2O†	2.10	2.02	2.08	2.27	2.16	2.31	2.19	2.21
K_2O	0.52	0.42	0.43	0.42	0.58	0.39	0.50	0.35
P_2O_5	0.06	0.06	0.06	0.10	0.06	0.06	0.06	0.10
TOTAL	99.03	99.01	97.64	100.20	99.05	98.48	99.59	100.38
LOI	0.64	1.28	0.86	nd	1.95	0.75	0.79	nd
Trace elements in ppm								
Nb	1	1	1	1	1	1	1	1
Zr	48	46	46	47	52	46	49	48
Y	23	22	22	21	24	22	23	22
Sr	294	294	295	287	288	294	293	285
Rb	7	6	4	8	13	2	7	3
Zn	98	92	71	90	94	77	82	78
Cu	175	184	72	197	181	141	196	133
Ni	7	9	10	11	11	11	10	12
Cr	11	11	11	43	8	9	11	19
V	407	428	387	374	354	408	370	392
Ce	18	32	15	nd	17	26	23	nd
Ba	169	142	165	196	158	280	177	159

a) Analyses performed on board the D/V JOIDES RESOLUTION, analyst: D. Sims

b) Analyses performed at the University of Hawaii, analysts: T. Husslebosch, L. Johnson

nd=not determined § Fe2O3*= total iron caluclated as Fe2O3

† Na2O values for "a" analyses corrected on the basis of factor determined by Arculus et al., (this volume).

Table 5.3. ODP Leg 125, Site 781, basalt layer,
REE analyses of three representative samples.

Core 9R1 Interval (ppm)	10R2 69-71	10R3 68-71	dev.[a] 65-67	factor[b] % Std.	Norm.
La	2.89	3.37	3.17	na	0.315
Ce	8.54	9.11	9.46	1.9	0.813
Nd	6.19	7.60	7.44	1.7	0.597
Sm	2.09	2.51	2.42	1.9	0.192
Eu	0.81	0.92	0.92	0.5	0.072
Gd	2.92	2.99	3.18	0.4	0.259
Dy	2.80	3.58	3.48	1.6	0.325
Er	1.82	2.56	2.23	1.2	0.214
Yb	1.80	2.26	2.20	1.6	0.208
Lu	0.30	0.36	0.34	1.9	0.032

Data determined by directly coupled plasma (DCP), at
Lamont-Doherty Geological Observatory, analyst: L. Johnson.

[a] Percentage of standard deviation [(1 std. dev. /average)*100]
for four analyses of a Mid-Atlantic ridge basalt.

[b] Chondrite factor used for normalization for Figure 2;
na=La values not determined.
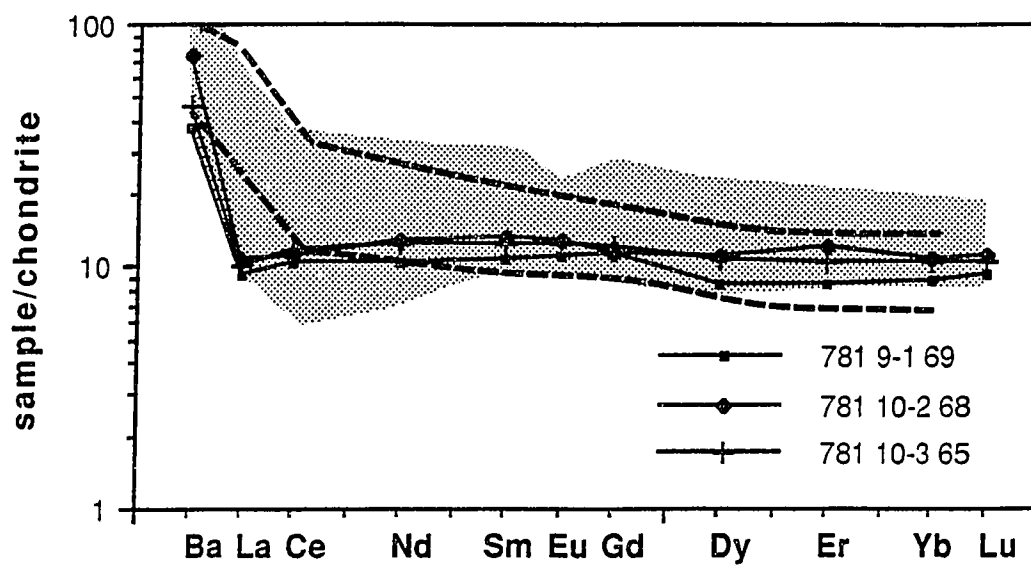
Figure 5.9. Chondrite normalized rare earth element patterns. Note the relatively flat pattern with a small "sway" in the middle rare earth elements that is characteristic of Mariana arc lavas. The fields are from the Mariana subaerial (stippled) and submarine (dashed outline) volcanoes of Stern et al., (1989).

consistent with a single, chemically homogeneous intrusion, and there is little evidence for internal fractionation.

Compatible elements (Sr, V, Cr, Ni) show a similar pattern to the major elements with small variations that probably relate to the relative proportion of plagioclase and mafic phenocrysts. As in the case of K, the mobile elements Rb, Ba, Cu show small variations that may be related to alteration. REE patterns from three samples representing the top, center, and base of the recovered basalt are essentially flat at about 10 times chondrite (Fig. 5.9). The patterns show a slight LREE and HREE depletion that gives a "humped" effect. The shallowest sample (781A-9R-1, 69-71 cm) has slightly lower abundances than the deeper samples and a more distinct, heavy REE depletion. The patterns fall at the lower end of the range of active Mariana arc lava patterns (Fig. 5.9; Stern et al., 1989), that vary from flat to LREE-enriched; the latter in particular have distinct negative Ce-anomalies that are not apparent in the Site 781 basalt.

The incompatible trace-element characteristics of basalts can be portrayed using multi-element plots, normalized to N-MORB (normal MORB; Pearce, 1983). On such a diagram, magmas derived from a depleted convecting mantle source similar to a MORB source will show a flat pattern. Magmas derived from the mantle overlying a subducting slab typically give patterns that are depleted in the incompatible HFS elements (Y, Ti, Zr and the middle-heavy REE) and are selectively enriched in the LIL elements (Sr, K, Rb, Ba and usually also light REE and Th) that are derived from the subducted oceanic lithosphere and its sediment cover through dehydration and partial melting. The type of enrichment pattern will also vary from arc to arc according to the nature of material being subducted, and with the thermal and geodynamic parameters of the subduction system (Pearce, 1983). The MORB normalizing values
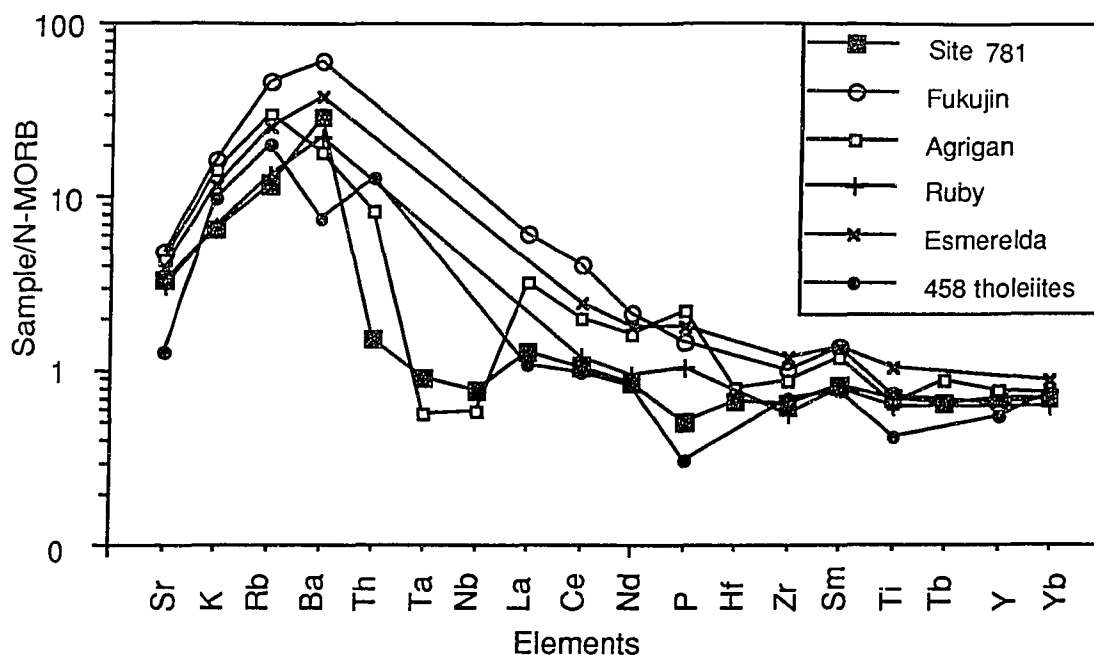
Figure 5.10. MORB-normalized incompatible trace element patterns for Site 781 basalt in comparison to: Agrigan, an active subaerial, calc-alkaline volcano in the central Mariana arc (JA Pearce unpublished ICP-MS data); Fukujin an active, submarine, calc-alkaline volcano in the northern Mariana arc (Bloomer et al, 1989; Lin et al., 1989); Ruby and Esmerelda Banks seamounts, active volcanoes in the southern Mariana arc with tholeiitic chemical characteristics (Stern et al., 1989); and to DSDP Hole 458 tholeiites from the outer Mariana forearc (Mattey et al., 1980; Wood et al., 1981). N-MORB normalizing values are from Sun and McDonough, (1989).

used in Figure 10 are taken with slight modifications from the compilation by Sun and McDonough (1989), and the ordering of the elements (with the exception of Sr and K) is based on the relative incompatibility (increasing from left to right) during lherzolite melting and is taken from Pearce (1983).

Patterns from four Mariana arc volcanoes, the forearc tholeiitic suite from DSDP Site 459, and from the ODP Site 781 rocks show selective enrichments (relative to N-MORBs) in all LIL elements from Sr through Th and relatively flat, though slightly depleted, patterns for the HFS elements (Hf-Yb; Fig. 5.10). Agrigan Island and Fukujin Seamount are calc-alkaline volcanoes in the central and northern Mariana arc, respectively, (Bloomer et al. 1989). Esmerelda Bank and Ruby Seamount are submarine volcanoes in the southern Mariana arc that erupts lavas with some tholeiitic characteristics (Stern et al., 1989).

Abundances of Sr, K and Rb are all lower for the basalt at Site 781 than for the arc volcanoes, however Ba content is in the range of the values for the arc volcanoes. The Site 781 lavas most closely resemble the lavas from Ruby Seamount, although Ba is slightly enriched and P slightly .depleted in Site 781 lavas relative to Ruby. Th is depleted and Ta and Nb enriched in the Site 781 basalt relative to Agrigan and Pagan lavas, however, data for Th, Ta and Nb are unavailable for other arc volcanoes. La in the Site 781 basalt is depleted relative to Fukujin and Agrigan lavas but the same as in samples from Ruby Seamount and in DSDP Site 458 tholeiites. Site 781 lavas are slightly depleted in HFS elements (Hf-Yb) relative to many of the arc volcanoes (Fig. 5.10), but are similar to those from Ruby Seamount. Site 458 samples show similar patterns to the arc volcanoes although they are more distinctly more depleted in Ti, P and Ba. Although the enrichment in the mobile LIL elements for

samples from Site 458 may be caused by alteration, the enrichments for the Site 781 basalt and the arc volcanoes must be primary features.

The enrichment of the mobile elements (Sr, K, Rb, and Ba), relative to N-MORB, suggests that the magma source was in the mantle overlying, not beneath, the subducting plate. Because mobile elements (ie.: Sr, K, Rb, and Ba) are released from subducted sediment and basaltic crust at subsolidus temperatures during prograde dehydration of the subducted slab, the source of these mobile elements in arc lavas must be at depths less than 50 km and is probably within the upper part of the subducted slab. Th and the LREEs are only mobilized when temperatures are higher, when sediment melting can take place. Thus they would be expected to be released from the subducted slab at greater depths. The higher Th and La content in Agrigan lavas than in the Site 781 basalt may reflect a higher sediment contribution to the Agrigan source. The apparently lower sediment contribution to Site 781 lavas may indicate a shallower source, perhaps trenchward of the source for Agrigan and Fukujin. The amounts of the HFS elements (Y, Zr, Nb) in Site 781 basalts are comparable with volcanic rocks from the active arc. This suggests a like degree of melting and involvement of similar mantle for the origin of the sill as for the volcanoes in the active arc. Models for small degrees of hydrous melting of the shallower, more harzburgitic, lithosphere of the mantle are not favored, as they should produce more boninitic compositions with major depletions in many HFS elements (e.g., Hickey-Vargas and Reagan, 1987). The slightly lower abundances of the HFS elements in the dredged and previously drilled forearc sites suggest a slightly lower proportion of melting or a more depleted source than that for Site 781.

Table 5.4: ODP Leg 125, Site 781, basaltic layer, Incompatible elements, REE[a] and isotopic values[b]

sample: 781, 9R-1, 72-77 cm

Incompatible elements (ppm)			REE (ppm)
Zr	43	La	3.62
Y	19.4	Ce	7.64
Nb	1.8	Pr	1.2
Hf	1.37	Nd	6.15
Ta	0.12	Sm	2.16
Pb	2.52	Eu	0.79
Th	0.18	Gd	2.73
U	0.20	Tb	0.43
Sr	270	Dy	2.84
Ba	156	Ho	0.60
		Er	1.70
		Tm	0.30
		Yb	1.79
		Lu	0.30

ISOTOPIC RATIOS

$^{87}Sr/^{86}Sr$ 0.703487 $\pm$ 10

$^{143}Nd/^{144}Nd$ 0.513048 $\pm$ 4

$^{206}Pb/^{204}Pb$ 18.740

$^{207}Pb/^{204}Pb$ 15.569

$^{208}Pb/^{204}Pb$ 38.386

(a) ICP-MS, performed at Durham University, analyst: B. Murton.(b) Mass Spectrometer, performed at Royal Holoway and Bedford New College, London, The Sample was leached in 6N HCl for 3 hours at 180°C for Sr isotope analysis. Analyst: J. A. Pearce
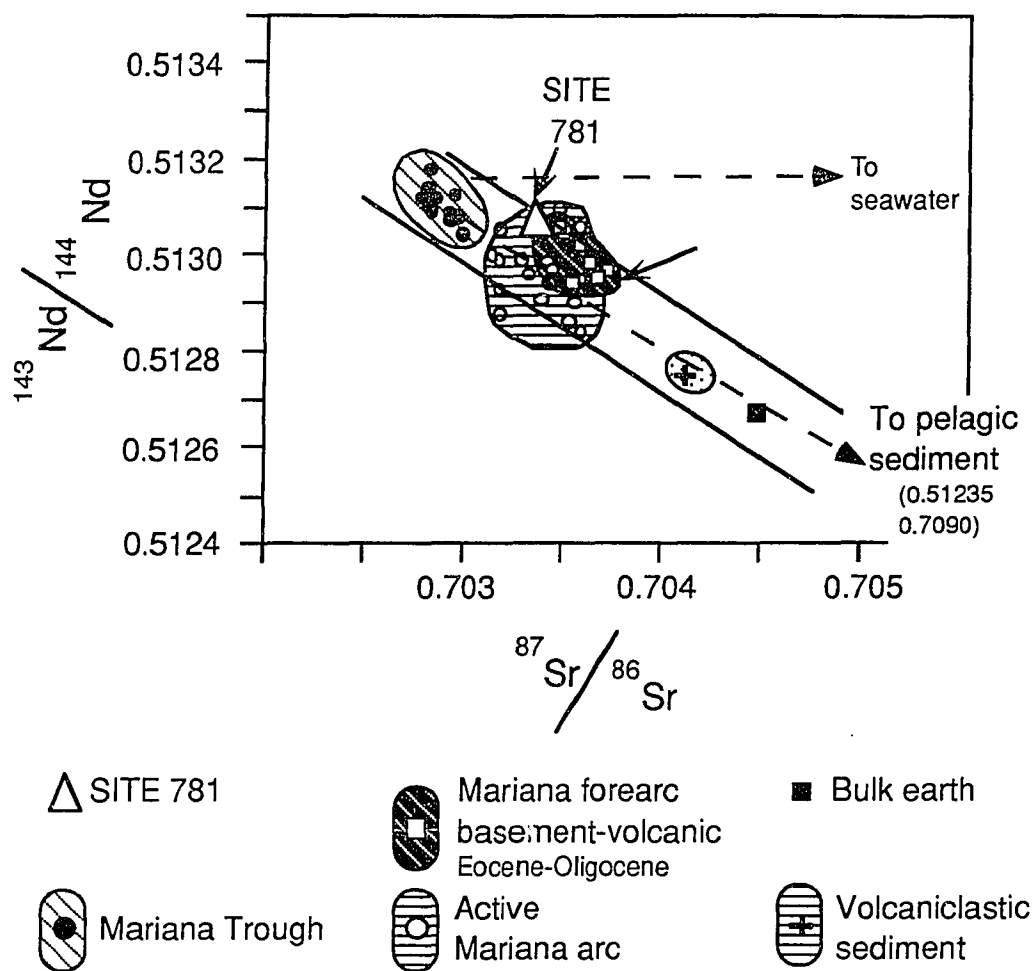
Figure 5.11. Sr-Nd isotope co-variation diagram for the basalt sill at Site 781 in comparison with Eocene-Oligocene forearc boninitic-tholeiitic lavas and lavas from the Mariana Trough and active Mariana arc.
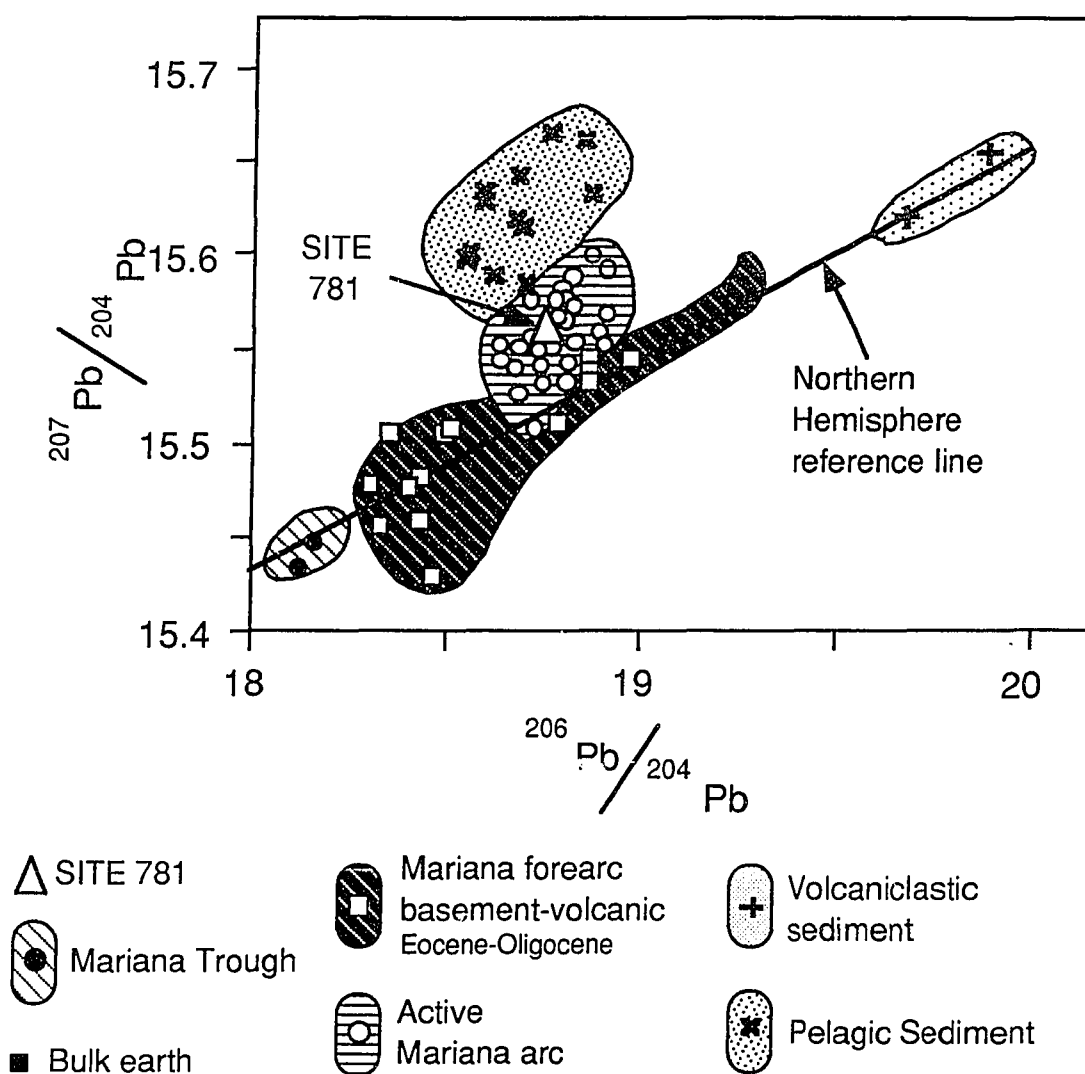
Figure 5.12. Pb isotope diagram for the basalt sill at Site 781 in comparison with Eocene-Oligocene forearc boninitic-tholeiitic lavas and lavas from the Mariana Trough and active Mariana arc.

5.5.5 Isotope Systematics

Figure 11 compares Sr and Nd isotope ratios for Site 781 basalts with isotope ratios for lavas from the active Mariana arc (Woodhead, 1989), Mariana Trough (Volpe et al., 1987), and from the Eocene to Oligocene Mariana forearc basement (Hickey-Vargas, 1989; Hickey-Vargas and Reagan, 1987). Active arc rocks have higher Sr and lower Nd ratios than rocks from the Mariana Trough. The basalt from Site 781 plots at the high end of the active arc field in terms of Nd isotope ratios, although its Sr isotope ratio is comparable.

In a Pb-isotope diagram (Fig. 5.12), the lavas from the active Mariana arc plot off the Northern Hemisphere Reference Line (NHRL) (the line containing MORB and northern hemisphere oceanic islands) of Hart (1984) toward pelagic sediments (or a mixture of pelagic and volcanogenic sediments). The Eocene to Oligocene forearc basement (Meijer, 1976; 1983) plots along or near the NHRL. The Site 781 sample plots in the center of the active arc field.

5.6 Discussion of Forearc Volcanism ·

Sedimentary strata recovered above and below the basalt have a biostratigraphic age of late Pliocene (Nannofossil Subzone CN12b). The mineralogy, texture, and chemistry of the Site 781 basalt are remarkably constant throughout the unit. The compositional homogeneity and the absence of any distinct internal flow boundaries suggest that basalt formation was a single intrusive event. The contact between the basalt and upper sedimentary strata is a narrow glassy margin with no pillow structures or breccia. These observations, along with the K-Ar age of 1.7 Ma, indicate that the basalt layer was injected *in-situ* as a sill. The magma was probably intruded from the fault zone bounding the graben and then was quenched against the

overlying sediment. Petrographic and geochemical evidence for interaction of the basalt with the overlying sediment are absent; however, low recovery (28%-55%) and a gap of 29 m following the last recovered rock at 92 mbsf (Fryer, Pearce, Stokking, et al., 1990) may have prevented the identification of flow contacts. This basalt is the youngest *in-situ* igneous layer reported in the Izu-Bonin and Mariana forearcs (Marlow et. al., 1988), and its genesis is important for understanding the emplacement of volcanic rocks in forearc settings.

Several models for the generation of igneous rocks in forearc settings have been discussed by Hussong and Uyeda, 1981a; Kobayashi, 1983a; Marlow et al., 1988). However, as presented in the following discussion, none of the models offers a satisfactory explanation for the generation of basalt at Site 781.

An early model for generating forearc volcanic rocks is shown in Figure 5.13A (from Hussong and Uyeda, 1981a), and this model involves a vertical sub-arc magma source that formed when the subducting slab was seaward of its present location. This model would imply tectonic erosion of the older forearc, so that the Site 781 basalt would now be in the forearc of a younger arc to the west. The young age of the Site 781 basalt (1.7 Ma) precludes such a model.

Another model proposed for forming forearc volcanic rocks is shown in Figure 5.13C. The forearc magma source here is from mantle beneath fractured oceanic crust. The resulting magmas should be MORB-like from such a mantle source. The magmas from Site 781 are not MORB-like but are tholeiitic and characteristic of an island arc source, not an oceanic mantle source.

Yet another model involves the generation of magma form a sub-arc source that is diverted either as a lateral sill or inclined dike that eventually reaches the middle of the forearc (Fig. 5.13C). However, Site 781 is 100 km from the island

A. Subarc source when
    subducting slab is
    seaward of present
    location (tectonic
    erosion of forearc) -
    basalt is too young
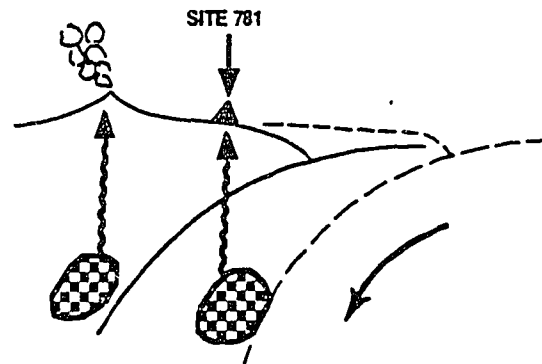
B. Source in fractured
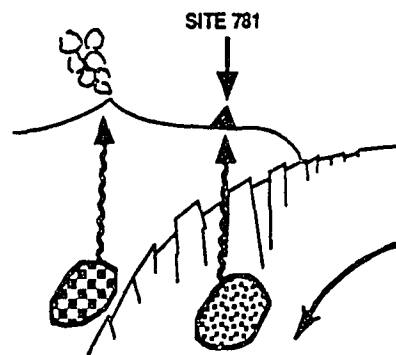   oceanic crust - basalt
    chemistry wrong

Figure 5.13. Schematic diagram showing models for forearc volcanism: (A) A deep source (about 150-200 km or normal depths for island arc volcanoes) during an earlier time period when the subducting slab was located seaward of its present location and implying tectonic erosion of the forearc. The basalt at Site 781 is too young for this model. (B) A magma source from within or below the fractured and subducting oceanic lithosphere. The chemistry of the Site 781 basalt does not fit this model.

C. Subarc source and
   lateral sill injection
   into the forearc -
   mechanically difficult
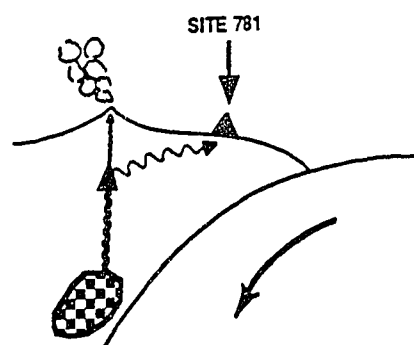
D. Simplest model -
   vertical injection of
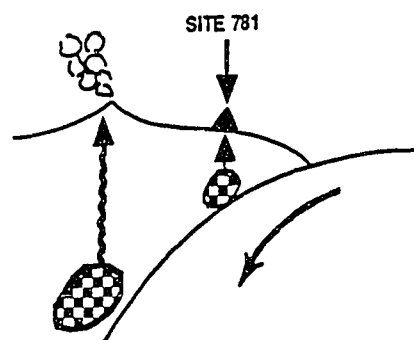   magma from a source
   directly beneath Site 781

Figure 5.13. (C) Lateral magma transport along a nearly horizontal conduit from near the magma sources for the active volcanoes. This model is mechanically difficult. (D) Simplest model showing vertical dike injection from a sub-forearc source beneath Site 781. Diagram is adapted from Hussong and Uyeda (1981a).

arc and the sill or dike would have to travel at least this distance through cold crust and sediment to reach the middle of the forearc, a supposition that is difficult to accept.

The simplest model for the emplacement of the basalt at Site 781 involves a source vertically beneath the site (Fig. 5.13D). Such a source would presumably involve the melting of oceanic crust and sediment and the mantle wedge above the subducting slab to generate a tholeiitic basalt with the chemistry described earlier (Fig. 5.14). However, a vertical feeder system directly under the forearc would require magma production where the depth to the subducted Pacific plate is only about 20 or 30 km deep (Hussong and Uyeda, 1981a; Eguchi, 1984). This region of the subducted slab beneath the forearc is probably too shallow to have generated sufficient heat to melt the overlying mantle wedge, unless there is sufficient hydration of the region by extensional fracturing. If the magma source is directly beneath Site 781, then thermal models of this forearc will undoubtedly have to be revised to allow for shallow melting. Without deep penetration seismic reflection data, no specific model can be confirmed.

5.7 Conclusions

Seismic reflection surveys revealed a small horst and graben structure in the midregion of the Mariana forearc at 19°30'N and near Conical Seamount, a serpentine mud volcano. A high-amplitude reflection occurs about 70 mbsf within the horst and can be seen on both sides of the fault bounding the graben. Drilling at Site 781 intersected 13 to 25 m of reversely-polarized, Pleistocene (1.7 Ma) tholeiitic basalt sill in normally-polarized, late Pliocene (2.5 Ma) sediment. The basalt sill is chemically and petrographically homogeneous and appears to be a single cooling unit.

Geochemical analysis indicates that the basalt sill is an island-arc tholeiite (IAT) similar to lavas from the active Mariana arc volcanoes. Multi-element analysis of the basalt indicates a magma source from the mantle above the subduction zone. Further drilling and seismic reflection surveys are necessary to delineate the magma conduits that fed the sill at Site 781.
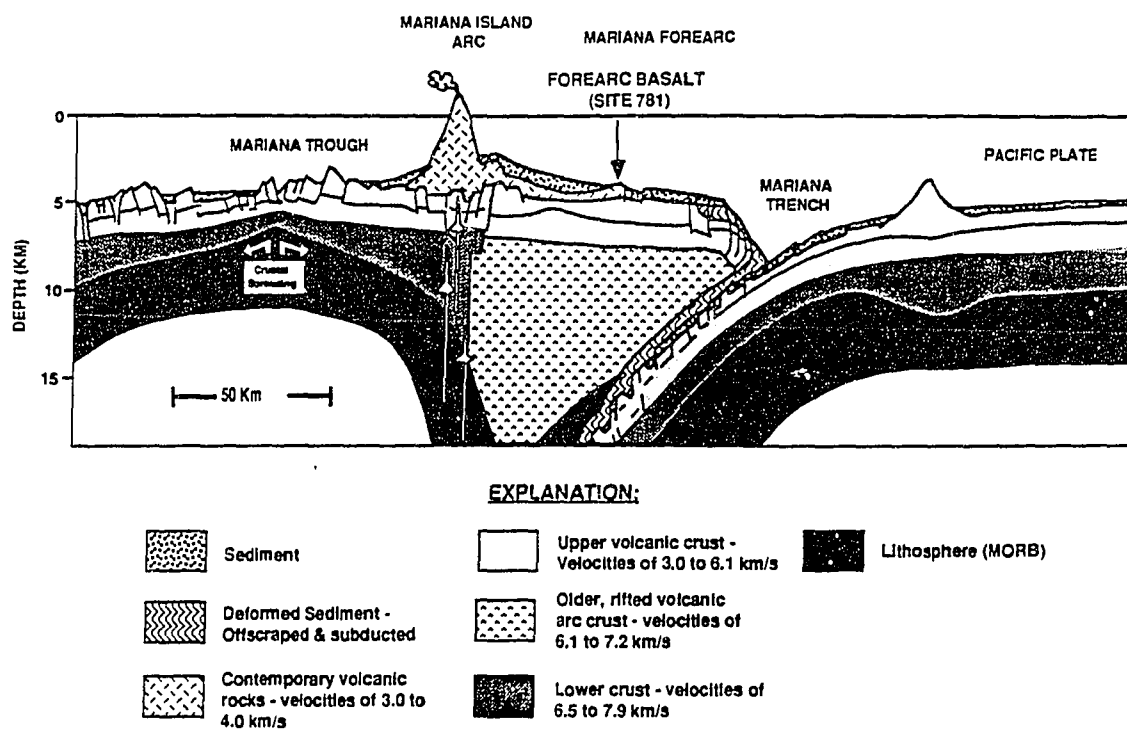
Figure 5.14. Cross section of the Mariana arc system, with ODP Site 781 projected on to the crustal section. Crustal section adapted from Hussong and Uyeda (1981a). The basalt sill drilled at Site 781 is seen as a continuous body of contemporary volcanic rocks extending back to the Mariana Island arc.

Table 5.5a: MODERN AND ANCIENT VOLCANIC ARCS WITH IGNEOUS ROCKS OR IGNEOUS ACTIVITY IN THE FOREARC REGION

REGION	ROCK TYPE	COMMENTS	REFERENCES
Eastern Aleutian Forearc	Granodiorite, granite, basalt, and andesite;	Dates range from 62 to 40 Ma. Attributed to passage of ridge-trench-trench triple junction (Kula-Farallon Ridge).	Marshak and Karig (1977); Hill et al. (1981); Moore et al. (1983); Hudson et al. (1977)
Eastern Aleutian Forearc	Basalt	K/Ar age of 22.5 Ma. on a basalt sample from Unimak Seamount along with early and middle Miocene sediment recovered in a dredge haul 50 to 60 km from the trench. Attributed to arc volcanism followed by truncation of the arc margin.	Bruns et al. (1987a,b)
Bonin Forearc	Boninite, tholeiite, serpentinized ultramafic rocks	K/Ar ages of 26 and 40 Ma. Forearc is 100 km or less from Bonin Trench. Presently active volcanic island arc is 250 km from associated trench.	Kuroda and Shiraki (1975) Shiraki et al. (1978, 1980); Cameron et al. (1979); Kobayashi (1983a,b); Ishii (1985); Fryer, Pearce, Stokking, et al. (1990)
Mariana Forearc	Boninite, arc tholeiitic basalt and differentiates, ocean island basalt (OIB), mid-ocean ridge basalt (MORB)	Eocene age. DSDP Site 458. Island arc affinities are a product of subduction-related volcanism, suggesting subduction erosion of the forearc.	Hussong, Uyeda, et al. (1981); Bloomer (1983); Chapter 3
Mariana Trench	Gabbro, ultramafic rocks, boninite, altered basalt, andesite and dacite, and alkalic basalt	Landward slope of trench. Probably a late Eocene arc complex exposed by subduction erosion. May include some offscraped seamount rocks.	Bloomer (1983); Bloomer and Hawkins (1983)
Yap-Mariana Trenches	Arc tholeiitic basalt, alkalic	K/Ar ages of 7.8 and 10.8 Ma; dredged from forearc close to trenches.	Beccaluva et al. (1980, 1986); Crawford et al. (1981, 1986)

Table 5.5b: MODERN AND ANCIENT VOLCANIC ARCS WITH IGNEOUS ROCKS OR IGNEOUS ACTIVITY IN THE FOREARC REGION

REGION	ROCK TYPE	COMMENTS	REFERENCES
Eastern Papua New Guinea	Basalt, nephelinite, basanite, tephrite, trachybasalt, and trachyandesite	Tabar to Feni Islands off the east coast of New Ireland; Pre-middle-Miocene but mostly Quaternary	Johnson et al. (1976); Johnson (1979)
'Eua, Tonga	Andesitic and silicic andesitic dikes and flows, serpentinized ultramafic, ultramafic, and arc tholeiitic rocks	Late Eocene island arc tholeiitic rocks rifted from an arc (Lau-Fiji Ridge?) older than the presently active Tonga arc and tectonically emplaced in the forearc.	Ewart and Bryan (1972); Hawkins and Falvey (1985); Bloomer and Hawkins (1987)
Japan (Oyashio paleoland)	Dacite conglomerate	K/Ar age of 23.4 +/- 5 Ma. DSDP Site 439. Below Oligocene sandstone; suggested tectonic erosion of ancient forearc that once lay seaward of the drill site.	von Huene et al. (1980); Kobayashi (1983b)
Southwest Japan	Siliceous igneous (extrusive and intrusive)	Age 17 to 13 Ma. Belt less than 50 km from coeval trench. Attributed to passage of Japan-Ryukyu-IZu-Bonin Trench triple junction and associated passage of Izu-Bonin volcanic are along the accretionary Japanese forearc (Marshak and Karig, 1977). Or volcanism may be related to subduction of young crust of the Shikoku Basin (Kobayashi, 1983a).	Marshak and Karig (1977); Shibata (1978); Kobayashi (1983a); Miyake (1985)
Nicoya Peninsula	Tholeiitic basalt	Late Cretaceous. Oceanic plateau, intraplate oceanic volcanism, or primitive are volcanism.	Lundberg (1983)
Western Sumatra	Scattered intrusive and extrusive rocks	Probable Oligocene age, within 100 km of trench and seaward of associated volcanic arc axis positions throughout Cenozoic time. Attributed to northeastward migration of ridge-trench-trench triple junction along Sunda Trench.	Marshak and Karig (1977)

Table 5.5c: MODERN AND ANCIENT VOLCANIC ARCS WITH IGNEOUS ROCKS OR IGNEOUS ACTIVITY IN THE FOREARC REGION

REGION	ROCK TYPE	COMMENTS	REFERENCES
Southern Chile	Granodiorite plutons and porphyritic stocks and sills	Age 4.0 to 3.5 Ma. 150 km seaward of the Quaternary volcanic arc associated with the Peru-Chile Trench. Attributed to subduction of the Chile Rise (Chile margin triple junction).	Forsythe and Nelson (1985); Forsythe et al. (1986)
Solomon Islands	High K_2O/TiO_2 basalt and basaltic andesite	Volcanism in the New Georgia Group within 30 km of associated trench. Attributed to subduction of the Woodlark spreading center beneath the Solomon Islands.	Stanton and Bell (1969); Weissel et al. (1982); Taylor and Exon (1982); Bunkley (1983); Ramsay et al., (1984); Perfit and Langmuir (1984)
Western California	Gabbro, basalt, serpentinite ultramafic rocks	Gabbro intrusions in Franciscan assemblage. Gabbro intruded into accretionary prism while convergence and subduction active as evidenced by blueschist-facies metamorphism. Mantle origin for magma. May be related to bending of plate or intersection of a fracture zone with margin.	Echeverria (1980); Johnson and O'Neil (1984); Phipps (1984); Shervais and Kimbrough (1985)
Southern California	Basalt, pyroxene andesite, and dacite	Age 25 to 15 Ma. Rocks occur in the northwestern Los Angeles Basin and the continental borderland. Erupted within 0 to 100 km of contemporaneous plate boundary (ridge-trench-transform triple junction) and may have been emplaced in an extensional environment as a result of ridge subduction.	Hurst (1982); Miyake (1985); See also Gill (1981) for summary and references
Troodos, Cyprus	Andestie-dacite-rhyolite assemblage and basalt-basaltic andesite assemblage; boninite	Overlain by Cretaceous sediment. Chemistry of lava indicates origin similar to forearc rocks of the Mariana and Bonin arcs.	Robinson et al. (1983); Miyake (1985)

Table 5.5d: MODERN AND ANCIENT VOLCANIC ARCS WITH IGNEOUS ROCKS OR IGNEOUS ACTIVITY IN THE FOREARC REGION

REGION	ROCK TYPE	COMMENTS	REFERENCES
Western Washington	Tholeiitic basalt	Crescent volcanic rocks beneath the Olympic Peninsula of early and middle Eocene age and as much at 15 km thick; apparently extruded on the Juan de Fuca plate and western margin of the North America plate. May be offscraped seamounts of an oceanic island chain (Snavely et al., 1968). Later volcanism (45 to 32 Ma) in forearc consisted of basaltic pillow lavas and tuff - from the ancestral Yellowstone hotspot? (Duncan and Kulm, 1989.	Snavely et al. (1968); Cady (1975); Miyake (1985); Duncan and Kulm (1987)

Chapter 6:

New evidence for crustal accretion in the outer Mariana forearc:

Cretaceous Radiolarian cherts and MORB-like lavas

6.1 Abstract

New age determinations on radiolarian cherts, foraminifers, and volcanic rocks document the presence of allochthonous fragments of Cretaceous oceanic plate, indicating accreted terrane, in the outer Mariana forearc, more than 50 km from the trench. Three dredges, from a 3 km^2 area along a steep scarp, recovered a diverse assemblage of rocks representing an ophiolite suite (chert, mafic and intermediate lavas and intrusive rocks). Trace element patterns of the lavas suggest at least three tectonic associations (island arc, ocean island, and oceanic plate). The cherts contain two deep-water assemblages of radiolaria of middle to late Valanginian (131-138 Ma) and Albian (97-112 Ma) age. Foraminifera recovered with the chert are Aptian to Albian in age. The lavas record a wide range of K-Ar ages, 85 Ma for a metabasalt with trace element signatures of mid-ocean-ridge basalt, 71 Ma for a highly metamorphosed alkalic basalt, and 39 Ma for a fresh glassy boninite. These ages imply multiple volcanic events and at least two tectonic settings for magma genesis. The cherts and meta-basalts are too old to have formed in situ or to be part of trapped West Philippine Basin crust. The mix of old oceanic plate with younger arc rocks requires complex tectonic relationships. We suggest that one or more fragments of Cretaceous oceanic plate (chert, mid-ocean ridge basalt and alkalic lavas) were accreted to the Mariana forearc and have been extensively faulted and likely intruded by arc lava (island arc tholeiite and boninite).
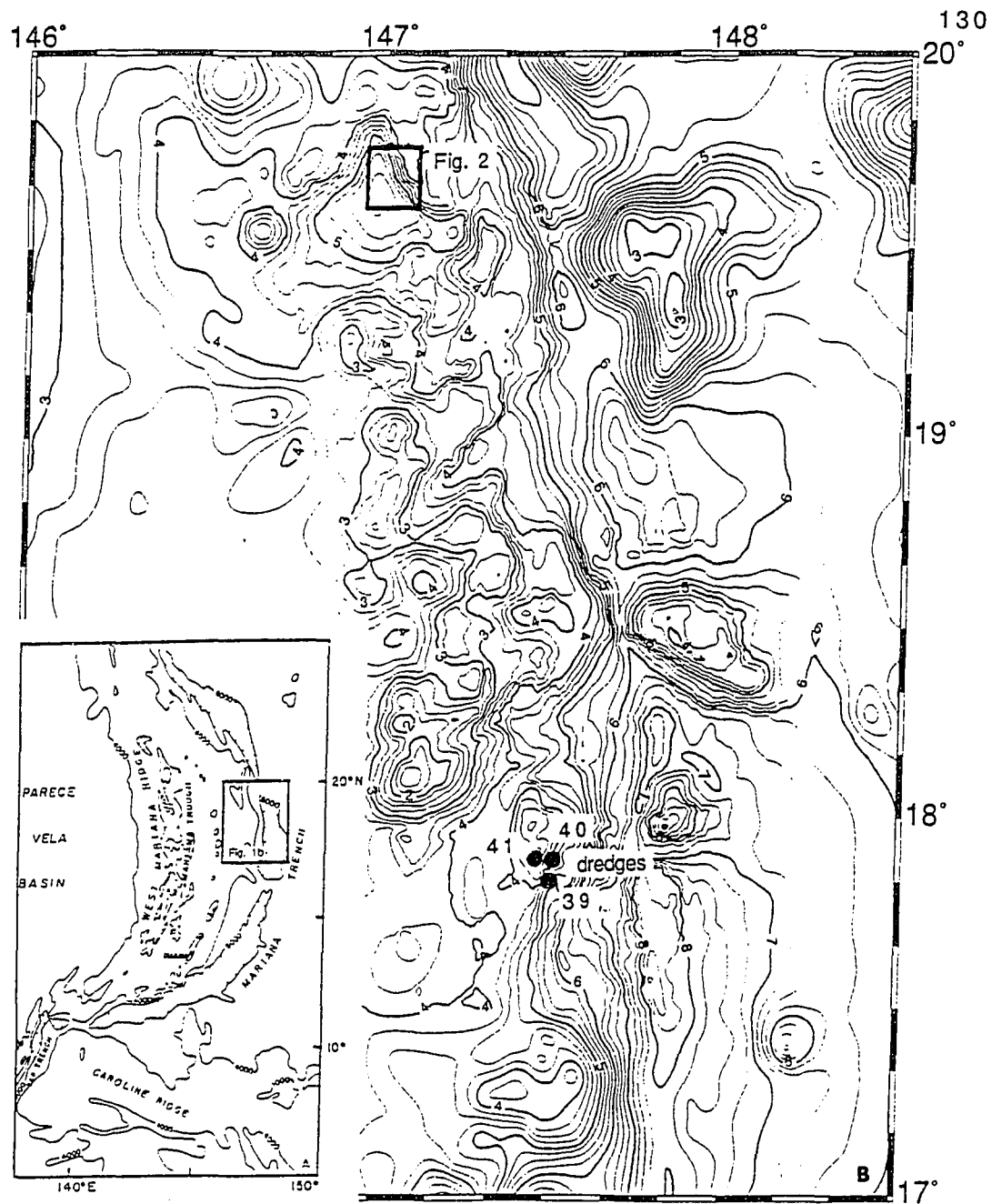
Figure 6.1. Location diagram for dredges. (A) Generalized map of western Pacific. (B) Central Mariana forearc, latitude 17-21°N, box shows area of Figure 6.2; bathymetry contoured in 250 m intervals from 3.5 kHz and SeaMARC II bathymetry. Dredge sites at latitude 17°50'N are shown by filled circles. Note the large seamount chains on the Pacific plate that are colliding with the Mariana forearc.
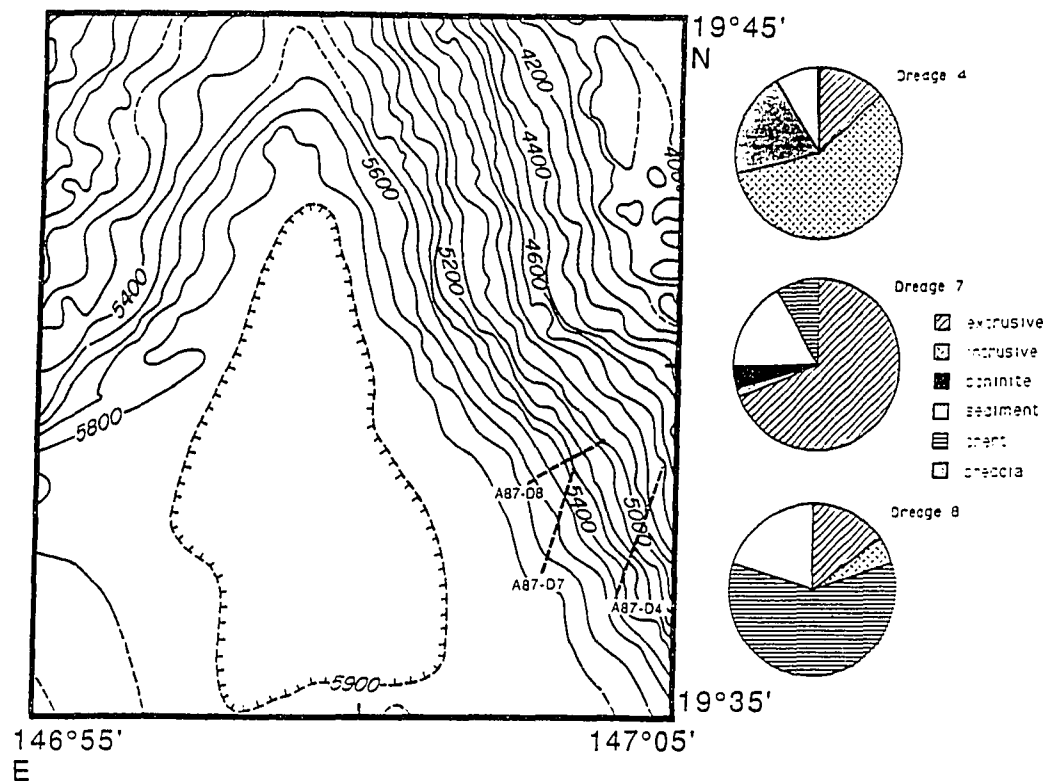
Figure 6.2. Dredge locations in the outer Mariana forearc and approximate percentages of rock types recovered from the steep fault scarp for samples of Chapter 3. Dredges at latitude 19°36'N are spaced about 1 km apart and recovered extremely diverse rock assemblages. Bathymetry is from SeaMARC II data contoured at 100 meter intervals.

6.2 Introduction

Some models for the formation of the Mariana forearc invoke entrapment of oceanic plate between the trench axis and the volcanic front upon initiation of subduction in the middle Eocene (about 45 Ma; (Uyeda and Ben-Avraham, 1972; Hilde et al., 1977; Dickinson and Seely, 1979; Mrozowski and Hayes, 1980; Bloomer, 1983). Other models suggest that arc lithosphere was already present or was later introduced into the forearc region (Klein and Kobayashi, 1980; Bloomer, 1983; Ogawa and Naka, 1984). Geophysical surveys of the Mariana forearc and inner trench wall reveal an unusually complex crustal structure: sediment thicknesses of as much as 1 km in the forearc basin, and an inner trench wall dominated by outcropping igneous rock (Mrozowski et al., 1981; Hussong et al., 1981). Early models for the evolution of the forearc region (Karig, 1971; Karig and Sharman, 1975) proposed that accretion of oceanic plate, seamounts, and sediment have created an unusually thick and wide forearc. However, the lack of an accretionary prism, the lack of sediment in the trench axis (Hussong and Uyeda, 1981), and the crustal structure determined from seismic refraction studies (LaTraille and Hussong, 1980) suggested that little, if any, of the subducting plate was preserved in the forearc. Diverse rock types recovered through dredging in the outer forearc, south of latitude 18°N, include siltstone, chert, lava, gabbro, and ultramafic rocks; they represent all the elements of an ophiolite suite (Bloomer and Hawkins, 1983). The composition of lavas recovered by dredging (Bloomer, 1983; Bloomer and Hawkins, 1983; Bloomer and Hawkins, 1987) and drilling in the forearc during DSDP Leg 60 (Meijer et al., 1981; Sharaskin, 1981; Wood et al., 1981) are all, with one exception, of arc-related composition (island arc tholeiites [IAT], boninite). A few fragments of alkalic basalt, thought to be locally accreted seamount fragments, were recovered during dredging of the inner trench wall (Bloomer, 1983). No rocks with mid-ocean-ridge

basalt (MORB) compositions were recovered from the forearc during these studies.

Sparse Cretaceous microfossils were recovered at DSDP Sites 460 and 461 (Azema

and Blanchet, 1981; Hussong et al., 1981) in the inner trench wall. On the basis of

these seismic and geochemical data, tectonic erosion and arc volcanism were proposed

as the dominant mechanisms of forearc evolution (Bloomer, 1983; Bloomer and

Hawkins, 1983; Hussong and Uyeda, 1981; Mrozowski and Hayes, 1980). However,

interpretations of seismic data, from the southern-most portion of the Mariana

forearc (12°N; Karig and Ranken, 1983) suggest at least one post-Oligocene episode

of accretion.

Recently, a suite of rocks representing the crustal sections of an ophiolite

suite -sediment (15%), radiolarian chert (27%), and mafic to intermediate

extrusive and intrusive rocks (55%)- was dredged from a steep, 2000-m-high,

southwest facing scarp in the outer forearc at latitude 19°38'N about 50 km arcward

from the trench (Chapter 3) (Figs. 6.1 and 6.2). A similar suite which included

sparse ultramafic rocks (<3%) was recovered at latitude 17°50'N (Johnson and

Fryer, 1990), no dates are available from this site. Geochemical data indicate that

the lavas from both sites represent at least three tectonic associations: (1) mid-

ocean ridge, represented by tholeiitic basalts (MORB), (2) ocean island, represented

by alkalic ocean-island basalt (OIB), and (3) island arc, represented by IAT and

boninites. These data show that oceanic plate lavas are present in the Mariana forearc

but that they are associated intimately with island-arc lavas. The close proximity of

ocean-plate and island-arc lavas, and the presence of Cretaceous cherts at latitude

19°38'N suggest that this exposure is an accreted block (or blocks) of oceanic plate

that has been tectonically disrupted and possibly intruded by arc volcanism. The

presence of mixed lava types in two sites suggests multiple emplacement and

disruption events. This interpretation is contrary to the predominantly accepted idea

that the major forces shaping the Mariana forearc have been tectonic erosion and arc-related volcanism.

6.3 Age Relationships of Forearc Rocks

The earliest suggestion of ancient rocks in the forearc is from a pebble conglomerate containing *Calpionella*, a late Jurassic to early Cretaceous planktonic microfossil recovered from the base of Deep Sea Drilling Project (DSDP) Hole 460 in the inner trench wall (Azema and Blanchet, 1981). Sparse, reworked, radiolaria were recovered at DSDP Sites 460, identified as Campanian, and 461, identified only as Cretaceous (Hussong et al., 1981). Upper Cretaceous foraminifers were recovered in the volcaniclastic apron from DSDP Site 290, just west of the Palau-Kyushu Ridge (Karig and Ingle, 1975). Because of the small size and isolated nature of these samples they were dismissed as pieces of transported, reworked sediment. However, recently determined paleontological and radiometric dates document the presence of Cretaceous oceanic crust in the Mariana forearc more than 50 km west of the trench axis and more than 100 km north of DSDP Sites 460 and 461. Radiolarian cherts from our recent dredge hauls at latitude 19°30'N yield two distinct deep-water assemblages, which fix the age of the cherts at middle to late Valanginian and Albian (Fig. 6.3). These zones correspond to Mesozoic magnetic anomalies M14-10 (131-138 Ma) and M0 into the beginning of the Cretaceous magmatic quiet period (97-112 Ma) (Harland et al., 1982). Foraminifers (Hedbergella planispira and H. sigali) extracted from the cherts with the radiolaria have been dated as Aptian to Albian, coincident with the radiolarian ages from the same samples. No foraminifers were present in the Valanginian age samples. The Early Cretaceous radiolaria are similar to faunas found in the Great Valley Group and the Franciscan Complex of California

Table 6.1. WHOLE ROCK K-Ar AGES
MARIANA FOREARC

Sample	K (wt %)	radiometric ^{40}Ar (10^{-8}ccSTP/g)	non-radio-metric Ar (%)	K-Ar age (Ma)
7-1 *	0.62	214.7 ± 2.4	13.7	87.1 ± 2.7
7-49†	3.83	1064 ± 12	14.7	70.2 ± 1.6
4-10§	0.73	111.3 ± 1.1	6.3	38.9 ± 1.2

Note: Analyses by T. Itaya; decay constants after
Steiger and Jager (1977).

* Fine-grained metabasalt with MORB-like trace
element characteristics (from Chapter 3).

† Medium grained, highly metamorphosed, alkalic
basalt. From T. Ishii (1988, unpublished data).

§ Fresh, glassy boninite (from Chapter 3).

(Pessagno, 1977a) and from DSDP Leg 7 Sites 60 and 61 just east of the present day trench (M. Silk, unpublished data). K-Ar ages determined for three lavas yield 87.1 ±2.7 Ma for an altered fine grained lava with MORB-like incompatible element abundances, 70.2 ±1.6 for a highly altered medium grained alkalic lava, and 38.9 ±1.2 Ma for a fresh, glassy boninite (Table 6.1). The 87 and 70 Ma ages are minima because of the degree of alteration of the samples and thus may be consistent with the 125 Ma age for the cherts. The boninite is relatively fresh and the K-Ar date is interpreted as a true age. Although the dated samples are from two different dredges (Fig. 6.2), these dredges are within 3 km of one another, and rocks representative of the entire suite --cherts and lavas with MORB-like, alkalic and boninitic compositions-- were recovered in a single dredge (dredge 7, Fig. 6.2).

6.4 Discussion

The current episode of subduction in the Mariana system began about 45 Ma, just before the change in motion of the Pacific plate (Clague and Jarrard, 1973). Rocks or sediments older than 45 Ma must represent either accreted or trapped fragments of oceanic plate. On the basis of crustal ages of the West Philippine Basin, it is estimated that the age of the oceanic plate that could have been trapped to form the forearc is less than 56 m.y. (Hilde and Lee, 1984). Thus, rocks older than 56 m.y. are probably accreted.

We suggest two possible mechanisms for the accretion of oceanic plate in the outer Mariana forearc. First, accretion may have occurred following collision with a seamount chain or an aseismic ridge (Lallemand and Le Pichon, 1987; von Huene and Lallemand, 1990) (Fig. 6.4). Steep-walled reentrants in the inner trench wall appear to form where such collisions are occurring (Fig. 6.4B). Crustal fragments, broken off the deforming subducting ridge, may become emplaced along the walls of

the reentrant (Fig. 6.4C). Further accretion(?) and/or extensive lateral faulting in the forearc may close off the reentrant; a graben structure would form and accreted oceanic plate would be trapped far from the trench axis (Figs. 6.2 and 6.4D). Accretion of faulted oceanic plate may also occur in a similar manner. Second, if a slice of oceanic crust becomes underplated at a shallow depth beneath the outer forearc, perhaps by downstepping of the décollement, it could later be exposed along steep faults in the outer forearc. Faults, thought to reach as deep as the décollement, are inferred from preliminary three-dimensional gravity modeling (Newsom and Fryer, 1987; and unpublished data) and appear to control the northwest wall of the graben (Fig. 6.2). These faults have been suggested as conduits for serpentine muds (Fryer and Fryer, 1987). Either of these mechanisms would allow for the juxtaposition of oceanic plate with preexisting island-arc rocks. Further mapping, dredging, seismic studies, diving, and deep drilling are needed to determine which, if either, model is most appropriate.

6.5 Conclusions

The ages of lavas and cherts from the outer Mariana forearc at latitude 19°38'N suggest that the sampled rock suite is an accreted piece of Lower Cretaceous normal ocean crust overlain by a thick chert accumulation (Valanginian to Albian). This crust is too old to have formed in situ or to have been part of an original plate trapped to form the Mariana forearc. The presence of two "ophiolite suites," one of supra-subduction zone origin (Bloomer and Hawkins, 1983) and one of oceanic plate (mid-ocean ridge) origin (Chapter 3), requires multiple tectonic events in the evolution of the Mariana forearc. Simple arc volcanism and obduction models are insufficient to explain the complex relationships observed. A combination of tectonic erosion of the inner trench wall, extensive vertical and possibly lateral tectonic

deformation, and episodes of accretion of fragments of oceanic plate is required. If this forearc were to become emplaced at the edge of a continent, interpretations based on only a small number of the observed ophiolite suites could lead to incorrect conclusions regarding the source of the obducted rocks. Thus, tectonic reconstructions of ancient forearc exposures on land must take into account the diversity of currently forming convergent margins such as the Mariana forearc. The controversy regarding the origin of the highly complex ophiolite terranes in the Coast Ranges of California (MacPherson et al., 1990) is one such example where a model incorporating multiple emplacement events and source areas might apply.

	UPPER JURASSIC				LOWER CRETACEOUS						SERIES		Zonal Terminology for Upper Jurassic -- Lower Cretaceous

UPPER JURASSIC

LOWER CRETACEOUS

SERIES

STAGE

UPPER KIMMERIDGIAN / LOWER TITHONIAN · LOWER TITHONIAN · UPPER-MIDDLE TITHONIAN · BERRIASIAN · VALANGINIAN · BARREMIAN HAUTERIVIAN · APTIAN · ALBIAN

Zonal Terminology for Upper Jurassic -- Lower Cretaceous

RADIOLARIAN ZONATION — ZONE / SUBZONE

Sample codes for presence

Eucyrtidium (?) ptyctum -- Parvicingula s. s. — 0

Parvicingula s. s. -- Emiluvia hopsoni — 1

Emiluvia hopsoni / Mirifusus guadalupensis · Mirifusus baileyi — 2 (a / b)

Tsilosche ordinaria -- Parvicingula hsui — 3

Parvicingula altissima — 4

Obesacapsula rotunda / Parvicingula jonesi · Pseudoeucyrtis paskentaensis · Cecrops septemporatus — 5 (a / b / c)

Parvicingula -- Thanaria conica — 6

Kozurium zingulai — 7

Petasiderma foremanae — 8

NUMBER

Sample codes: 8-1 ◑ Oɜ-2 ● 8-12 ◖ 8-13 ▣ 8-29 △ 8-69 ▶

samples with open symbols also contain foraminifera

Sample symbol	Taxon	
▶◑●	Acanthocircus	dicranocanthus
▣	Archaeodictyomitra	apiara
○	Crolanium	triquetrum
△	Dictyomitra	multicostata
○	Mita	magnifica
▣◖	Obesacapsula	rotunda
●	Obesacapsula	Sp. aff. O. morroensis
▶	Pantanellium	corriganesis
◖●●	Podobursa	tricantha
○	Pseudodictymitra	lodogaensis
▪	Pseudodictymitra	pentacolaensis
△	Stichomitra (?)	euganea
▶△	Xitus	antelopensis
△○	Xitus	plenus
▶○	Xitus	spicularius
▣	Xitus	spineus

Figure 6.3. Radiolarian zonation for the Lower Cretaceous of the Outer Mariana forearc at latitude 19°38'N. Zones after Pessagno, (1977a; 1977b); analyses by M. Silk, and D. Jones.
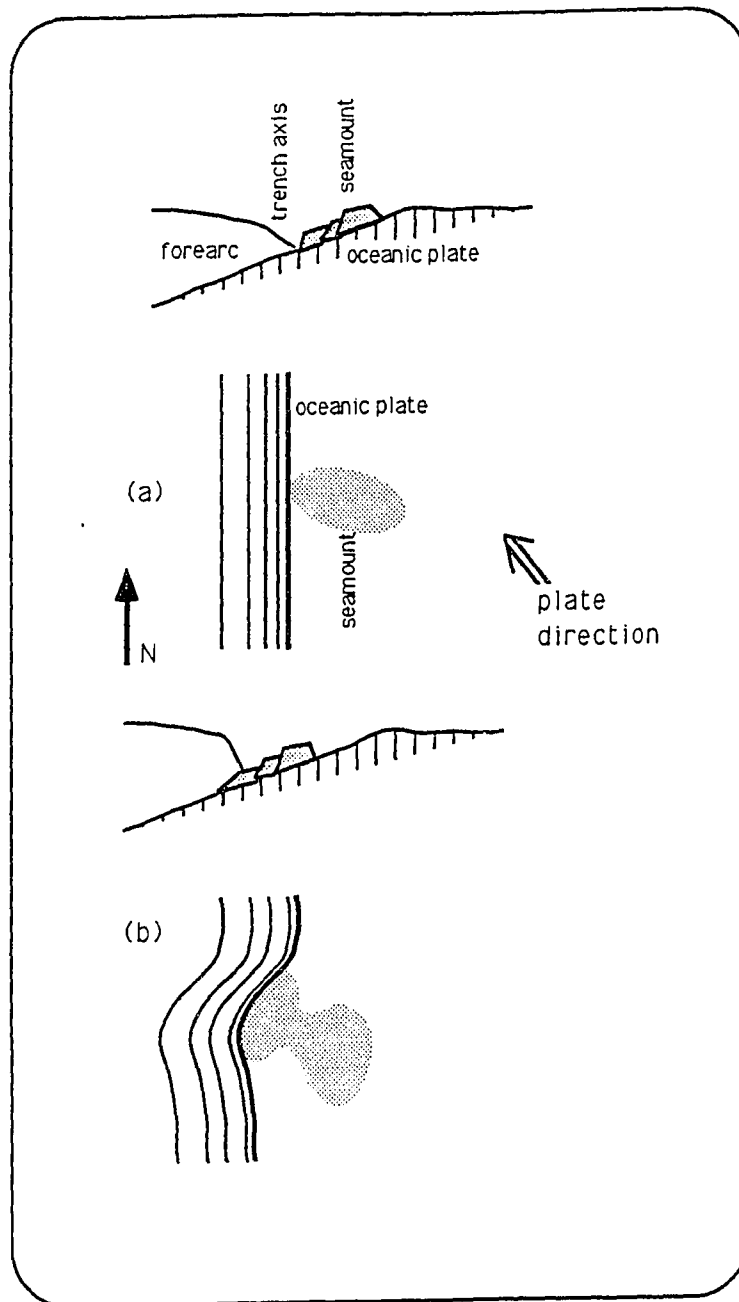
Figure 6.4. Schematic drawing of one model for accretion of oceanic crust and the formation of steep walled grabens. Dotted areas denote seamount or aseismic ridge, all contours are generalized. In plan view the heavy contour is meant to represent the trench axis. Plate motion direction is schematic. (A) Situation before seamount reaches trench axis. (B) Seamount, or aseismic ridge, entering subduction zone will be faulted and fractured and deform inner trench wall, creating steep-walled reentrant.
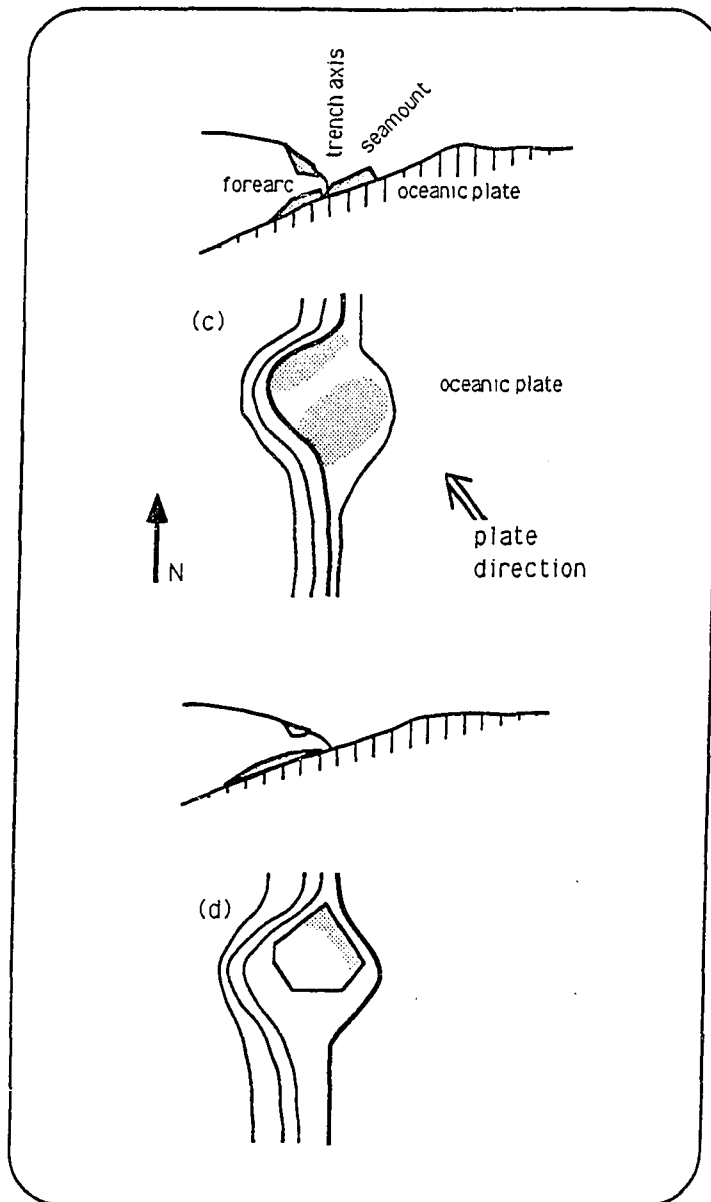
Figure 6.4. (C) Piece of subducting crust may be torn from main edifice and become accreted to walls of reentrant, remainder of edifice subducts. If seamount were moving northward with respect to trench axis, as in Mariana region, accretion would preferentially take place along northern walls of reentrant. (D) Geomorphic setting observed today: graben with very steep northern side and shallow southern side (see Fig. 6.2). Accreted rocks crop out on the northeast wall. Steep-walled reentrant has been closed off by faulting of arc material parallel to trench and/or by additional accretion of oceanic crust.

Chapter 7:

Ridge Collision and Forearc deformation in the

Northern Mariana Subduction Zone:

Implications for tectonic erosion and accretion in hardrock forearcs

7.1 Abstract

Interpretation of geophysical data at 20°20'N, where the Dutton Ridge (DR) is colliding with the outer Mariana forearc, indicate three tectonically defined regions. (1) A faulted near-trench region of the Pacific plate and the fractured seamounts of the DR; (2) over-steepened and faulted inner trench wall and locally shallow trench axis, and (3) tectonically deformed outer forearc consisting of an outer forearc high, two small (volcanic ?) seamounts, a shallow basin and a broad uplifted block. Geophysical data include SeaMARC II sidescan, analog single channel seismic profiles, magnetics and free air gravity.

Single channel seismic and 3.5 kHz bathymetric profiles running north-south across the DR show an increase in fracturing and breakup of the edifice as it approaches the trench. Large faults that cut the DR seamount and inner trench wall generally trend 135-145° similar to spreading fabric on the Pacific plate. The occurrence of faults with similar trends on the DR seamount and inner trench wall suggest a coupling of stresses across the plate boundary. The trench shallows by over 1500 m at the intersection with the subducting ridge and is cut by minor bathymetric reentrants. Hummocky topography in the trench axis and regions of mottled backscatter on the sidescan images suggest egress of fluids along the décollement or over-pressuring of water rich sediments in the convergence zone. The inner trench wall is over-steepened north of the subducting ridge and cut by faults, with offsets of

200-450 m, and slump structures, up to 7500 m across. The outer forearc high is a semi-continuous ridge trending 120°, approximately parallel to the trench axis. Two small seamounts, one with over 500 m of relief, sit on top of the high. The northern seamount lacks significant sediment cover, is 8 km from the break in slope of the inner trench wall and is adjacent to a small basin. The southern seamount is highly sedimented and coincides with the break in slope of the inner trench wall. A shallow basin, situated about 18 km from the trench axis at 20°15'N, is 16 by 34 km across and bounded on the SW side by a 450 m scarp that trends 105°. Small faults are common across the outer forearc but do not cross either the small seamounts or the small basin. At the western edge of the survey area is a regional uplift rising over 1500 m from the surrounding forearc.

A highly faulted forearc and inner trench wall adjacent to a fractured, elevated block of lithosphere (seamount plus underlying plate) may be the ideal place for accretion. I have demonstrated the presence of accreted oceanic plate along a steep wall of a basin at approximately 19°30'N (Chapters 3 and 6) and hypothesize that regions of seamount subduction and basin formation may be sites of tectonic accretion events.

7.2 Introduction

The interaction of seamounts or ridges with a subduction zone has profound morphologic effects on the inner trench wall, the outer forearc and the colliding edifice. Studies of these effects may provide clues to the evolution of forearc and trench regions. The effect that colliding bodies will have on the forearc and inner trench wall must be influenced by the structure of the subduction margin. Erosional forearcs are characterized by rock outcrops in the inner trench wall, little or no

sediment in the outer forearc and the lack of an accretionary wedge, and erosion of the overriding plate at the toe of the forearc or inner trench wall is common (Mrozowski and Hayes, 1980; Hussong and Uyeda, 1981; Bloomer, 1983). An accretionary forearc is characterized by a thick prism of off-scraped sediment and perhaps accreted crustal fragments (Karig and Sharman, 1975; Dickinson and Seely, 1979). Accretionary margins may be more prone to the effects of seamount collision than are erosional margins. Erosional forearcs, including the Mariana and Tonga forearcs, are sometimes referred to as sediment starved (Ballance et al., 1989) or "hardrock" forearcs.

Ridges and isolated seamounts are quite common on the Pacific plate; eventually these edifices reach the trench and must either be subducted or become part of the overriding plate (tectonic accretion). The subducting edifice and underlying oceanic crust are fractured and faulted during the subduction process (Fryer and Smoot, 1985). Both morphologic and geophysical effects of seamount collision/subduction are recorded in the forearc region. Morphologic effects include: (1) structural disruption and over-steepening of the inner trench wall and shallowing of the trench axis (Fryer and Hussong, 1985; Collot et al., 1985); (2) subsidence and basin formation in the forearc (Collot and Fisher, 1989) and uplift of the forearc (Fryer and Smoot, 1985; Yamazaki and Okamura, 1989); (3) accretion of oceanic plate rocks, seamount rocks and sediment to the inner trench wall and the outer forearc (e.g., Ballance et al., 1989; Yamazaki and Okamura, 1989; Chapter 6); and (4) accelerated tectonic erosion of the inner trench wall (Ballance et al., 1989). Geophysical effects include anomalous gravity and magnetic signatures caused by the addition or removal of forearc crust (Yamazaki and Okamura, 1989), and deep structural disruption that can be observed on seismic profiles (Fisher et al., 1986).
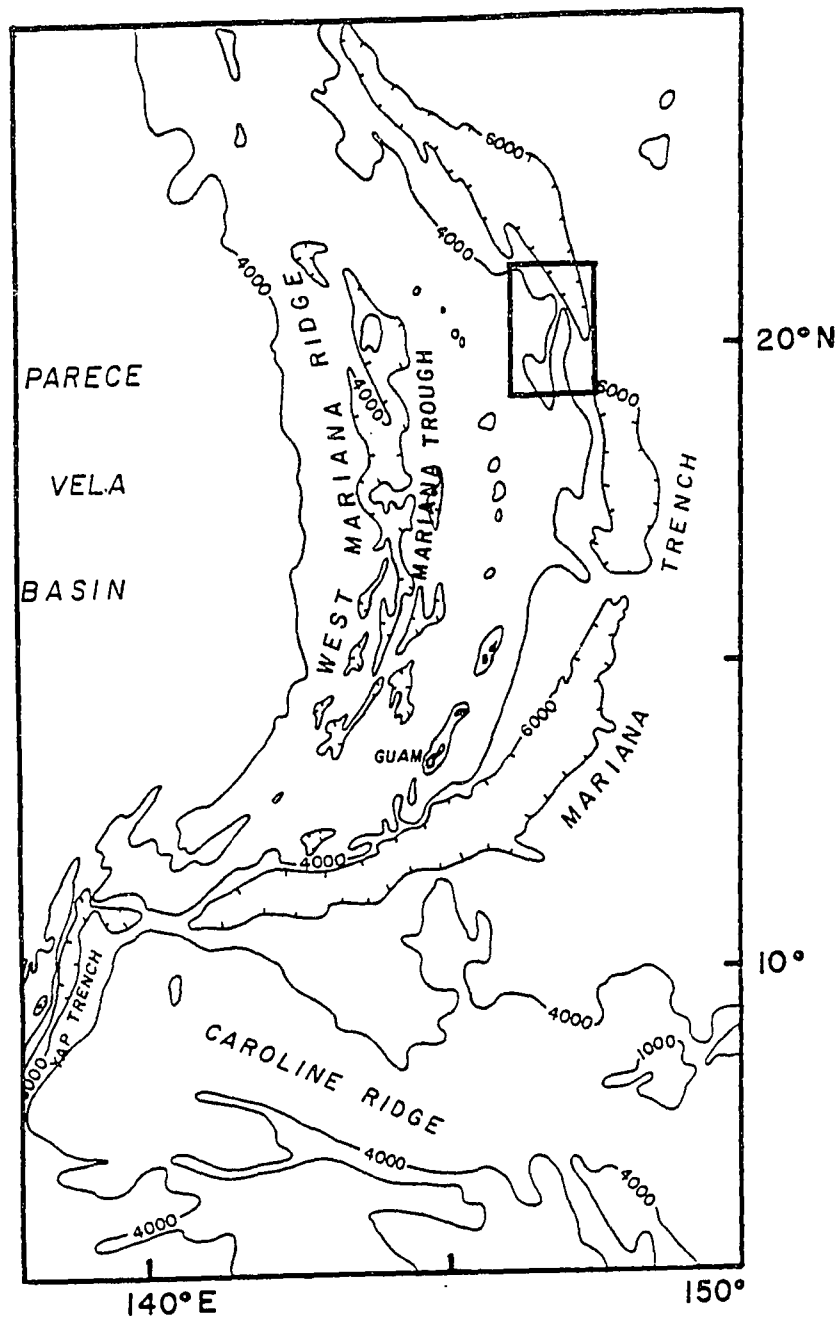
Figure 7.1a. General location map of Mariana Island Arc system. Box denotes area of figure 7.1b.

21°

20° 30'

20°

19° 30'
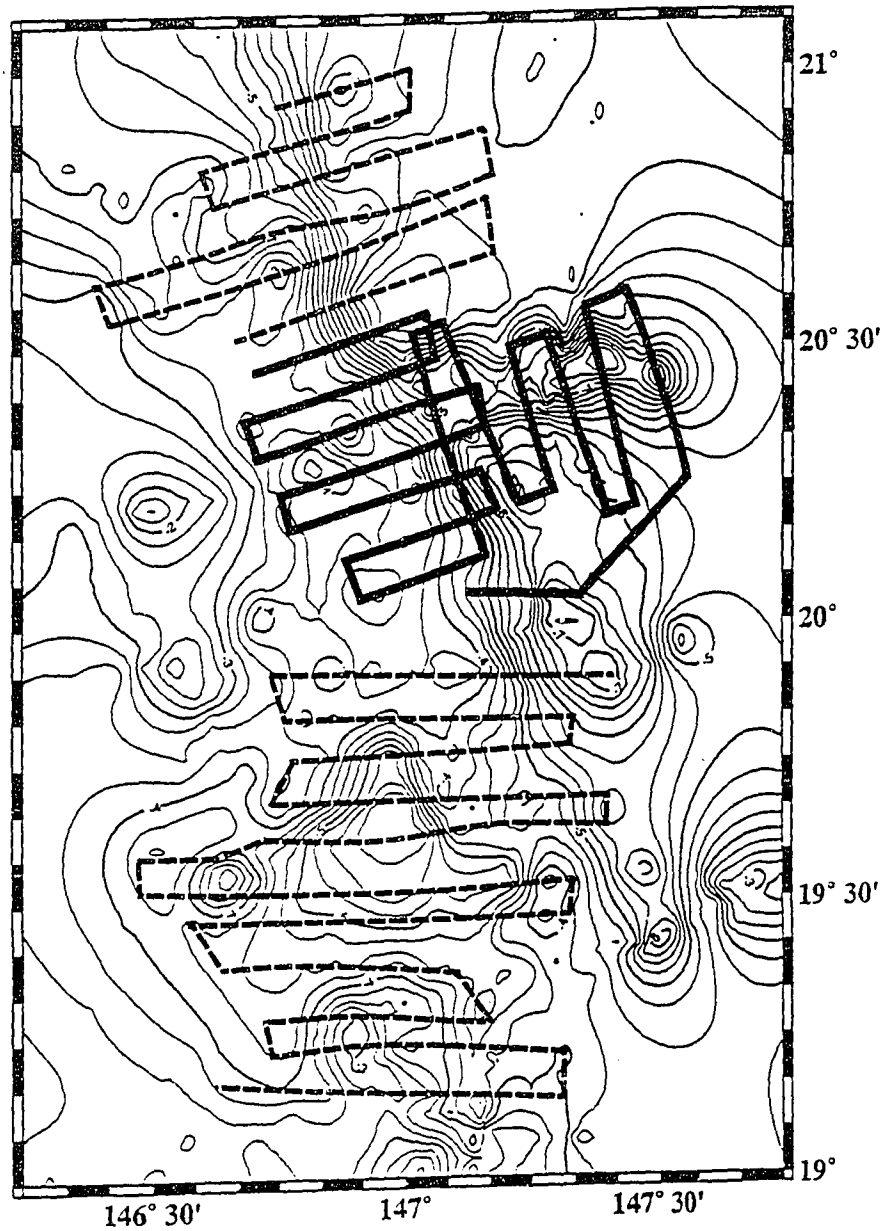
19°

146° 30'   147°   147° 30'

Figure 7.1b. 3.5 kHz bathymetry map. Contour interval is 250 m, tracklines from 1983 SeaMARC II surveys are shown. Thick black lines are the survey discussed in this paper. Dashed lines north of this study are Fryer and Hussong, (1985) and south of this study are Hussong and Fryer, (1985).

Other effects such as gaps in arc volcanism (e.g., McGeary et al., 1985) have been observed in some areas, but will not be discussed in this chapter.

In this Chapter I describe the forearc morphology at 20°20'N, where a collision is presently occurring (Figs. 7.1 and 7.2). I then compare this area to the forearc at 18°N, where there is no present day collision, and to the the forearc at 19°30'N (Chapter 3) and 20°45'N (Fryer and Hussong, 1985) where I infer past collision events.

7.3 Background to Studies of Subducting Seamounts and Accretion

Seamount fracturing. Fryer and Smoot, (1985) found that seamounts smaller than 40 km diameter fracture similar to the surrounding plate, whereas those between 40-100 km diameter show less evidence of fracturing. The enhanced fracturing of smaller seamounts may facilitate subduction, and the less fractured, larger edifices may be more likely to become partially accreted. The part of DR chain presently at the trench axis is approximately 10-15 km in diameter.

Accretion. On the basis of a study of the Tonga forearc, Ballance et al. (1989) suggested that seamount debris have little chance of permanently remaining in the forearc, and little hard evidence for accretion in either the Mariana or Tonga forearcs exists. A small volume of Cretaceous sediments was recovered in DSDP sites 460 and 461 in the Mariana forearc (Azema and Blanchet, 1981) and alkalic basalts, presumably derived from subducting intraplate seamounts, were recovered by dredging in the inner trench wall (Bloomer, 1983). However, I have shown in Chapter 6 that igneous oceanic plate and seamount fragments as well as sedimentary cherts from the oceanic plate are present, over 60 km from the trench axis, in the outer Mariana forearc at 19°30'N.

Erosion. Seamounts on the Pacific plate that are colliding with the Tonga forearc seem to create a tunnel in the inner trench wall as they subduct (Ballance et al., 1989). This may leave holes in the outer forearc, allowing the collapse of overlying crust. Ballance et al. (1989) suggested that erosion rates as high as 50 km/my may occur where the Louisville ridge intersects the inner trench wall of the Tonga trench. Supra-subduction zone (SSZ) rocks, including island arc tholeiite and boninite, have been drilled in the outer Mariana forearc (Hussong and Uyeda, 1981; Sharaskin, 1981; Wood et al., 1981) and are exposed in the inner trench wall (Bloomer, 1983). Because the formation of such rocks is thought to occur at least 50-100 km from the trench axis, their presence in the outer forearc and inner trench wall requires at least 50 km of erosion of the forearc since inception.

Uplift and Embayment. Yamazaki and Okamura (1989) suggested a sequence of morphologic effects in the outer forearc during subduction of a seamount in the Izu-Bonin subduction zone. As subduction commences a topographic swell forms ahead and an embayment behind the subducting edifice; later the uplifted rocks will slump into the embayment and the swell eventually becomes the outer forearc high (Yamazaki and Okamura, 1989). They conclude that the type of forearc, accreting or eroding, does not effect this process. However forearc regions that are not opposite subducting seamounts (e.g., Karig, 1971) also have outer forearc highs, suggesting that other processes must be involved. In contrast, studies of the d'Entrecausteaux collision in the New Hebrides conclude that subducting ridges do not always disrupt the forearc (Fisher et al., 1986).

7.4 Background to the Northern Mariana Area

In the Western Pacific, at approximately 20°20'N, the DR is colliding with at the Mariana trench. Detailed Navy SASS bathymetry of the DR, a series of 5 seamounts and guyots, was collected and described by Smoot, (1983a). These seamounts are characteristically "star shaped" in map-view, rather than circular, with ridges extending from the central part of the edifice. Our SeaMARC II survey imaged the western limb of the seamount that is presently at the trench axis. The linear nature of the DR suggests that seamounts may have continued to the west, like many of the western Pacific seamount chains, but have since been subducted. A SeaMARC II survey just north of our survey area (Fryer and Hussong, 1985) reveals a small seamount that has become partially subducted. Further north at about 26°N another seamount chain, the Michelson Ridge, is colliding with the Izu-Bonin forearc and may have disrupted subduction in that area (Smoot, 1983b). Other seamounts and ridges are present on the Pacific plate in the Western Pacific, and subduction of these edifices is a common occurrence today and was probably so in the past. It is likely that forearc regions of the western Pacific record the effects of past collisions.

7.4.1 Forearc Morphology in the Absence of Active Collision

The forearc just south our survey area (Hussong and Fryer, 1985; Fryer et al., 1985; Fryer and Fryer, 1987) is broken by two large seamounts of serpentinized ultramafic rocks and a deep basin. Rocks from a steep fault bounding this basin are a diverse mix of SSZ rocks and accreted oceanic plate rocks (mid-ocean ridge basalt, alkalic ocean island basalt, cherts) (Chapters 3 and 6). I suggest that the formation of this basin may have been caused by seamount subduction in the past,

and that regions around such basins may be likely sites for accretion of oceanic plate rocks.

Extensive surveys were conducted across the Mariana island arc system, at about 18°N, in association with DSDP Leg 60 drilling (Hussong et al., 1981; Hussong and Uyeda, 1981); thus the crustal structure of the Mariana forearc at 18°N is well known. Seismic surveys included refraction (LaTraille and Hussong, 1980; Ambos, 1984) and reflection (Mrozowski and Hayes, 1980) profiles. Refraction studies revealed a continuous layer at about 3 km sub-bottom depth with a velocity of 6.1-6.5 km/s (LaTraille and Hussong, 1980) underlain by a low-velocity layer (Ambos, 1984). The Moho was not imaged in the outer forearc although estimates just east of the arc place it at between 21.5-18 km (LaTraille and Hussong, 1980; Ambos, 1984). Reflection studies revealed two forearc provinces: (1) a western province (inner forearc) with thick layered sediment, increasing in thickness toward the arc, and (2) an eastern province (outer forearc) with thin (<1 km) sediment that pinches out toward the trench. The outer forearc is cut by numerous normal faults that trend subparallel to the trench and have offsets up to 300 m (Mrozowski and Hayes, 1980). No evidence for compressional features was observed (Hussong and Uyeda, 1981).

7.5 This Study

7.5.1 Methods

The present study is based on simultaneously collected SeaMARC II sidescan, single channel seismic reflection profiles, 3.5 kHz profiles, and magnetic and gravity data collected over the DR and outer forearc between 19°56'-20°40'N and 146°36'-147°40'E aboard the R/V Kana Keoki in 1983. Because of errors in recording bottom
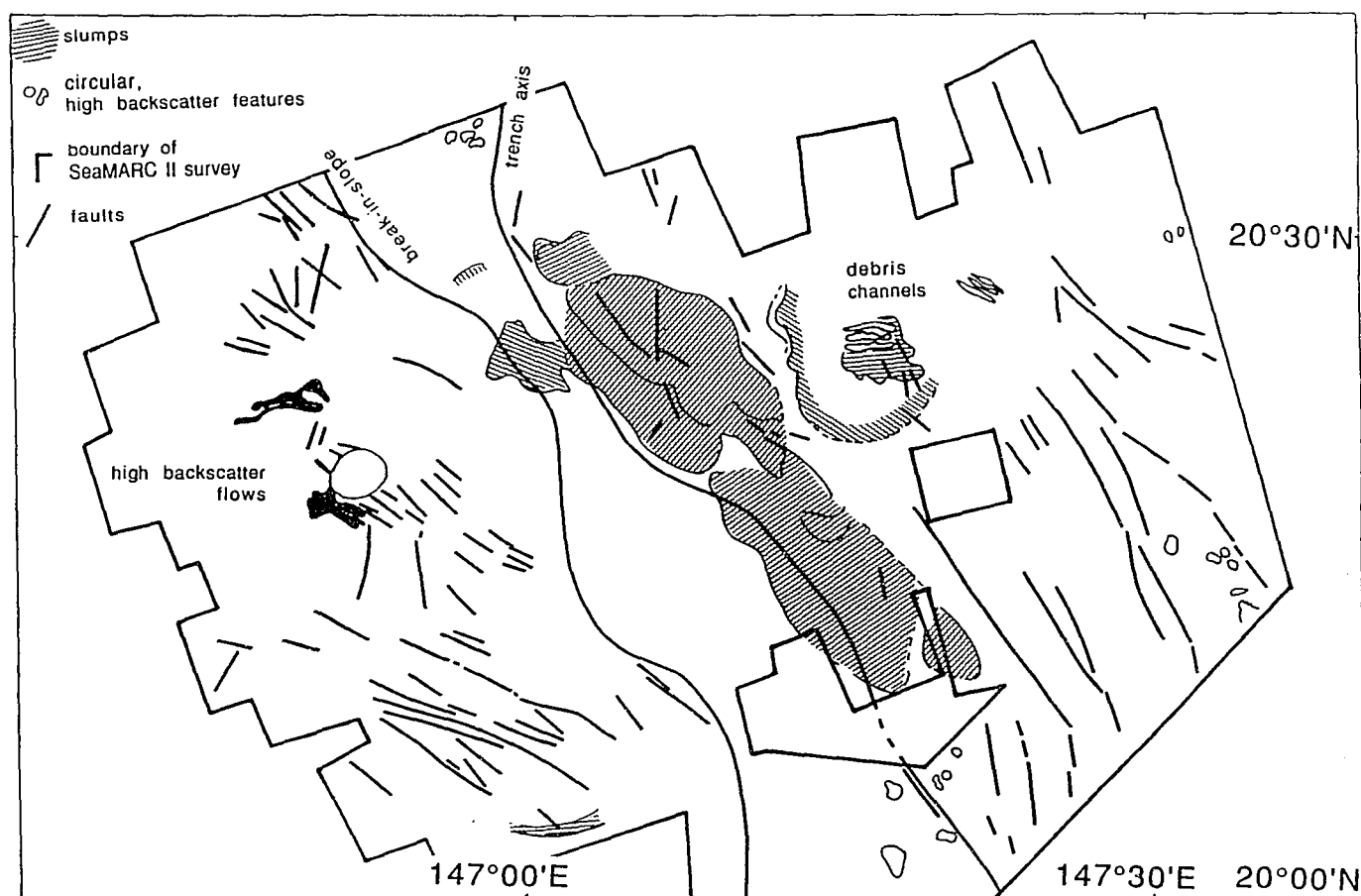
Figure 7.2. Geologic interpretation of SeaMARC II, seismic and bathymetric data.

detection time, SeaMARC II swath bathymetry is presently unavailable. However, re-digitized SASS, 3.5 kHz and other SeaMARC II data have been compiled and contoured to produce Figures 7.1b and 7.3.

Seismic data are mixed frequency (150 kHz to 250 kHz) analog data, collected with a 40 cubic inch air gun (Figs. 7.4 and 7.5). Collection parameters and processing methods for SeaMARC II data are described by Hussong and Fryer (1983) (Fig. 7.6). Gravity and magnetic data were collected simultaneously with the SeaMARC II survey. These data were combined with data from the NGDC database and contoured to produce Figures 7.7, 7.8, and 7.9.

Navigation was accomplished with Loran C and traditional dead reckoning between transit satellites. Further navigational accuracy is achieved by overlap of SeaMARC II sidescan resulting in a relative accuracy of about 100 m. Ship tracks are approximately perpendicular to the trend of features being imaged: those over the DR are generally north-south and those over the inner trench wall and outer forearc are northwest-southeast, perpendicular to the trench (Fig. 7.1b). The objective of this survey was to study the interaction between a subducting seamount and the inner trench wall and outer forearc. Because of the extreme changes in depth from the DR (2700 m) to the trench axis (over 7000 m), the backscatter shown on the SeaMARC II image (Fig. 7.6) was processed to maximize along track variability. This type of presentation is most useful for looking at structural details.

7.5.2 Morphology and Reflection Characteristics of the Dutton Ridge and Outer Forearc

Three tectonic regions are defined by the geophysical data: (1) The western end of DR and surrounding Pacific plate, (2) the inner trench wall and trench axis, and (3) the outer forearc. Each region is described below.
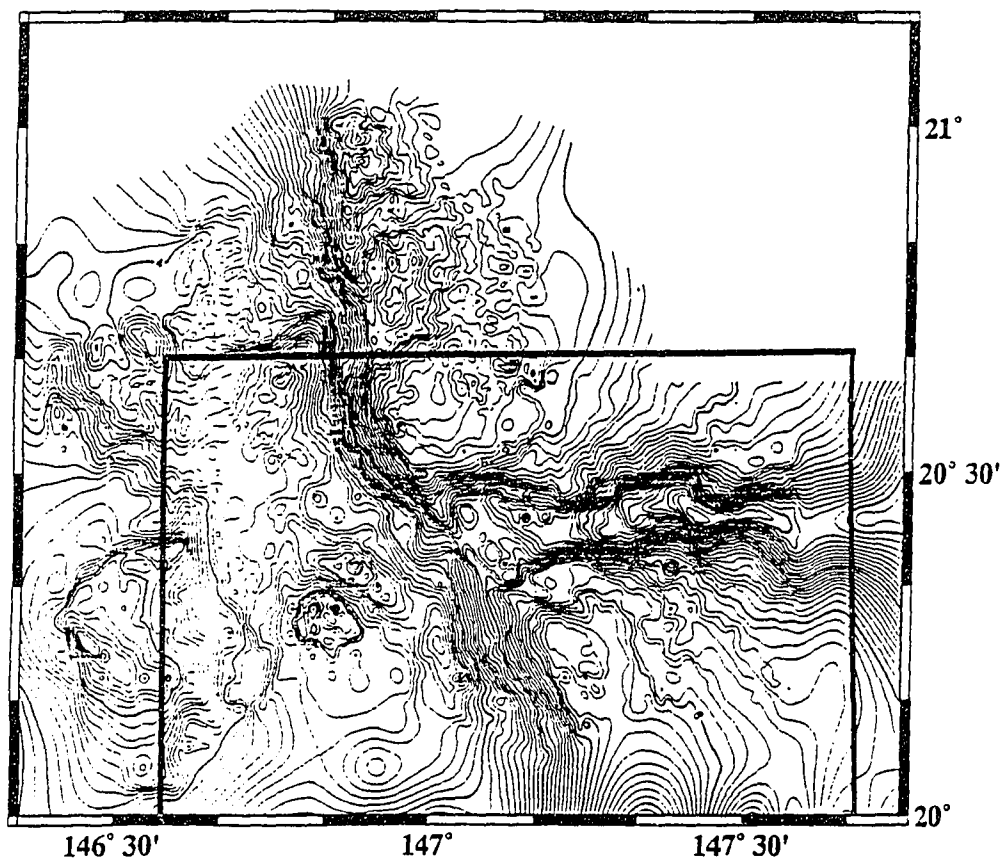
Figure 7.3. Bathymetric map of survey area (in box) and of Fryer and Hussong, (1985) survey (north of box). Data is digitized SASS, SeaMARCII and 3.5 kHz data contoured at 100 m. Tracklines for SeaMARC II survey are shown in Figure 7.1b.

7.5.2.1 Pacific Plate and Dutton Ridge:

Sidescan, Seismics and Bathymetry. The abundance and scale of faults and slumps on the DR imaged in seismic and 3.5 kHz profiles (Figs. 7.4 and 7.5) and imaged on the sidescan (Fig. 7.6) increase to the west as the ridge approaches the trench. The morphology of the seamount limb imaged in our survey changes from a conical, steep-sided edifice (line 10) on the east to a broad, faulted platform to the west (seismic lines #8-16; Figs. 7.3 and 7.4). However, because the edifice is partially subducted and the survey has a limited north-south it is impossible to determine if this effect is caused solely by the interaction with the inner trench wall or if it is a regional feature of the seamount. Small slump features from 50 m high (lines 8-10) to over 250 m high (lines 16; Fig. 7.4) occur on the flanks of the seamounts and increase in frequency and size towards the trench axis. Seismic profiles 8 and 10 (Fig. 7.4), show an unfaulted, steep sided edifice with a rounded top and a small amount of layered sediment on the flanks, however, small faults that strike approximately 120° are observed on the sidescan (lines 8, 10; Fig. 7.6). The top of the seamount flattens out and exhibits incipient faulting in seismic profiles (line 12; Fig. 7.4) about 30 km from the trench axis. About 20 km from the trench the summit of the seamount breaks up into several local highs and faults are clearly visible across the top. Large blocks over 15 km wide, nearly 30 km long (parallel to the trench) and over 700 m high appear to be sliding into the trench (line 16; Fig. 7.4: line 14 and 16; Fig. 7.6). Linear features that strike 080° across lines 12-14 and are floored with low-backscatter material (Fig. 7.6) may be debris channels. Large faults that cut the subducting seamount chain and inner trench wall generally have two orientations, 135-145° and 005°. Line 18 runs nearly along the trench and primarily shows chaotic sediments (Fig. 7.4).

On the Pacific Plate. Lines 5 and 6, south of the seamount, image the Pacific plate. Faults sub-parallel to the trend of the trench axis, 150-160°, have an average throw of 50-75 m and probably represent original seafloor spreading fabric reactivated by bending of the Pacific plate as it subducts. Similar features are imaged to the north (Fryer and Hussong, 1985). A region of hummocky topography and mottled backscatter at the eastern end of line 31 (Fig. 7.6) on the Pacific plate near the trench axis suggests egress of fluids along the décollement. Similar features are imaged south of this survey on the forearc immediately north of the steep scarp at 19°30'N and were the object of an ALVIN dive in 1987 (All-118-15, Dive 1850). On the basis of morphology observed in that dive I suggest that these features may be exposed edges of small fault blocks composed of lithified forearc sediment. One manganese mound, approximately 4 m long by 3 m wide and 2 m high, was discovered at the the top of a local rise in slope and is likely related to egress of fluids along fault block boundaries.

Gravity and Magnetics. DR has a free air gravity high greater than +60 mgals at the summit of the subducting limb (Fig. 7.7), generally consistent with topography. The largest magnetic signature in the map area, -400 nanoteslas (nt) (Fig. 7.8) is over the two eastern peaks imaged in this survey. This signatures rapidly diminishes as the trench is approached and fracturing of the seamounts increases.

7.5.2.2 Inner Trench Wall and Trench Axis

Sidescan, Seismics and Bathymetry. There is a distinct change in the regional trend of the trench axis where it intersects the DR (Figs. 7.3 and 7.7) and shallows from a typical depth of 6000 m to about 4500 m (lines 23-27; Figs. 7.3 and 7.5).
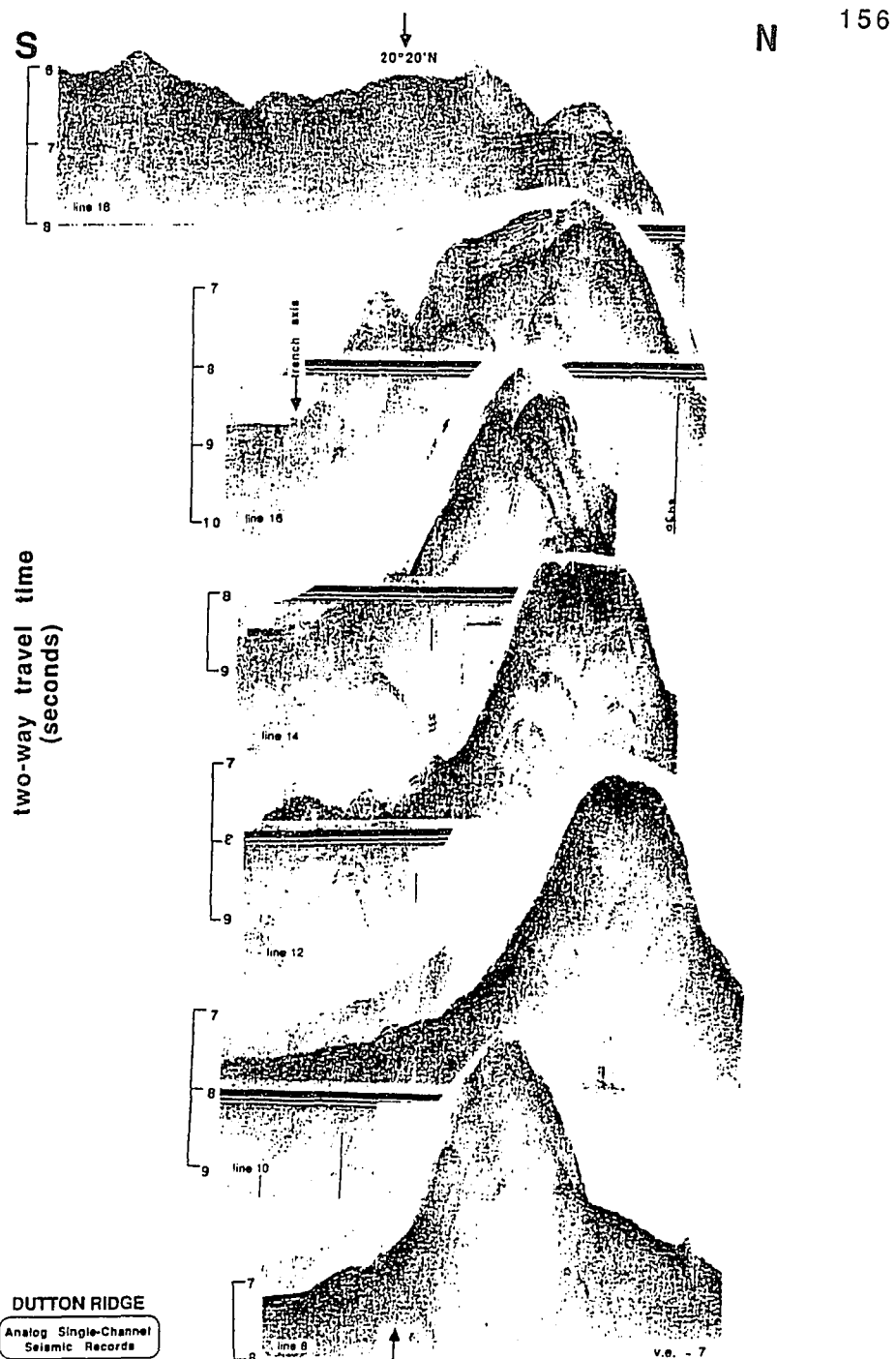
Figure 7.4. Single channel seismic lines over Dutton Ridge where it intersects the Mariana forearc. Note the progressive change from smooth unfaulted ridge at line 8 (eastern margin of survey) to the faulted and slumped ridge at line 16. Line 18 is approximately in the trench axis.
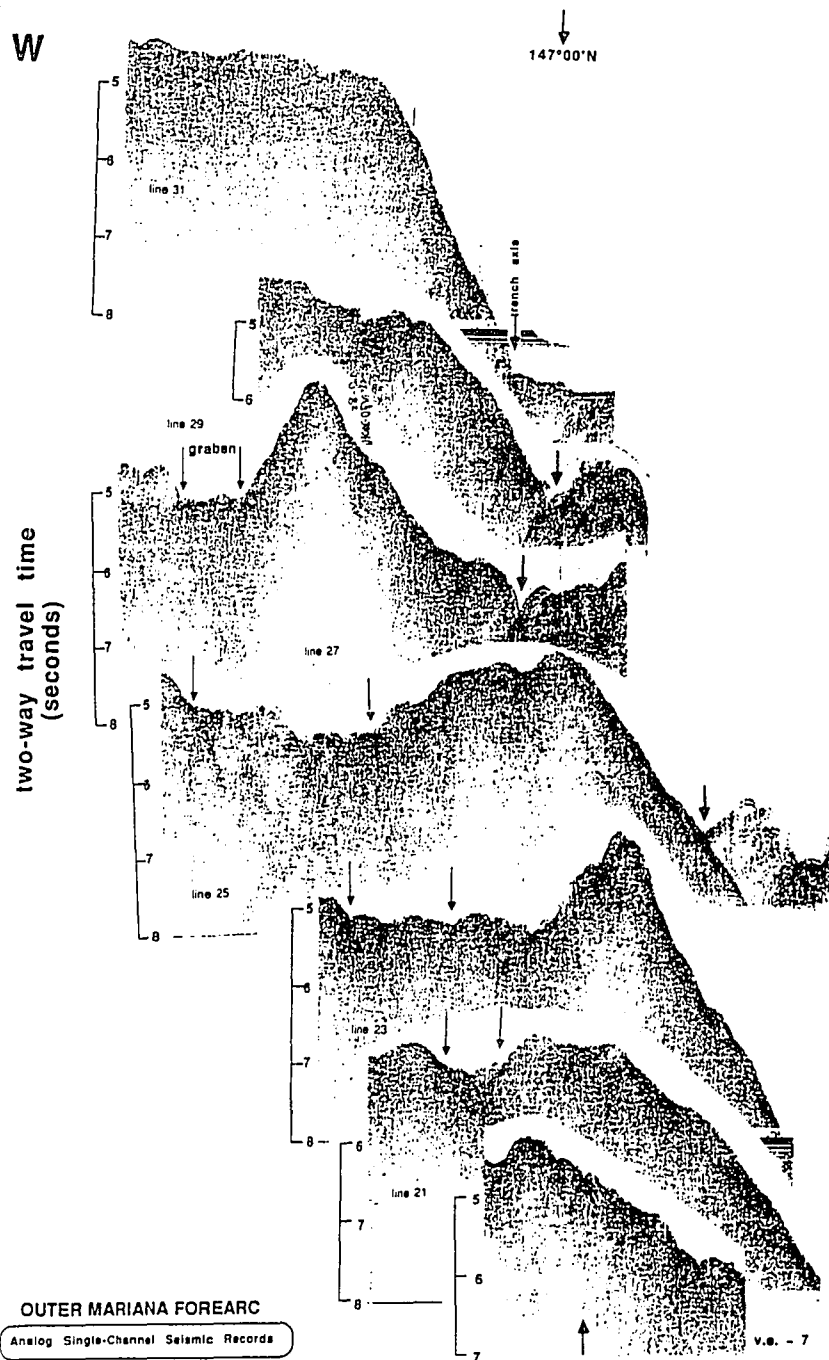
W

147°00'N

E

two-way travel time
(seconds)

line 31

trench axis

line 29

graben

line 27

line 25

line 23

line 21

OUTER MARIANA FOREARC

Analog Single-Channel Seismic Records

v.e. − 7

Figure 7.5. Single channel seismic lines over the outer Mariana forearc at 20°20'N. The trench axis is imaged on lines 25 - 31. The break in slope of the inner trench wall is poorly developed south of the collision (approximately line 25). Note the two small seamounts on lines 23 and 27 and the shallow basin on lines 21-27. The basin floor is hummocky and lacks layered sediments.
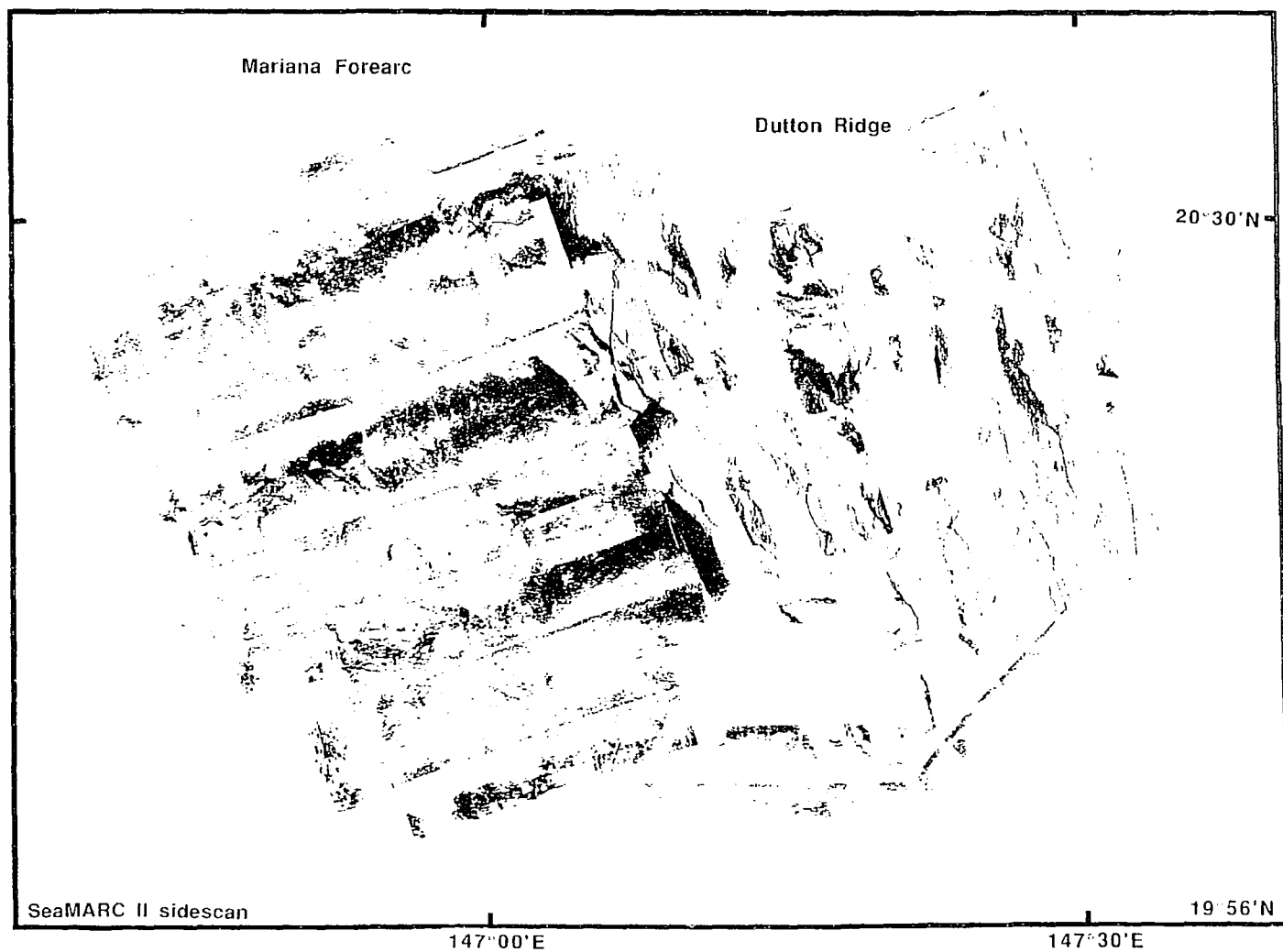
Figure 7.6. SeaMARC II sidescan image. Data was collected on Hawaii Institute of Geophysics (HIG) cruise KK83-01-14, Leg 4 and processed at HIG by K. Sender and L. Johnson. The area of very high backscatter in the center of the image is the trench axis.

The inner trench wall is over-steepened north and south of the subducting guyot (compare lines 23 and 27 21, 25 and 29; Figs. 7.3 and 7.5) and is nearly devoid of sediment except for some small terraces that are best imaged on lines 27 and 23. These small terraces may be related to two small seamounts on the break in slope of the inner trench wall (discussed below). The trench axis is well defined in the SeaMARC II image by an abrupt change from very high backscatter returns (black) to lower energy returns over the chaotic sediments slumping off of the guyot. Unfortunately such high backscatter returns make the sidescan difficult to interpret. The 3.5 kHz profiles show faults, with offsets of 200-450 m that are down on the east side. Slump structures up to 7500 m across are clearly visible in the inner trench wall (Fig. 7.6, between lines 27-29). Faults with similar strike to those found on the DR crosscut the bathymetric trench axis (especially on line 29), suggesting there may be some coupling of stresses across the trench axis. Similar faults have been recognized in the Tonga-Kermadec region (Gnibidenko et al., 1985). These faults, however, may be scarps bounding the edges of large slump blocks that have become (temporarily?) accreted to the inner trench wall.

Over-steepening of the inner trench wall may result from erosion caused by the collision of the DR. The strike of the DR and the direction of motion of the Pacific plate would cause the point of collision to migrate north with time, I thus expect that the inner trench wall south of the ridge to be steeper (more erosion) and has less sediment than to the north. The inner trench wall is steeper north of the collision zone (Fig. 7.3) suggesting that over-steepening occurs in advance of ridge collision. South of the collision there is no true break in slope of the inner trench wall to the outer forearc (Fig. 7.5). Minor bathymetric reentrants observed on the sidescan in

the inner trench wall may provide channels for the products of accelerated erosion of the forearc to reach the trench axis rapidly.

Gravity and Magnetics. The typical free air gravity anomaly along the trench axis both north and south of the intersection with the DR ranges from 120 to -140 mgals. However, at the intersection this value increases to almost 70 mgals (Fig. 7.7). This change is probably simply a consequence of the shallowing of the trench axis and the excess mass of the DR thrust beneath the forearc. The magnetic signature in this area is generally between -100 nt and +100 nt, but there is no distinct anomaly associated with the trench axis and inner trench wall (Fig. 7.8).

7.5.2.3 Outer Forearc

The typical depth of the Mariana forearc is about 3500 m (Fig. 7.1b); however, it is frequently interrupted by seamounts, basins and faults (Fig. 7.2). In the survey area small, semi-continuous faults, a shallow basin elongate subparallel to the trench, and two small (possibly volcanic?) seamounts disrupt the continuity of the outer forearc. Although no distinct uplift correlating to the subducting ridge is observed, a broad, regional high, elongate north-south with over 1500 m of relief ,is present at the western boundary of the study area.

Sidescan, Seismics and Bathymetry. Two small seamounts, on lines 23 and 27 (Figs. 7.2, 7.3 and 7.5), are quite distinct on the SeaMARC II image and bathymetric profiles (Figs. 7.3, 7.5, and 7.6). The southern seamount (line 23; Fig. 7.9), at the break in slope of the inner trench wall, is just under 500 m high and 8 km in diameter, is elongate parallel to the trench, has concentric fractures, and is moderately sediment covered. The western side of the seamount slumps toward the arc. The northern seamount, (line 27; Fig. 7.9) about 15 km to the north, has a

Figure 7.7. Free-air gravity map contoured at 5 mgal intervals; box marks area of SeaMARC II survey (Fig. 7.6). Note the positive signal of the Dutton Ridge and the low signal over the trench. The two small seamounts have small positive anomalies and the shallow basin a negative anomaly.
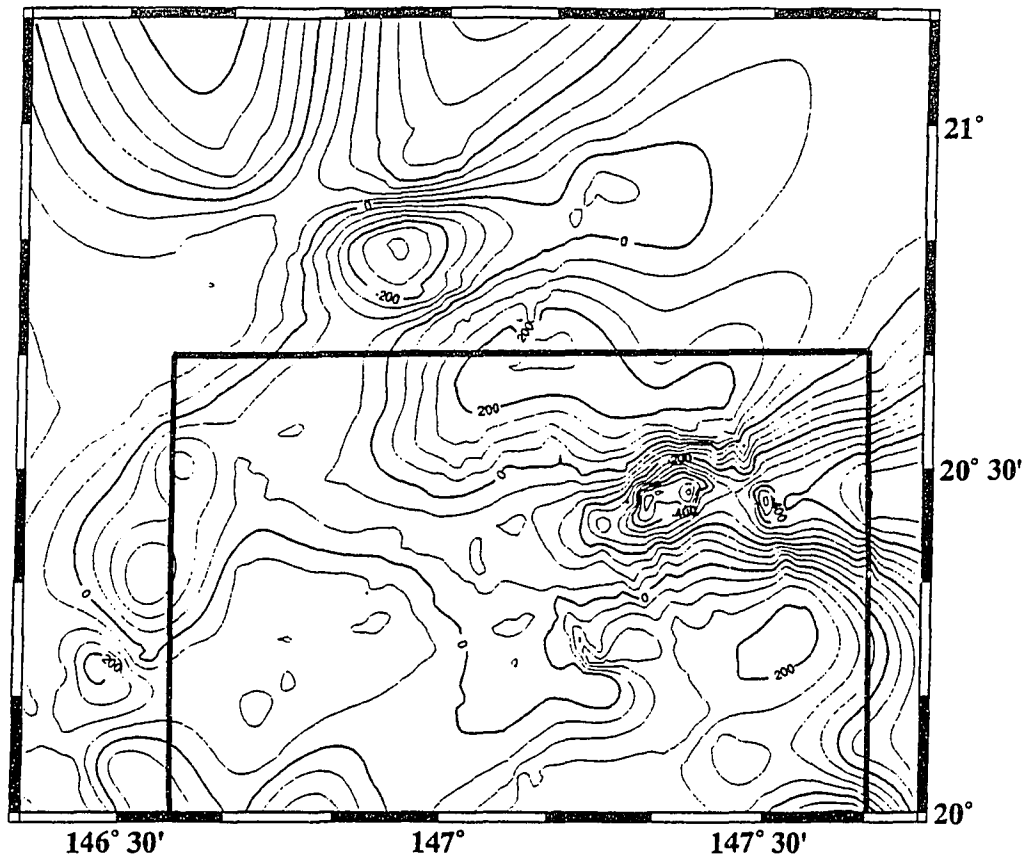
Figure 7.8. Magnetic data, contoured at 50 nanoteslas; box marks area of
SeaMARC II survey (Fig. 7.6). The Dutton Ridge is a distinct magnetic high up
to about 20 km from the trench axis; there is no distinct signal from the
trench axis or in the forearc.

distinctly circular plan view with smooth sides and strong backscatter characteristics (Fig. 7.6). Although the darkest feature on the sidescan is only 4.5 km across, the bathymetric expression of the seamount is about 9 km in diameter and is over 750 m high. The high backscatter return suggests that the northern seamount is unsedimented or only thinly sediment covered and may be quite young. A dark sinuous feature extends from the western flank of the seamount across the bounding scarp of a small basin just west of the seamounts (described below) and may be either a lava or sediment flow.

The break in slope from the inner trench wall to the outer forearc is well-defined north of the collision but less well defined to the south. The inner trench wall is smooth and breaks at a depth of about 4.5 sec. two-way travel time on all lines except 23, where small sedimented terraces are present. At line 25, midway through the the collision zone and between the two small seamounts, the break in slope deepens to about 6 sec two-way travel time. (Fig. 7.5).

At 20°15'N and about 18 km from the trench axis (at line 25). There is a shallow basin, measuring 16 by 34 km across and bounded on the SW side by a 450 m high scarp that trends 105° (Figs. 7.2, 7.3, 7.5, and 7.7). The floor of the basin is essentially devoid of layered sediments and has a hummocky and irregular topography. The basin is poorly defined on the sidescan image (Fig. 7.6) except for the north-west boundary. Total relief between the basin and the northern seamount is over 1250 meters. Small faults that trend about 120°? with small throws (<100 m) down to the west are present across the outer forearc but do not appear to connect from one line to another. This fabric does not continue through the northern seamount nor is it developed across the floor of the shallow basin.

Gravity and Magnetics. The two small forearc seamounts are well-defined on the gravity map (Fig. 7.7) as distinct positive anomalies of -30 mgals, over 20 mgals higher than the adjacent basin. Neither the seamounts nor the basin have a magnetic signature strong enough to dominate the contoured magnetic map (Fig. 7.8). However, profiles over each of the seamounts show a magnetic high offset to the west from the coincident bathymetric and gravity highs by approximately 15-20 km (Fig. 7.9).

Regional Uplift. West of the basin is a large bathymetric high rising to depths shallower than 2000 m (Figs. 7.1b and 7.3). This bathymetric feature is distinct as a gravity high (Fig. 7.7) at +40 mgals and as a small asymmetric magnetic dipole (Fig. 7.8).

7.6 Summary and Discussion

The effects of the collision of the DR with the Mariana forearc are apparent in the morphology of both the overriding and subducting plates. The accumulated effects of subduction over a long period of time may also be observed in the regional bathymetry.

Dutton Ridge. Normal faults on the Pacific plate are reactivated by bending of the Pacific plate as it approaches the Mariana trench. The DR is faulted and disrupted to a progressively greater degree as it approaches the trench. Some of this faulting is sub-parallel to that on the underlying Pacific plate suggesting that the structure of the seamount is coupled to the plate. Over a distance of approximately 30 km the morphology of the ridge changes from smooth and rounded with some layered sediment to fractured with large slump blocks and faults. This change in morphology may be inherited from the original (pre-collision) morphology; however, the increasing

abundance of faults and slumps suggests the change in morphology is caused by the collision. Debris channels, sub-parallel to the trench of the ridge, begin to form about 25 km from the trench axis (line 10; Fig. 7.6) and may indicate the first stages of collision related erosion of the subducting seamount. Sediment and rocks dislodged by extensive faulting and slumping on the seamount are probably moved into the trench axis by these channels. The magnetic signature of the DR decreases rapidly at about the same place where faulting and slumping become pervasive. This may suggest that faulting is sufficiently deep seated to disrupt a previously existing coherent magnetic signature. However, if the ridge itself is a rift feature extending from a central edifice or is composed of sills and interdigitated flows, it may not have had an originally coherent magnetic signature.

Trench Axis. An asymmetric morphology should be created as the DR moves northward, with respect to the forearc, over time. The regional strike of the trench axis bends to the west, the trench axis shallows and the inner trench wall is over-steepened north of where the DR intersects. The shallowed trench axis is caused by the excess sediment provided by erosion of the inner trench wall in the collision zone and by slumping off of the DR. The deflection in trend of the trench axis may be a regional change. The over-steepening north of the collision is probably caused by the interaction between the ridge and the inner trench wall. The smoother inner trench wall and the lack of a well-defined break in slope from the inner trench wall to the forearc south of the collision may be caused by accelerated erosion or it may reflect a return to equilibrium slope conditions following over-steepening in advance of the subducting ridge. Debris is probably transported to the trench axis by small fault bounded or erosion channels in the inner trench wall, however, the shallowed trench axis may act as a dam preventing debris movement along strike of the trench.

Inner Trench Wall. Sidescan images and seismic profiles around 20°20'N and dredges further south demonstrate that the inner trench wall is composed predominantly of outcropping igneous rock. It seems likely that an igneous forearc would be affected differently, and perhaps less, by collision than would a highly sedimented forearc and inner trench wall. The locally over-steepened inner trench wall, the deepened break in slope on line 25, and the slumps and faults in the inner trench wall, some with similar orientations to those on the DR, suggest that stresses may be coupled across the subduction zone and not accommodated solely by uplift and deformation of the forearc. In fact the forearc does not appear to be significantly uplifted by the subducting ridge. Such a coupling would cause fracture of both the subducting ridge and the forearc and may result in increased tectonic erosion and facilitate accretion by moving seamount and oceanic plate fragments into contact with a faulted forearc. Around 19°30'N SSZ rocks exposed presumably by erosion (Bloomer, 1983) and accreted rocks (Chapters 3 and 6) are both present. At 20°20'N the collision with the DR appears to have enhanced erosion of the inner trench wall. However, just north of this survey a subducting seamount fragment appears to be uplifting the forearc without increasing erosion of the inner trench wall (Fryer and Hussong, 1985). Thus it appears that erosion and accretion both can be present along strike in a single forearc and may alternate over the history of the forearc. The cause or causes of the change from erosion to accretion are unknown.

Because the bulk of the ridge appears to be subducted and there is evidence for increased tectonic erosion, the volume of rock and sediment being subducted at 20°20'N is likely greater than that along other parts of the trench. The increased volume of subducted rocks and sediment and the water and other volatiles contained in them may have an effect on the composition of arc lavas.
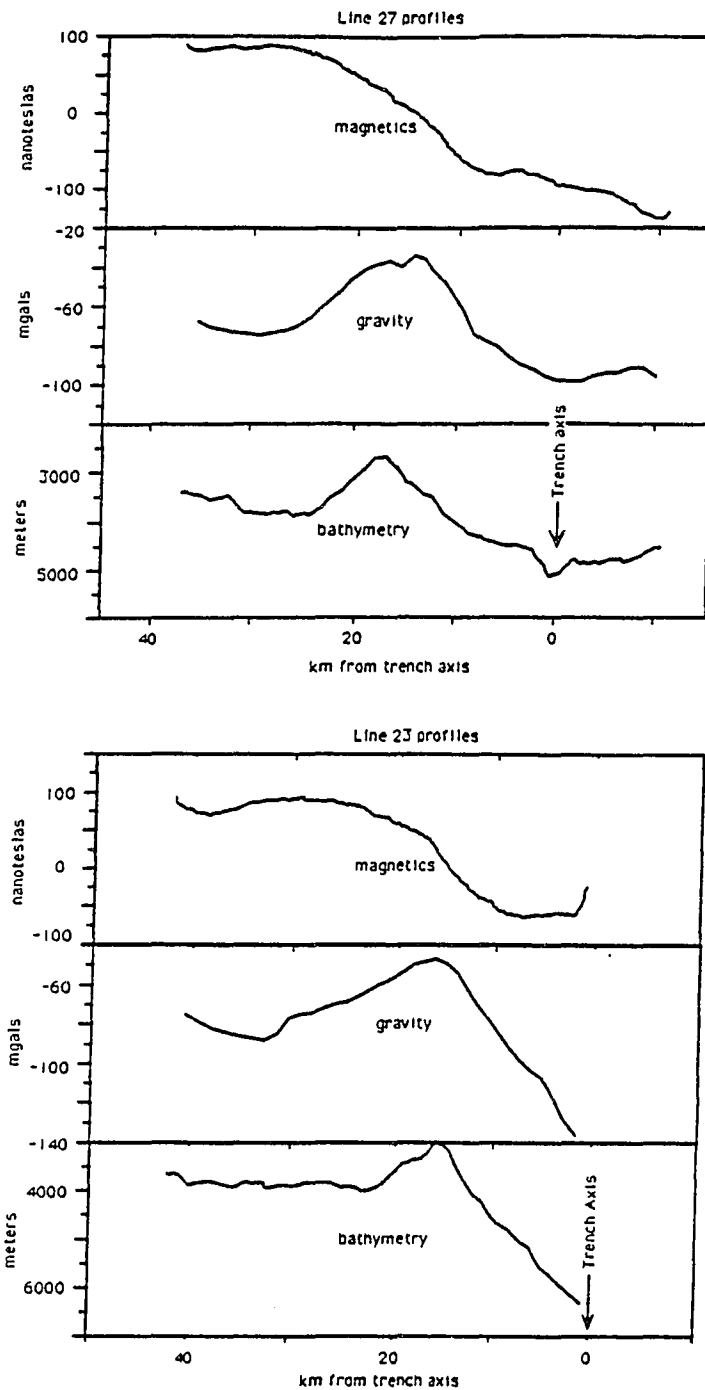
Figure 7.9. Bathymetry, gravity and magnetics profiles for lines 23 and 27, over the two small seamounts. Note the good correlation between the gravity and bathymetry profiles. The small magnetic high is offset approximately 20 km arcward from the bathymetric high.

Seamounts. The apparent relative age relationships (given by the sediment cover and relative size) between the two small seamounts on the break in slope of the inner trench wall supports an origin related to the subducting ridge. As the ridge sweeps northward features related to the passage of the ridge beneath the forearc would be older to the south. These seamounts may be faulted blocks of forearc crust, accreted blocks of subducting plate, sediment accumulations or they may be young volcanism in the forearc. The circular shape, smooth sides and lack of deep faults is not consistent with an origin as uplifted or accreted blocks, however, these seamounts are much too close to the trench axis (and thus the top of the subducting slab) to be volcanic features formed in-situ. A sinuous feature originates from the summit and appears to flow into the basin on the southwest. If the sinuous feature is in fact a flow (volcanic, metamorphic or debris), then it must be younger than the initial formation of the north-east wall of the basin, that I infer to be young (see below). This feature can be compared to small seamounts imaged in the Sumisu rift and lava flows emanating from them (Taylor et al., 1990). Sinuous flows of serpentinized muds issue from the summit of a serpentinite seamount (Conical Seamount) at about 19°25'N in the outer Mariana forearc (Hussong and Fryer, 1985). The northern seamount is located less than 10 km above the top of the subducting slab, much too shallow to permit normal magma generation that is thought to require at least a 70-80 km separation. However, boninite, a lava type found only in forearcs and ophiolites is thought to form at a separation of only about a 30 km. If the increased volatile input to the sub-forearc mantle west of the two seamounts lowers the melting temperature enough to allow shallow melting, such melts may travel along faults in the outer forearc and be erupted near the trench slope break. An intrusion that may have traveled up to 100 km was drilled during Ocean Drilling Program Leg 125

(Chapter 5). If these are in fact recently active seamounts they are quite anomalous. Magma generation in the outer forearc has been suggested to result from fracturing of the subducting plate as it bends beneath the forearc causing decompression melting of the mantle beneath the subducting plate. Near-trench magmatic intrusions in ocean-continent forearcs have been documented from the Paul Revere Ridge near the triple junction of the American-Pacific-Juan de Fuca plates (MacLeod and Pratt, 1973), in the Franciscan Complex of California (Echeverria, 1980), and in southern Chile (Forsythe et al., 1986). An origin of this type is highly speculative, however, the general disruption of the outer forearc and the apparent coupling between the subducting plate and DR (faults with similar strike) is consistent with intense disturbances.

Basin. The small basin just west of the two seamounts may be analogous to the deep, steep-sided basin imaged at 19°30'N (Hussong and Fryer, 1985) (Chapter 3). The lack of layered sediments in the basin (Fig. 7.5), and the disruption of the fault fabric across it suggest that it is an actively deforming feature. Extensive disruption including relative subsidence of the outer forearc is occurring and may be caused by one or more of the following mechanisms. (1) Subduction of seamounts cause localized uplift resulting in fracturing and structural disruption of the forearc. This may eventually cause removal of sub-crustal rocks and subsequent downdropping of the forearc crust. Alternatively the accelerated erosion of the inner trench wall may destabalize the outer forearc creating a tensional environment allowing normal faulting as blocks slump into the trench. (2) Metamorphism of upper mantle may result in the formation of serpentine seamounts causing "voids" in the lower forearc, as well as local expansion and uplift of surrounding country rock. (3) A subducting ridge may create a reentrant in the inner trench wall that is later "plugged" by

accretion of oceanic plate or faulting of arc rocks, subparallel to the trench (von Huene and Lallemand, 1990) (Chapter 6). The initial reentrant may eventually be trapped as a forearc basin (Collot and Fisher, 1989). (4) Regional tensional stresses may cause normal faulting resulting in downdropped features. These mechanisms apply equally to formation of both the small basin at 20°20'N and at 19°30'N, the larger fault bounded basin discussed in Chapter 3. Regardless of the mechanism of formation, the basin at 19°30'N has proved quite unique. Accreted Cretaceous sediments, lavas, and plutonic rocks as well as igneous rocks with SSZ compositions have been recovered from it (Chapters 3 and 6). Although there is no present day seamount subduction at 19°30'N, nor is the inner trench wall over-steepened or indented, a large seamount is present just east of this basin (Fig. 7.1b). This seamount and the general continuity of seamount chains in the Pacific prompt us to propose that seamount subduction has occurred here in the past. I suggest that the subduction of seamounts or ridges leads to the creation of deep basin structures. The presence of oceanic plate in the forearc at 19°30'N suggests that the effects of seamount subduction on the inner trench wall and outer forearc create the necessary environment for the accretion (or obduction) of oceanic plate into the outer forearc. If the association of obviously accreted rocks with outer forearc basins is more than a local association, I expect that the basin at 20°20'N is a site of accreted rocks.

Broad High. One of the largest bathymetric features in the study area is the broad high located just west of the SeaMARC II survey. Over 2000 m of relief exist between this high and the typical forearc depth. Recent drilling has revealed a Pleistocene intrusion, about 100 km from the active arc, and near the southern edge of this high (Figs. 7.1b and 7.2) (Chapter 5). In Chapter 5 I suggest the uplift of this block, that forms the western boundary of the present survey area, may be

responsible for rupture of the forearc providing a pathway from the arc for magma emplacement. Smoot et al., (1983) suggested that regional uplift is caused by the westward extension of the DR beneath the Mariana Forearc. However, the forearc between the high and the trench does not appear to be uplifted suggesting a less continuous response between ridge subduction and forearc uplift. Instead of a direct tectonic connection, I suggest that the increased volatile input from the subducting DR and accelerated forearc erosion may cause excess magma generation that may in turn be responsible for this high.

7.7 Conclusions

Collision of seamount chains with subduction zones causes faulting and disruption of the subducting edifice, over 30 km from the collision zone, as well as the forearc and inner trench wall. Collision may locally cause shallowing of the trench axis, over-steepening of the inner trench wall in advance of the collision, and disruption of the trench slope break. Accelerated tectonic erosion and accretion may occur as the consequence of collision, thus, more sediment and rock than usual is subducted in the area of a collision. Near trench volcanism may be possible in areas of collision, or perhaps fracturing of the outer forearc allows the formation of serpentine seamounts or mud volcanoes. The mechanism for basin formation and complex fault patterns at 20°20'N is apparently a consequence of ridge subduction. By analogy to the area at 19°30'N this basin forming event and collision may facilitate the accretion of oceanic plate rocks in the outer Mariana forearc. A consequence of the increased volume of rock and sediment subducted at 20°20'N may be the addition of abundant fluids to the forearc causing greater than usual melting and creating a broad uplift over 150 km from the trench.

Chapter 8:

Summary and Conclusions:

New ideas about the Mariana Forearc

A new model for the evolution of the Mariana forearc can be proposed based on the primary conclusions of this dissertation. Erosional, intra-oceanic subduction margins, such as the Mariana forearc, are frequently considered simple systems. In the simplest model, volcanism from the arc builds forearc crust and erosion at the inner trench wall (ITW) destroys forearc crust exposing supra-subduction zone (SSZ) rocks (those rocks generated in an arc environment overlying a subduction zone) over 200 km from the active arc. This dissertation attempted to answer two fundamental questions relating to the Mariana forearc. (1) What is the nature, geochemical and structural, of the crust of the Mariana forearc between 19-21°N? (2) What evolutionary history could explain the present composition and structure? My studies of the outer Mariana forearc discuss the geochemical nature of the forearc crust and document evidence that requires a reassessment of the simple erosion/non-accretion model for the evolution of the Mariana forearc.

I have characterized the geochemical composition of mafic rocks from three sites in the Mariana forearc. At each of these widely separated locations, rocks with chemical compositions indicative of formation at a mid-ocean ridge (i.e., mid-ocean ridge basalt: MORB) have been documented. Location 1 is a steep scarp bounding a 2000 m deep basin, at 19°30'N, west of the break in slope of the ITW and over 50 km from the trench axis (Chapters 3, and 6). Location 2 is a smaller scarp at the break in slope of the ITW at 17°50'N (Johnson and Fryer, 1990; Chapter 6), and location 3 is a serpentine seamount over 80 km from the trench axis (Chapter 4). At each of

these locations rocks with MORB chemical characteristics were recovered in the same dredge (locations 1 and 2) and drillhole (location 3) as rocks with SSZ chemical characteristics, (island arc tholeiites). Rocks unquestionably identifiable as boninites were only recovered from location 1. Rocks with ocean island type characteristics (ocean island alkalic basalts: OIB) were recovered from locations 1 and 2 and rocks with possible characteristics of shoshonites (alkalic arc rocks) were recovered at location 3. Cherts with Cretaceous radiolaria and foraminifera were recovered at location 1 (identifications by M. Silk, D. Jones, and W. Sliter, personal communication).

This geochemically complex crust must have a comparably complex structure. The likely source of the SSZ rocks is the active arc and its related magma systems and magmatic processes active in the forearc (boninite). The likely source of the OIB is accretion of seamount fragments. However, there are several possible sources for the MORB-like rocks. These include: (1) accreted Pacific plate emplaced into the outer forearc prior to subduction; (2) subducted plate emplaced into the lower forearc by faulting across the décollement; (3) trapped, foundered, oceanic plate left from initiation of subduction; (4) magmatism of a BABB (backarc basin basalt) nature emplaced into the forearc during an arc rifting event; and or (5) forearc magmatism of a MORB-like composition (Fig. 4.7). Because of alteration of these samples it is not presently possible to distinguish geochemically between these possibilities (especially between MORB and BABB), thus we must rely on structural constraints. Although limited single channel and 6-channel seismic profiles are available, the structure of the forearc is not well known around 19°30'N (locations 1 and 3). (Hussong and Fryer, 1985; Fryer et al., 1990b). At approximately 18°N the crustal structure of the forearc is well known (see Chapter 7 for a summary).

Despite the present location, over 50 km from the trench axis, the source of MORB-like rocks at location 1 is likely to be accretion of Pacific plate prior to subduction. This is consistent with the recovery of OIB and Cretaceous chert at this site. These rocks may have been thrust or pushed over the break in slope or emplaced into the outer forearc and later vertically faulted into place. The steep scarp at location 1 requires at least 2000 m of vertical faulting in the forearc. This faulting may move rocks from depth, in the forearc crustal structure, to the surface. Such faults may be related to subduction of seamounts and the erosion of lower crustal rocks. Alternatively, the formation of serpentine bodies may remove material from the lower crust/upper mantle leaving a void for crustal blocks to slip into. The steep scarp, the presence of SSZ rocks (including boninites), and the distance from the trench axis require that post-obduction faulting, including some component of vertical movement, must have occurred.

The source of MORB-like rocks at location 2 is likely also to be accretion prior to subduction. This is consistent with the presence of OIB and the location near the break in slope of the ITW. No sedimentary or igneous rocks have been dated from this site. DSDP Leg 60 drillholes are at this latitude, though further west, and no MORB-like rocks were recovered there. Dated sediments from Leg 60 were primarily Eocene, although sparse reworked Cretaceous microfossils were recovered (see Chapter 6). This may suggest that instead of a simple accretionary source for the MORB-like rocks at location 2 that a more complex crustal structure is present. Seismic refraction studies suggest the crustal structure at about 18°N may include a trapped piece of oceanic plate (Ambos, 1984).

Rocks from location 3 may have several different sources and are unlikely to be simply accreted from the Pacific plate prior to subduction. The rodingitized fragments (see Chapter 4) are likely to have been emplaced into the serpentine mud at depth in the forearc and are thus likely to be derived by methods 2, 3, 4, or 5 (see above) but not 1 (simple accretion). The lack of high pressure minerals in the FeTi basalt fragment (Chapter 4) is consistent with derivation from a foundered slab of oceanic crust. The presence of high pressure minerals (lawsonite and blue amphibole) indicates rocks from deep crustal levels or the subducting slab are involved. The shoshonitic rocks may represent a fragment of an older arc complex. The rising serpentine mud itself helps to mix rocks with both MORB-like and SSZ compositions. Thus, I suggest that the crustal structure of the outer Mariana forearc at about 19°30'N is quite complex and likely includes elements from several different tectonic environments.

The presence of the SSZ rocks has been documented well by previous workers (see Chapter 1 for a summary). The close spatial association of obviously accreted rocks with SSZ rocks (Chapters 3 and 6) suggests that mixing of the forearc occurs at a small scale (<3 km^2). This mixing may be either tectonic, including lateral and vertical faulting in the forearc, or magmatic, including intrusions of SSZ lavas into accreted MORB-like rocks (Chapter 5). The available data suggest that a combination of these has occurred. The rocks recovered from the serpentine seamount (Chapter 4) imply this mixing must be widespread (over 70000 km^2 between the three locations), and involve deeper forearc rocks, indicated by the presence of high pressure minerals in clasts (Chapter 4; table 4.1).

Despite these conclusion an enigma remains. This is the recovery of abundant SSZ rocks in drillholes from the outer forearc and dredges in the ITW and the lack of MORB-like rocks from the same locations (see Chapters 1 and 3 for a summary). The large area where I have documented the presence of MORB-like rocks suggests they should also be present in the ITW. One model that may help to explain this problem is presented in Chapter 7. When seamounts and aseismic ridges begin to subduct they collide with the outer forearc and ITW. This causes extensive faulting of the outer forearc and ITW as well as the colliding edifice and underlying oceanic plate. Such extensive faulting accelerates erosion, facilitating the exposure of SSZ rocks in the ITW; however, the faulted nature of the subducting edifice, the underlying plate and the outer forearc also facilitates accretion. The faulting in the outer forearc may assist mixing of the accreted rocks into the forearc crustal structure. Thus, seamount collision may create the necessary conditions for the combination of erosion and accretion. This conclusion is consistent with discovery of MORB-like, OIB, and SSZ volcanic rocks and Cretaceous sediments from the outer forearc. Intrusion of SSZ lavas into the outer forearc also will assist mixing in the forearc at the observed scale of 2-3 km, allowing for a petrologically and structurally complex forearc crust.

References Cited

Ambos, E.L., 1984, Applications of ocean bottom seismometer data to the study of forearc and transform fault systems [Ph. D.]: University of Hawaii,

Azema, J., and Blanchet, R., 1981, The Late Jurassic-Early Cretaceous Genus Calpionella in reworked pebbles from Deep Sea Drilling Project Site 460, Mariana transect, in Hussong, D.M., and Uyeda, S., eds., Initial reports of the Deep Sea Drilling Project: Washington, D.C., U.S. Government Printing Office, v. 60, p. 574-575.

Ballance, P.F., Scholl, D.W., Vallier, T.L., Stevenson, A.J., Ryan, H., and Herzer, R.H., 1989, Subduction of a late Cretaceous seamount of the Louisville Ridge at the Tonga Trench: A model of normal and accelerated tectonic erosion: Tectonics, v. 8, p. 953-962.

Beccaluva, L., Macciotta, G., Savalli, C., Serri, G., and Zeda, O., 1980, Geochemistry and K/Ar ages of volcanics dredged in the Philippine Sea (Mariana, Yap, and Palau trenches and Parece Vela Basin), in Hayes, D.E., ed., The tectonic and geologic evolution of Southeast Asian seas and islands: Part I, Washington, D. C., American Geophysical Union, p. 247-268.

Bloomer, S., 1983, Distribution and origin of igneous rocks from the landward slopes of the Mariana Trench: Implications for its structure and evolution: Journal of Geophysical Research, v. 88, p. 7411-7428.

Bloomer, S., and Hawkins, J.W., 1983, Gabbroic and ultramafic rocks from the Mariana trench: An island arc ophiolite, in Hayes, D.E., ed., The tectonic and geologic evolution of Southeast Asian seas and islands: Part II, Washington, D. C., American Geophysical Union, p. 294-317.

Bloomer, S., and Hawkins, J.W., 1987, Petrology and geochemistry of boninite series volcanic rocks from the Mariana Trench: Contributions to Mineralogy and Petrology, v. 97, p. 361-377.

Bloomer, S.H., Stern, R.J., Fish, E., and Geschwind, C.H., 1989, Shoshonitic volcanism in the northern Mariana Arc 1. Mineralogic and major and trace element characteristics: Journal of Geophysical Research, v. 94, p. 4469-4496.

Bruns, T.R., Vallier, T.L., Pickthorn, L.B., and R., v.H., 1987, Volcanic-arc dacite and early Miocene basalt dredged from the Shumagin margin, Alaska., in Hamilton, T.D., and Galloway, J.P., eds., Geologic Studies in Alaska by the U.S. Geological Survey During 1986: U.S. Geol. Surv., p. 143-146.

Byerly, G.R., Melson, W.G., and Vogt, P.R., 1976, Rhyodacites, andesites, ferro-basalts and ocean tholeiites from the Galapagos spreading center: Earth and Planetary Science Letters, v. 30, p. 215-221.

Cameron, W.E., Nisbet, E.G., and Dietrich, V.J., 1979, Boninites, komatiites, and ophiolitic basalts: Nature, v. 280, p. 550-553.

Cande, S.C., Lewis, S.D., Bangs, N., Tebbens, S.F., and Westbrook, G.K., 1990, The Chile Ridge/Chile Trench collision zone: A rift valley disappears beneath a continental margin: EOS Trans. Am., Geophs. Union, v. 71, p. 1565.

Cann, J.R., 1970, Rb, Sr, Zr and Nb in some ocean floor basaltic rocks: Earth and Planetary Science Letters, p. 7-11.

Clague, D.A., and Jarrard, R.I., 1973, Tertiary Pacific plate motion deduced from Hawaiian-Emperor chain: Geological Society of America Bulletin, v. 84, p. 1135-1154.

Coleman, R.G., 1966, New Zealand Serpentinites and Associated Metasomatic Rocks : N. Z. Geological Survey, Bull. 76.

Coleman, R.G., 1967, Low-temperature reaction zones and Alpine ultramafic rocks of California, Oregon and Washington : U. S. Geol. Surv., Bull. 1247.

Collot, J.-Y., and Fisher, M.A., 1989, Formation of forearc basins by collision between seamounts and accretionary wedges: An example from the New Hebrides subduction Zone: Geology, v. 17, p. 930-933.

Collot, J.Y., Daniel, J., and Burne, R.V., 1985, Recent tectonics associated with the subduction/collision of the D'Entrecasteaux zone in the central New Hebrides: Tectonophysics, v. 112, p. 325-356.

Crawford, A.J., Beccaluva, L., Serri, G., and Dostal, J., 1986, Petrology, geochemistry and tectonic implications of volcanics dredged from the intersection of the Yap and Mariana trenches: Earth and Planetary Science Letters, v. 80, p. 265-280.

Crawford, A.J., L. Beccaluva, and Serri, G., 1981, Tectono-magmatic evolution of the West Philippine-Mariana region and the evolution of boninites: Earth and Planetary Science Letters, v. 54, p. 346.

DeLong, S., Fox, P., and McDowell, F., 1978, Subduction of the Kula Ridge at the Aleutian Trench: Geological Society of America bulletin, v. 89, p. 83-95.

Dickinson, W.R., and Seely, D.R., 1979, Structure and stratigraphy of forearc regions: American Association of Petroleum Geologists Bulletin, v. 63, p. 1-31.

Dixon, T.H., and Batiza, R., 1979, Petrology and chemistry of recent lavas in the northern Marianas: Implications for the origin of island arc basalts: Contributions to Mineralogy and Petrolgy, v. 70, p. 167-181.

Dixon, T.H., and Stern, R.J., 1983, Petrology, chemistry, and isotopic compositions of submarine volcanoes in the southern Mariana arc: Geological Society of America Bulletin, v. 94, p. 1159-1172.

Duncan, R.A., and Kulm, L.D., 1989, Plate tectonic evolution of the Cascades arc-subduction complex, in Winterer, E.L., Hussong, D.M., and Decker, R.W., eds.,

The Eastern Pacific Ocean and Hawaii: Geol. Soc. Am. The Geology of North
America, p. 413-438.

Dunkley, P.N., 1983, Volcanism and the evolution of the ensimatic Solomon Islands arc, *in* Shimozuru, D., and Yokoyama, I., eds., Arc Volcanism: Tokyo, Terra Scientific, Publishing Company, p. 225-241.

Echeverria, L.M., 1980, Oceanic basaltic magmas in accretionary prisms: The Franciscan intrusive gabbro: American Journal of Science, v. 280, p. 697-724.

Ewart, A., and Bryan, W.B., 1972, Petrography and geochemistry of the igneous rocks from Eua, Tongan Islands: Geological Society of America Bulletin, v. 83, p. 3281-3298.

Fisher, M.A., Collot, J.-Y., and Smith, G.L., 1986, Possible causes for structural variation where the New Hebrides island arc and the D'Entrecasteaux zone collide: Geology, v. 14, p. 951-954.

Floyd, P.A., J. A. Winchester, 1975, Magma type and tectonic discrimination using immobile elements: Earth and Planetary Science Letters, v. 27, p. 211-218.

Forsythe, R., and Nelson, E., 1985, Geological manifestations of ridge collision: Evidence from the Golfo de Penas-Taitao basin, southern Chile: Tectonics, v. 4, p. 477-495.

Forsythe, R.D., Nelson, E.P., Carr, M.J., Kaeding, M.E., Herve, M., Mpodozis, C., Soffia, J.M., and Harambour, S., 1986, Pliocene near-trench magmatism in southern Chile: A possible manifestation of ridge collision: Geology, v. 14, p. 23-27.

Fryer, P., Ambos, E.L., and Hussong, D.M., 1985, Origin and emplacement of Mariana forearc seamounts: Geology, v. 13, p. 774-777.

Fryer, P., and Fryer, G.J., 1987, Origins of non-volcanic seamounts in a forearc environment, *in* Keating, B.H., Fryer, P., Batiza, R., and Boehlert, G.W., eds., Seamounts, islands and atolls: Washington, American Geophysical Union, p. 61-69.

Fryer, P., and Hussong, D.M., 1981, Seafloor spreading in the Mariana Trough: Results of Leg 60 drill site selection surveys, *in* Hussong, D.M., and Uyeda, S., eds., Initial reports of the Deep Sea Drilling Project: Washington, D.C., U.S. Government Printing Office, v. 60, p. 45-55.

Fryer, P., and Hussong, D.M., 1985, SeaMARC II studies of subducting seamounts, *in* Nasu, N., ed., Formation of Active Ocean Margins: Tokyo, Terra Sci. Pub. Co., p. 291-306.

Fryer, P., and Smoot, N.C., 1985, Processes of seamount subduction in the Mariana and Izu-Bonin trenches: Marine Geology, v. 64, p. 77-90.

Fryer, P., Haggerty, J., Tilbrook, B., Sedwick, P., Johnson, L., Saboda, K., Newsom, S., Karig, D., Uyeda, S., and Ishii, T., 1987, Results of ALVIN studies of Mariana forearc serpentinite diapirism: EOS Trans. Am., Geophs. Union, v. 68, p. 1534.

Fryer, P., Pearce, J.A., and The Shipboard Scientific Party, 1989, Leg 125 drills forearc crust and mantle: Geotimes, v. 37, p. 18-20.

Fryer, P., Pearce, J.A., Stokking, L.B., and The Shipboard Scientific Party, 1990a, Proceedings of the Ocean Drilling Program: Initial reports, 125 : College Station, TX, Ocean Drilling Program, 1092 p.

Fryer, P., Saboda, K.L., Johnson, L.E., Mackay, M.E., Moore, G.F., and Stoffers, P., 1990b, Conical Seamount: SeaMARC II, ALVIN submersible and seismic reflection studies, *in* Fryer, P., Pearce, J.A., Stokking, L.B., et al., eds., Proc. ODP, Init. Repts., 125: College Station, TX, Ocean Drilling Program,

Fryer, P., Sinton, J.M., and Philpotts, J.A., 1981, Basaltic glasses from the Mariana Trough, in Hussong, D.M., and Uyeda, S., eds., Initial reports of the Deep Sea Drilling Project: Washington, D.C., U.S. Government Printing Office, v. 60, p. 601-609.

Fryer, P., Taylor, B., Langmuir, C.H., and Hochstaedter, A.G., 1990c, Petrology and geochemistry of lavas from the Sumisu and Torishima backarc rifts: Earth and Planetary Science Letters, v. 100, p. 161-178.

Gill, J., 1976, Composition and age of Lau Basin and Ridge volcanic rocks: Implications for evolution of an interarc basin and remnant arc: Geological Society of America Bulletin, v. 87, p. 384-1395.

Gill, J., 1981, Orogenic andesites and plate tectonics : New York, Springer-Verlag, 385 p.

Gnibidenko, H.S., Anosov, G.I., Argentov, V.V., and Pushchin, I.K., 1985, Tectonics of the Tonga-Kermadec Trench and Ozburn Seamount Junction area: Tectonophysics, v. 112, p. 357-383.

Harland, W.B., Cox, A.V., Llewellyn, P.G., Pickton, C.A.G., Smith, A.G., and Walters, R., 1982, A geologic time scale : Cambridge, Cambridge University Press, 131 p.

Hawkins, J.W., 1979, Petrology of Back-Arc Basins and Island Arcs: Their Possible role in the Origin of Ophiolites, Proceedings International Ophiolite Symposium: Cyprus, The Cyprus Geological Survey.

Hawkins, J.W., and Falvey, D.A., 1985, Petrology of andesitic dikes and flows from 'Eua, Tonga., in Scholl, D.W., and Vallier, T.L., eds., Geology and Offshore Resources of Pacific Island Arcs-Tonga Region: Circum-Pacific Council for Energy and Mineral Resources, p. 269-277.

Hawkins, J.W., Bloomer, S.H., Evans, C.A., and Melchior, J.T., 1984, Evolution of intra-oceanic arc-trench systems: Tectonophysics, v. 102, p. 175-205.

Hickey, R.L., and Frey, F.A., 1982, Geochemical characteristics of boninite series
volcanics: Implications for their source: Geochimica Cosmochimica Acta, v. 46,
p. 2099-2115.

Hickey-Vargas, R., 1989, Boninites and tholeiites from DSDP Site 458, Mariana forearc., *in*
In Crawford, A.J., ed., Boninites and related rocks: London, Unwin Hyman Ltd, p. 339-
356.

Hickey-Vargas, R., and Reagan, M.K., 1987, Temporal variation of isotope and rare-earth
element abundances in volcanic rocks from Guam: Implications for the evolution of the
Mariana arc: Contributions to Mineralogy and Petrology, v. 97, p. 497-508.

Hilde, T.W.C., and Lee, C.-H., 1984, Origin and evolution of the West Philippine Basin:
A new interpretation: Tectonophysics, v. 102, p. 85-104.

Hilde, T.W.C., and Uyeda, S., 1983, Geodynamics of the western Pacific-Indonesian region :
Washington, Am. Geophys. Union Geodynamics Series,

Hilde, T.W.C., Uyeda, S., and Kroenke, L., 1977, Evolution of the western Pacific and
its margin: Tectonophysics, v. 38, p. 145-165.

Hill, M., Morris, J., and Whelan, J., 1981, Hybrid granodiorites intruding the
accretionary prism, Kodiak, Shumagin, and Sanak Islands, southwest Alaska:
Journal of Geophysical Research, v. 86, p. 10569-10590.

Hochstaedter, A.G., Gill, J.B., Kusakabe, M., Newman, S., Pringle, M., Taylor, B., and
Fryer, P., 1990, Volcanism in the Sumisu Rift, I. Major element, volatile and
stable isotope geochemistry: Earth and Planetary Science Letters, v. 100, p.
179-194.

Hudson, T., Plafker, G., and Lanphere, M.A., 1977, Intrusive rocks of the Yakutat-St.
Elias area, south-central Alaska: U.S. Geological Survey Journal of Research, v.
5, p. 155-172.

Humphris, S.E., and Thompson, G., 1978, Trace element mobility during

   hydrothermal alteration of oceanic basalts: Geochimica Cosmochimica Acta, v.

   42, p. 127-136.

Hurst, R.W., 1982, Petrogenesis of the Conejo volcanic suite, southern California.

   Evidence for mid-ocean ridge-continental margin interactions: Geology, v. 10,

   p. 167-272.

Hussong, D.M., and Fryer, P., 1981, Structure and tectonics of the Mariana arc and.

   fore-arc: Drillsite selection surveys, in Hussong, D.M., and Uyeda, S., eds.,

   Initial reports of the Deep Sea Drilling Project: Washington, D.C., U.S.

   Government Printing Office, v. 60, p. 33-44.

Hussong, D.M., and Fryer, P., 1983, Back-arc seamounts and the SeaMARC II seafloor

   mapping system: EOS Trans. Am., Geophs. Union, v. 64, p. 627-632.

Hussong, D.M., and Fryer, P., 1985, Fore-Arc Tectonics in the northern Mariana Arc,

   in Nasu, N., ed., Formation of Active Ocean Margins: Tokyo, Terra Sci. Pub. Co.,

   p. 273-290.

Hussong, D.M., and Uyeda, S., 1981a, Tectonic processes and the history of the

   Mariana Arc: A synthesis of the results of Deep Sea Drilling Project Leg 60, in

   Hussong, D.M., and Uyeda, S., eds., Initial reports of the Deep Sea Drilling

   Project: Washington, D.C., U.S. Government Printing Office, v. 60, p. 909-

   929.

Hussong, D.M., and Uyeda, S., 1981b, Mariana Arc and fore-arc background

   objectives, in Hussong, D.M., and Uyeda, S., eds., Initial reports of the Deep Sea

   Drilling Project: Washington, D.C., U.S. Government Printing Office, v. 60, p.

   251-254.

Hussong, D.M., S. Uyeda, and et al., 1981, Initial reports of the Deep Sea Drilling

   Project: Washington D.C., U.S. Government Printing Office, v. 60, 937 p.

Irvine, T.N., and Baragar, W.R., 1971, A guide to the chemical classification of the common igneous rocks: Canadian Journal of Earth Science, v. 8, p. 523-45.

Iwabuchi, Y., 1979, General Bathymetric Chart of the Oceans (GEBCO): Canadian Hydrographic Survey, Ottawa, v. 5.06,

Jackson, M.C., Fryer, P., and Gill, J.B., 1987, Petrology of volcanic rocks collected on a recent Alvin cruise to the Kasuga Volcanoes, northern Mariana Arc: EOS Trans. Am., Geophs. Union. v. 68, p. 1532.

Johnson, L.E., and Fryer, P., 1990, Mariana forearc mafic crustal complex: a pre-emplacement analogue to the Coast Range Ophiolite, CA: EOS Trans. Am., Geophs. Union, v. 71, p. 1648.

Johnson, L.E., Fryer, P., and Ishii, T., 1987, Mariana forearc basement adjacent to serpentinite diapirs: EOS Trans. Am., Geophs. Union, p. 1534.

Johnson, L.E., Fryer, P., Pearce, J., and The Shipboard Scientific Party, 1989, Mariana Forearc crust sampled by serpentinite seamounts: EOS Trans. Am., Geophs. Union, v. 70, p. 1309.

Johnson, R.W., 1979, Geotectonics and volcanism in Papua New Guinea. A review of the late Cainozoic: Journal Geology and Geophysics, Bureau of Mineral Resources, Australia,, v. 4, p. 181-207.

Johnson, R.W., Wallace, D.A., and Ellis, D.J., 1976, Feldspathoid-bearing potassic rocks and associated types from volcanic islands off the coast of News Ireland, Papua New: A preliminary account of geology and petrology., in Johnson, R.W., ed., Volcanism in Australasia: New York, Elsevier Scientific Publishing Company, p. 297-316.

Jones, G.M., Hilde, T.W.C., Sharman, G.F., and et al., 1978, Fault patterns in outer trench wall and their tectonic significance: Journal of the Physical Earth, v. 26 Supplement, p. S85-S101.

Karig, D.E., 1971, Structural history of the Mariana Island Arc system: Geological

Society of America Bulletin, v. 82, p. 323-344.

Karig, D.E., 1973, Plate convergence between the Philippines and the Ryukyu Islands:

Marine Geology, v. 14, p. 153-168.

Karig, D.E., 1974, Evolution of arc systems in the western Pacific: Annual Reviews of

Earth and Planetary Science, v. 2,

Karig, D.E., 1975, Basin genesis is the Philippine Sea, in Karig, D.E., and J. C. Ingle, J., eds.,

Initial reports of the Deep Sea Drilling Project: Washington, D.C., U.S. Government

Printing Office, v. 31, p. 857-879.

Karig, D.E., and Ingle, J.C., Jr., 1975, Initial reports of the Deep Sea Drilling Project:

Washington, D.C., U.S. Government Printing Office, v. 31, 927 p.

Karig, D.E., and Ranken, B., 1983, Marine geology of the forearc region, southern

Mariana Trough, in Hayes, D.E., ed., The tectonic and geologic evolution of

Southeast Asian seas and islands: Part II, Washington, D. C., American

Geophysical Union,, p. 266-280.

Karig, D.E., and Sharman, G.F., 1975, Subduction and accretion in trenches: Geological

Society of America Bulletin, v. 86, p. 377-389.

Klein, G.d.V., and Kobayashi, K., 1980, Geological summary of the north Philippine

Sea, based on Deep Sea Drilling Project Leg 58 results, in Klein, G.d.V., and

Kobayashi, K., eds., Initial reports of the Deep Sea Drilling Project:

Washington, D.C., U.S. Government Printing Office, v. 58, p. 951-961.

Kobayashi, K., 1983a, Cycles of subduction and Cenozoic arc activity in the

northwestern Pacific margin., in Hilde, T.W.C., and Uyeda, S., eds.,

Geodynamics of the Western Pacific-Indonesian Region: Washington, DC, Am.

Geophysical Union Geodynamics Series, p. 287-301.

Kobayashi, K., 1983b, Fore-arc volcanism and cycles of subduction, *in* Shimozuru, D., and Yokoyama, I., eds., Arc Volcanism: Physics and Tectonics: Tokyo, Terra Scientific Publishing Company, p. 153-163.

Kroenke, L., Scott R.B., S. et al., 1980, Initial reports of the Deep Sea Drilling Project: Washington, D.C., U.S. Government Printing Office, v. 59, 820 p.

Kuroda, N., and Shiraki, K., 1975, Boninite and related rocks of Chichijima, Bonin Islands, Japan: Rep. Fac. Sci., (Shizoka Univ.), v. 10, p. 45-155.

Kushiro, I., 1990, Partial melting of mantle wedge and evolution of island arc crust: Journal of Geophysical Research, v. 95, p. 15,929-15,939.

Lallemand, S., and Le Pichon, X., 1987, Coulomb wedge model applied to the subduction of seamounts in the Japan trench: Geology, v. 15, p. 1065-1069.

LaTraille, S.L., and Hussong, D.M., 1980, Crustal structure across the Mariana Island Arc, *in* Hayes, D.E., ed., The tectonic and geologic evolution of Southeast Asian seas and islands: Part I, Washington, D. C., American Geophysical Union, p. 209-221.

LaTraille, S.L., and Hussong, D.M., 1980, Crustal structure across the Mariana Island Arc, *in* Hayes, D.E., ed., The tectonic and geologic evolution of Southeast Asian seas and islands: Part II, Washington, D. C., American Geophysical Union, p. 209-221.

Lundberg, N., 1983, Development of forearcs of intraoceanic subduction zones: Tectonics, v. 2, p. 51-61.

MacLeod, N.S., and Pratt, R.M., 1973, Petrology of volcanic rocks recovered on Leg 18, *in* Kulm, L.D., and von Huene, R., eds., Initial reports of the Deep Sea Drilling Project: Washington, D.C., U.S. Government Printing Office, v. 18, p. 935-945.

MacPherson, G.J., Phipps, S.P., and Grossman, J.N., 1990, Diverse sources for

   igneous blocks in Franciscan melanges, California Coast Ranges: Journal of

   Geology, v. 98, p. 845-862.

Marlow, M.S., Merrill, D.L., and Party, S.S., 1990, Underway geophysics, *in* Fryer, P.,

   Pearce, J.A., and Stokking, L.B., eds., Proc. ODP, Init. Repts.: College Station, Ocean

   Drilling Program, p. 41-67.

Marshak, R.S., and Karig, D.E., 1977, Triple junctions as a cause for anomalously near-

   trench igneous activity between the trench and volcanic arc: Geology, v. 5, p. 233-

   236.

Mattey, D.P., Marsh, N.G., and Tarney, J., 1980, The geochemistry, mineralogy and

   petrology of basalts from the West Philippine and Parece Vela Basins and from

   the Palau-Kyushu and West Mariana Ridges, Deep Sea Drilling Project Leg 59,

   in Kroenke, L., and Scott, R., eds., Initial reports of the Deep Sea Drilling

   Project: Washington, D.C., U.S. Government Printing Office, v. 59,p. 753-

   797.

McGeary, S., Nur, A., and Ben-Avraham, Z., 1985, Spatial gaps in arc volcanism: The

   effect of collision or subduction of oceanic plateaus: Tectonophysics, v. 119, p.

   195-221.

Meijer, A., 1976, Pb and Sr isotopic data bearing on the origin of volcanic rocks from the

   Mariana island-arc system: Geological Society of America Bulletin, v. 87, p. 1358-

   1369.

Meijer, A., 1983, The origin of low-K rhyolites from the Mariana frontal arc: Contributions

   to Mineralogy and Petrology, v. 83, p. 45-51.

Meijer, A., Anthony, E., and Reagan, M., 1981, Petrology of volcanic rocks from the

   fore-arc sites, *in* Hussong, D.M., and Uyeda, S., eds., Initial reports of the Deep

Sea Drilling Project: Washington, D.C., U.S. Government Printing Office, v. 60, p. 709-729.

Miyake, Y., 1985, MORB-like tholeiites formed within the Miocene forearc basin, southwest Japan: Lithos, v. 18, p. 23-30.

Moore, J.C., Byrne, T., Plumley, P.W., Reid, M., Gibbons, H., and Coe, R.S., 1983, Paleogene evolution of the Kodiak Islands, Alaska: Consequences of ridge-trench interaction in a more southerly latitude: Tectonics, v. 2, p. 265-293.

Morrison, M.A., 1978, The use of "Immobile" trace elements to distinguish the palaeotectonic affinities of metabasalt: Applications to the Paelocene Basalts of Mull and Skye, Northwest Scotland: Earth and Planetary Science Letters, v. 39, p. 407-416.

Mrozowski, C.L., and Hayes, D.E., 1980, A seismic reflection study of faulting in the Mariana fore arc, in Hayes, D.E., ed., The tectonic and geologic evolution of Southeast Asian seas and islands: Part I, Washington, D. C., American Geophysical Union, p. 223-233.

Mrozowski, C.L., Hayes, D.E., and Taylor, B., 1981, Multichannel seismic reflection surveys of Leg 60 sites, in Hussong, D.M., and Uyeda, S., eds., Initial reports of the Deep Sea Drilling Project: Washington, D.C., U.S. Government Printing Office, v. 60, p. 57-70.

Natland, J.H., 1980, Effect of axial magma chambers beneath spreading centers on the compositions of basaltic rocks, in Rosendahl, B.R., and Hekinian, R., eds., Initial reports of the Deep Sea Drilling Project: Washington, D.C., U.S. Government Printing Office, v. 54, p. 833-850.

Newsom, S., and Fryer, P., 1987, Three dimensional gravity modeling of serpentinite seamounts in the Mariana forearc: EOS Trans. Am., Geophs. Union, v. 68, p. 1534.

Ogawa, Y., and Naka, J., 1984, Emplacement of ophiolitic rocks in forearc areas: Examples from central Japan and Izu-Mariana-Yap island arc system, *in* Gass, S.G., et al., eds., Ophiolites and Ocean Lithosphere: Oxford, Blackwell Sci. Pubs., p. 291-302.

Okada, H. and Bukry, D., 1980, Supplementary modifications and introduction of code numbers to the low-latitude cocolith biostratigraphic zonation, Mar. Micropaleontol. 5:321-325.

Pearce, J.A., 1975, Basalt geochemistry used to investigate past tectonic environments on Cyprus: Tectonophysics, v. 25, p. 41-67.

Pearce, J.A., 1983, Role of the sub-continental lithosphere in magma genesis at active continental margins, *in* Hawkesworth, C.J., and M. J. Norry, eds., Continental Basalts and Mantle Xenoliths: London, United Kingdom, Shiva Pub. Co., p. 230-249.

Pearce, J.A., and Cann, J.R., 1971, Ophiolite origin investigated by discriminant analysis using Ti, Zr, and Y: Earth and Planetary Science Letters, v. 12, p. 339-349.

Pearce, J.A., and Cann, J.R., 1973, Tectonic setting of basic volcanic rocks determined using trace element analysis: Earth and Planetary Science Letters, v. 19, p. 290-300.

Pearce, J.A., D. Wanming, 1988, The ophiolites of the Tibetan Geotraverse, Lhasa to Golmud (1985) and Lhasa to Kathmandu (1986): Philisophical Transactions of the Royal Society of London, series A, v. 327, p. 215-238.

Pearce, J.A., T. Alabaster, A.W. Shelton, R. Searle, 1981, The Oman ophiolite as a Cretaceous arc-basin complex: evidence and implications: Philisophical Transactions of the Royal Society London, v. 300, p. 299-317.

Peccerillo, A., and Taylor, S.R., 1976, Geochemistry of Eocene calc-alkaline volcanic rocks from the Kastamonu area, Northern Turkey: Contributions to Mineralogy and Petrology, v. 20, p. 2-35.

Perfit, M.R., and Langmuir, C.H., 1984, Geochemical effects of ridge subduction in the

    Solomon Islands-Woodlark Basin region: Geological Society of America Abstracts with

    Programs, v. 16, p. 622.

Pessagno, E.A.J., 1977a, Lower Cretaceous radiolarian biostratigraphy of the Great

    Valley Sequence and the Franciscan Complex, California Coast Ranges: Cushman

    Foundation for Foraminiferal Research, Special Publication, v. 15, p. 1-86.

Pessagno, E.A.J., 1977b, Upper Jurassic radiolaria and radiolarian biostratigraphy of

    the California Coast Ranges: Micropaleontology, v. 23, p. 56-113.

Phipps, S.P., 1984, Ophiolitic olistostromes in the basal Great Valley Sequence, Napa

    County, Northern California Coast Ranges: Geological Society of America Special

    Paper, v. 198,

Poldervaart, A., and Hess, H.H., 1951, Pyroxenes in the crystallization of basaltic

    magma: v. 59, p. 472-489.

Price, R.C., Johnson, L.E., and Crawford, A.J., 1990, Basalts of the North Fiji Basin:

    the generation of back arc basin magmas by mixing of depleted and enriched

    mantle sources: Contributions to Mineralogy and Petrology, v. 105, p. 106-

    121.

Ramsay, W.R.H., Crawford, A.J., and Foden, J.D., 1984, Field setting, mineralogy,

    chemistry, and genesis of arc picrites, New Georgia, Solomon Islands:

    Contributions to Mineralogy and Petrology, v. 88, p. 386-402.

Robinson, P.T., Melson, W.G., O'Hearn, T., and Schmincke, H., 1983, Volcanic glass

    compositions of the Troodos ophiolite, Cyprus: Geology, v. 11, p. 400-404.

Saboda, K.L., 1991, Petrology of ultramafic rocks from Conical Seamount based on

    Alvin submersible and Ocean Drilling Project studies [M.S.]: University of

    Hawaii.

Saboda, K.L., Fryer, P., and Fryer, G.J., 1987, Preliminary studies of metamorphic rocks collected during Alvin studies of Mariana forearc seamounts: EOS Trans. Am., Geophs. Union, v. 68, p. 1534.

Sample, J.C., D.E. Karig, 1982, A volcanic production rate for the Mariana Island Arc: Journal of Volcanological and Geothermal Research, v. 13, p. 73-82.

Sharaskin, A.Y., 1981, Petrography and geochemistry of basement rocks from five Leg 60 Sites, in Hussong, D.M., and Uyeda, S., eds., Initial reports of the Deep Sea Drilling Project: Washington, D.C., U.S. Government Printing Office, v. 60, p. 647-656.

Shervais, J., and Kimbrough, D., 1985, Geochemical evidence for the tectonic setting of the Coast Range ophiolite: A composite island arc-oceanic crust terrane in western California: Geology, v. 13, p. 35-38.

Shervais, J.W., 1982, Ti-V Plots and the petrogenesis of modern and ophiolitic lavas: Earth and Planetary Science Letters, v. 59, p. 101-118.

Shibata, K., 1978, Contemporanity of Tertiary granites in the outer zone of southwest Japan: Journal of the Geological Survey of Japan, v. 29, p. 551-554.

Shiraki, K., Kuroda, N., Maruyama, S., and Urano, H., 1978, Evolution of the Tertiary volcanic rocks in the Izu-Mariana arc: Bulletin Volcanologique, v. 412, p. 548-562.

Sinton, J.M., and Fryer, P., 1987, Petrology of Mariana Trough Lavas from 18°N and the Origin of Back-Arc Basin Basalts: Journal of Geophysical Research, v. 92, p. 12,782-12,802.

Smoot, N., 1988, The growth rate of submarine volcanoes on the South Honshu and East Mariana Ridges: Journal of Volcanology and Geothermal Research, v. 35, p. 1-15.

Smoot, N.C., 1983a, Guyots of the Dutton Ridge at the Bonin/Mariana trench juncture
as shown by multi-beam surveys: Journal of Geology, v. 91, p. 211-220.

Smoot, N.C., 1983b, Multi-Beam Surveys of the Michelson Ridge Guyots: Subduction of
Obduction: Tectonophysics, v. 99, p. 363-380.

Snavely, P.D., MacLeod, N.S., and Wagner, H.C., 1968, Tholeiitic and alkalic basalts of
the Eocene Siletz River volcanics, Oregon Coast Range: American Journal of
Science, v. 266, p. 454-481.

Stanton, R.L., and Bell, J.D., 1969, Volcanic and associated rocks of the New Georgia Group,
British Solomon Islands Protectorate: Overseas Geological Mineral Resources, v. 10, p.
113-145.

Steiger, R.H., and Jager, E., 1977, Subcommission on geochronology: convention on the
use of decay constants in geo- and cosmo-chronology: Earth and Planetary
Science Letters, v. 36, p. 359-362.

Stern, R.J., Bloomer, S.H., Ping-Nan, L., and Smoot, N.C., 1989, Submarine arc volcanism in
the southern Mariana Arc as an ophiolite analogue: Tectonophysics, v. 168, p. 151-
170.

Sun, S.S., and McDonough, W.F., 1989, Chemical and isotopic systematics of oceanic
basalts: Implications for mantle composition and processes: v. 42, p. 313-
345.

Taylor, B., and Exon, N., 1982, Forearc volcanism and subduction without a trench.
Peculiarities of ridge subduction in the Woodlark-Solomons Region: EOS Transactions
American Geophysical Union, v. 63, p. 1120-1121.

Taylor, B., Brown, G., Fryer, P., Gill, J.B., Hochstaedter, A.G., Hotta, H., Langmuir,
C.H., Leinen, M., Nishimura, A., and Urabe, T., 1990, ALVIN-SeaBeam studies
of the Sumisu Rift, Izu-Bonin arc: Earth and Planetary Science Letters, v. 100,
p. 127-147.

Taylor, B., Fujioka, K., and The Shipboard Scientific Party, 1990, Proceedings of the Ocean Drilling Program: Initial reports, 126 : College Station, TX, Ocean Drilling Program, 1002 p.

Thompson, G., 1973, A geochemical study of the low-temperature interaction of sea water and oceanic igneous rocks: EOS Transactions of the American Geophysical Union, v. 54, p. 1015.

Uyeda, S., and Ben-Avraham, Z., 1972, Origin and development of the Philippine Sea: Nature Physical Science, v. 240, p. 176-178.

von Huene, R., and Lallemand, S., 1990, Tectonic erosion along the Japan and Peru convergent margins: Geological Society of America Bulletin, v. 102, p. 704-720.

von Huene, R., Langseth, M., and Nasu, N., 1980, Summary: Japan Trench transect, *in* von Huene, R., and Nasu, N., eds., Initial reports of the Deep Sea Drilling Project: Washington, D.C., U.S. Government Printing Office, v. 56/57, p. 473-488.

Weissel, J.K., Taylor, B., and Karner, G.D., 1982, The opening of the Woodlark basin, subduction of the Woodlark spreading system, and the evolution of northern Melanesia since mid-Pliocene time: Tectonophysics, v. 87, p. 253-277.

Wood, D.A., Marsh, N.G., Tarney, J., Joron, L.J., Fryer, P., and Treuil, M., 1981, Geochemistry of igneous rocks recovered from a transect across the Mariana Trough, arc, fore-arc, and trench, Sites 453 through 461, Deep Sea Drilling Project Leg 60, *in* Hussong, D., and Uyeda, S., eds., Initial reports of the Deep Sea Drilling Project: Washington, D.C., U.S. Government Printing Office, v. 60, p. 611-645.

Woodhead, J.D., 1988, The origin of geochemical variations in Mariana lavas: A general model for petrogenesis in intra-oceanic Island arcs?: Journal of Petrology, v. 29, p. 805-830.

Yamazaki, T., and Okamura, Y., 1989, Subducting seamounts and deformation of overriding forearc wedges around Japan: Tectonophysics, v. 160, p. 207-229.